Progress in Nuclear Magnetic Resonance Spectroscopy 97 (2016) 82–125

Contents lists available at ScienceDirect

Progress in Nuclear Magnetic Resonance Spectroscopy

journal homepage: www.elsevier.com/locate/pnmrs

NMR in drug discovery: A practical guide to identification and validation of ligands interacting with biological macromolecules

Alvar D. Gossert *, Wolfgang Jahnke

Novartis Institutes for BioMedical Research, Novartis Campus, 4002 Basel, Switzerland

Edited by Geoffrey Bodenhausen and David Neuhaus

ARTICLE INFO

Article history:
Received 24 May 2016
Accepted 7 September 2016
Available online 30 September 2016

Keywords:
Drug discovery
Validation
Fragment-based screening
Protein-ligand Interactions

ABSTRACT

Protein-ligand interactions are at the heart of drug discovery research. NMR spectroscopy is an excellent technology to identify and validate protein-ligand interactions. A plethora of NMR methods are available which are powerful, robust and information-rich, but also have pitfalls and limitations. In this review, we will focus on how to choose between different experiments, and assess their strengths and liabilities. We introduce the concept of the validation cross, which helps to categorize experiments according to their information content and to simplify the choice of the right experiment in order to address a specific question. Additionally, we will provide the framework for drawing correct conclusions from experimental results in order to accurately evaluate such interactions. Out of scope for this review are methods for subsequent characterization of the interaction such as quantitative K_D determination, binding mode analysis, or structure determination.

© 2016 Elsevier B.V. All rights reserved.

Contents

* Corresponding author.
E-mail address: alvar.gossert@novartis.com (A.D. Gossert).

http://dx.doi.org/10.1016/j.pnmrs.2016.09.001
0079-6565/© 2016 Elsevier B.V. All rights reserved.

Introduction

NMR as a biophysical method in the context of drug discovery

Every drug discovery project typically comprises efforts to find lead compounds, where a chemical is sought that modulate the activity of a medicinal target. A typical drug discovery campaign can be divided into several steps: Hit finding, hit validation and subsequent characterization and optimization (Fig. 1). Hit finding can be undertaken with a variety of strategies, high-throughput screening (HTS) and fragment-based screening (FBS) being the most popular. In HTS, one starts by screening many compounds that modulate (most often inhibit) the activity of a target molecule. Since the assay is automated for high throughput, large compound libraries (more than a million compounds) can be screened. However, high-throughput assays are often prone to artifacts. Therefore, in a second step, initial "hits" need to be validated using more refined experiments such as NMR, with lower throughput but higher information content. Fragment-based screening goes the other way: Only few compounds (on the order of a few thousands) are screened, but using robust and sensitive biophysical methods, such as NMR or surface plasmon resonance (SPR). Because of the high sensitivity of such biophysical methods, even weak interactions can be detected. This allows screening of small compounds, so-called fragments, which in turn cover a wider diversity of chemical space than common HTS libraries. Even if the fragment hits are usually weaker in affinity than HTS hits, their "ligand efficiency"[1,2], that is their affinity per atom, is typically higher, making them valuable starting points for chemical optimization. A broad range of other hit-finding methods exist and are being applied, such as *in silico* screening, structure-based drug design, or DNA-encoded libraries. All of these approaches require validation of the hits by orthogonal methods, such as NMR. The result of these procedures is a validated ligand, which provides the basis for subsequent characterization and optimization. In this review, we only cover hit finding and validation, as this represents the basis for any subsequent activity. In other words, only a reliably validated ligand can justify high investments (e.g., a chemistry program) in a drug discovery project.

NMR is one of a plethora of biophysical methods that can reveal interactions between molecules, including surface plasmon resonance (SPR), isothermal titration calorimetry (ITC), thermal shift assays, microscale calorimetry (MST) and other methods [3–6]. NMR has some important assets that make it particularly valuable for studying interactions of ligands with macromolecules. Firstly, the studies are carried out in solution, that is, the biomolecule does not need to be attached to a surface or a column, and is in a nearly physiological state where it preserves its full conformational flexibility and steric accessibility from all sides. Secondly, the unmodified biomolecule and the ligand can be monitored directly. In other words, the NMR method is truly label-free, as there are no chemical compounds attached as labels to the biomolecule or the ligand. This makes NMR assays generally very robust. Additionally, most NMR methods can be multiplexed, that means that mixtures of several compounds can be screened at once and the one(s) that bind can directly be identified. In practical terms, NMR assays are

also very simple to set up without extensive method development – essentially only a stable preparation of the biomolecule in a buffer is needed and no lengthy optimization of parameters and assay windows is required.

Apart from these fundamental advantages of NMR, there is another important difference to most other biophysical techniques: its versatility. The value of NMR in drug discovery does not arise from a single "silver-bullet" experiment. NMR allows shedding light onto different aspects of a molecular interaction by applying several different types of experiments, sometimes tailor-made for the specific question under investigation, and the summed information will allow drawing educated conclusions. On the other hand, the wealth of NMR experiments that are available for drug discovery [7–9] represents a challenge to the scientist [10]. It may sometimes be difficult to choose the right experiment to address a specific question. Furthermore, the context of a drug discovery project will influence the decision about which experiments should be chosen. It is difficult to know the limitations, potential artifacts and intricacies of all NMR experiments. This review is intended to serve as a guide to put the different experiments and their information content into perspective.

Evaluating protein-ligand interactions using the validation cross

The goal of NMR in drug discovery is to provide validated ligands, which can be developed into drugs. But what is a validated ligand? How does one validate a protein-ligand interaction? What experiments are needed to validate a ligand?

We propose here a scheme termed the *validation cross* that may help to answer these questions. This scheme can be used for systematically evaluating a potential protein-ligand interaction. It consists in determining four main properties of the interaction:

- Ligand integrity
- Protein integrity
- Binding effects on the ligand
- Binding effects on the protein

Experimental data on these four aspects will enable proper validation or de-validation of an interaction.

Fig. 2 illustrates the modular application of NMR experiments in order to evaluate a protein-ligand interaction. Let's have a detailed look at the different fields of the validation cross and start with the top left field: ligand integrity. NMR is one of the few methods that can assess ligand quality in a stringent way, which not only includes ligand identity, but also ligand solubility and the mere presence of ligand. Although this may sound trivial, no other biophysical method is able to confirm that a ligand truly is in the sample and no pipetting errors or mislabeling of the tube have happened. Essentially, any binding experiment will be useless if the ligand identity and its presence in the sample have not been demonstrated. Therefore, the "ligand integrity" field can be marked green if experiments demonstrate that the ligand is present in the solution at a given concentration and that the ligand corresponds to the annotated structure. Experiments addressing the ligand integrity will also allow revealing self-aggregation or degradation of the ligand and detecting contaminants.

The field to the top right in Fig. 2 represents protein integrity. Protein aggregation, modification or degradation is one of the most important sources of artifacts in biochemical experiments. Various biophysical experiments can also suffer from protein degradation. For example, in most ligand-observed NMR experiments, the slowing-down of molecular motions of the ligand are used as an indication of binding. Unspecific binding of ligands to protein aggregates will therefore lead to a strong response, which will be interpreted as binding – a false-positive result. Therefore, protein integrity is a pre-requisite for validating an interaction. This field can be positively checked if the presence of the protein at the desired concentration and its integrity (with respect to unfolding, aggregation or degradation) can be demonstrated with experimental data.

At this point one can turn attention to binding experiments. Usually, these are divided into ligand-observed and protein-observed experiments – which is reflected in the bottom left and right fields of the validation cross, respectively. Protein-observed experiments, as the name says, will reveal binding effects on the protein. Finally, a ligand-observed experiment is needed in order to detect effects on the ligand. Such an experiment is necessary because the binding effects detected in the protein-observed experiment may for example arise from an interaction with a contaminant in the solution (e.g., a metal ion) and not with the intended organic ligand itself.

In summary, rigorous validation of a ligand requires addressing each aspect of the validation cross. This will exclude possible artifacts.

The different methods described in the following sections will have varying information content, which can be described by the

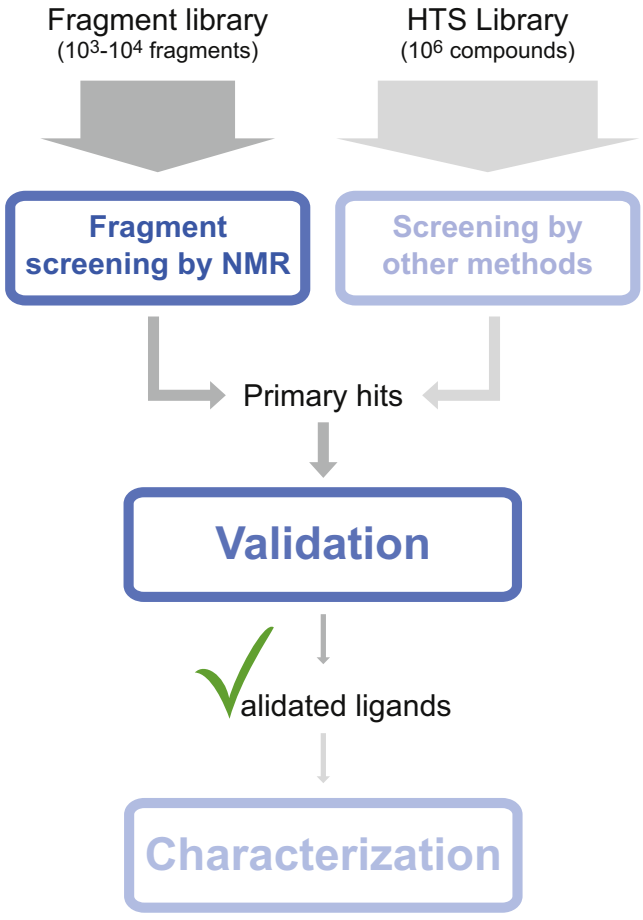

Fig. 1. Workflow in early drug discovery by NMR. Typically, a drug discovery campaign is started by screening a library of compounds for binding or modulation of activity (screening). This can be a fragment-based screening (FBS) by NMR or high-throughput screening (HTS) using alternative methods, like biochemical assays or computational methods. Initial screens yield "primary hits" that need to be validated in order to exclude artifacts (validation). The resulting validated ligands provide the basis for further optimization. Obtaining a validated ligand is the central theme of this review. Therefore, NMR screening and validation procedures are treated in depth (indicated by dark colors), but further characterization of ligand binding modes or determination of affinity and mode of action are not discussed (faint colors).

quadrants of the validation cross. Protein-observed experiments for example allow obtaining direct information about binding effects on the protein as well as direct information on its integrity. A protein-observed experiment can be represented as an operator which will determine the color of the two fields on the right hand side of the validation cross (Fig. 3). Each experiment can be represented by such an operator. This helps in identifying the most suitable experiment at each stage of a validation workflow, which should fill the blind fields. This approach will be illustrated in part III, after having dealt in detail with the information content of NMR experiments in sections 3.1 and 3.2.

Structure of this review

This review is divided into three parts. In part I, the physical principles of ligand binding and the NMR effects that arise from them are introduced. In part II, NMR experiments used in drug discovery are described. In part III, the information content and usage of these experiments is discussed, as well as how to validate or de-validate a protein-ligand interaction.

To structure the individual parts, the scheme of the validation cross will be used recurrently (Fig. 3).

In part II, experiments are grouped according to the field of the validation cross they primarily address. The most popular approaches will be discussed in detail, and pulse sequences are provided through the Bruker pulse program library [11]. The focus is mainly on practical aspects, the limitations of individual experiments as well as the necessary controls.

The validation cross is not only used to provide a structure to part II of this review. Its main value lies in helping to take the right decision on which experiments are needed in a given validation workflow. The information content of NMR experiments can be represented in shorthand notation using the validation cross, therefore allowing one to quickly identify the experiments that are most suitable to providing a missing piece of information. In part III, validation of interactions will be discussed including the information content (Section 3.1) and the range of application of experiments (Section 3.3). To illustrate applications to validation, several possible workflows and the correct interpretation of experimental outcomes will be discussed in section 3.5.

(For the sake of simplicity, instead of using the general term "biological macromolecule" for the target or host molecule, in the further text we will simply speak of "proteins" and "protein-ligand interactions". However, in most cases, the word protein can be replaced by DNA, RNA or other macromolecules of interest and the statements will still be valid.)

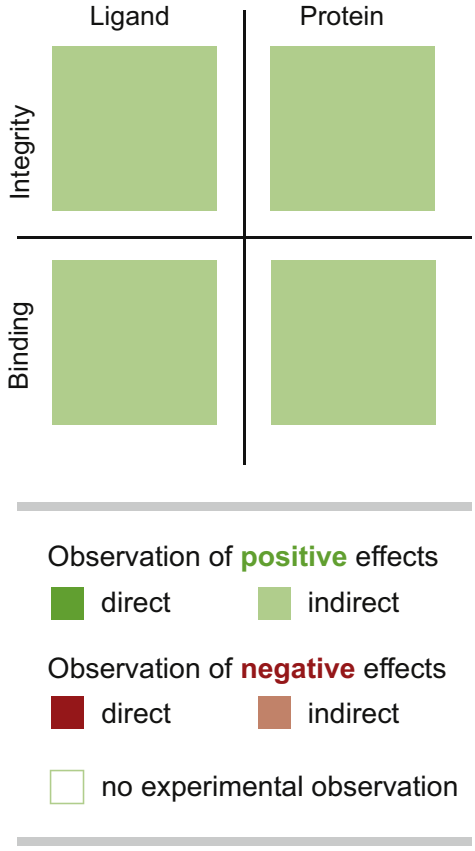

Fig. 2. The validation cross. This scheme describes four fields that must be addressed in order to validate an interaction between two binding partners, here between a protein and a low molecular weight (LMW) ligand. An interaction is said to be validated if the following features have directly been observed in experiments: binding effects on the ligand, binding effects on the protein, integrity of the ligand and integrity of the protein. As there is no single experiment that can address all of these fields simultaneously, several NMR experiments need to be carried out. The fields of the validation cross can be filled with green or red colors for positive or negative experimental effects, respectively. This can be refined by using dark or faint colors for direct or indirect observation of experimental effects, respectively. For example, if a ligand induces chemical shift changes in a protein-observed HSQC experiment, this will be represented by a green square in the protein-binding field. Because the effects are observed directly on the protein, the color will be dark. Since in the same spectrum the protein integrity is directly observed, the protein integrity field is filled with dark green. Another example: if a ligand displaces a reporter ligand, this is classified as a positive effect. Since the ligand was not observed directly in the experiment, but only the reporter signal, this is only represented by a faint color. This color code provides a shorthand notation that is valuable to capture the state of validation of a given protein-ligand interaction, as will be discussed in depth in Sections 3.4–3.6.

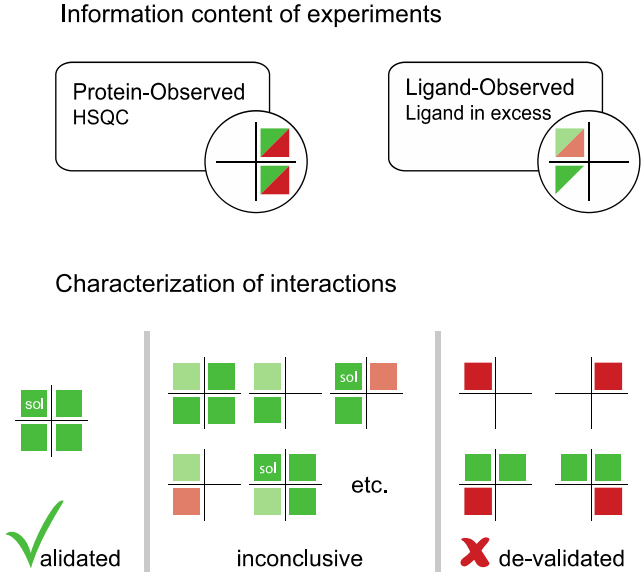

Fig. 3. Different usages of the validation cross and structure of this review. The validation cross is used in several ways in this review. **Information content of NMR experiments** (Section 3.1). NMR experiments can yield data on different fields of the validation cross, for example whether there are binding effects or not. The upper panel represents experiments and their information content. This is discussed in more detail in Sections 3.1–3.3. **Validation state of interactions** (Sections 3.4–3.6). In the lower panel, some examples of different outcomes of protein-ligand interactions are shown. The two well-defined situations are those of fully validated (all four fields are dark green) and clearly de-validated ligands (the four patterns shown in the figure). However, most ligands will fall into the "inconclusive" category. The shades of green or red represent the level of confidence. In a stringent analysis however, these ligands cannot be selected as truly validated ligands or disregarded as clearly de-validated ligands.

1. Part I: Setting the scene – physical effects and associated NMR parameters in protein-ligand interactions

Interactions between ligands and biological macromolecules are governed by several physical effects (Fig. 4). First, the physical consequences of interactions will be discussed, and in the next section the NMR parameters that are affected will be analyzed.

1.1. Physical effects of protein-ligand interactions relevant for NMR

1.1.1. Thermodynamics of ligand binding

The strength of a protein-ligand interaction is usually characterized by the dissociation constant K_D [13]. The K_D reflects the thermodynamic equilibrium of bound and free (= dissociated) states (Eq. (1a) in Table 1). In practice, for biological systems the lowest K_D values (i.e. those for the strongest binding interactions) are in the order of 10^{-15} M, as determined for example for the interaction of the ligand biotin with the protein avidin [2,14]. Typical drugs have K_D values in the range of 10^{-10} to 10^{-8} M, in other words their K_D values are in the sub-nanomolar or low nanomolar range. Initial hits from high-throughput screening often have K_D values in the range of 10^{-8} to 10^{-5} M, whereas hits from fragment-based screening (using organic compounds with MW < 250 Da) may have K_D values between $10^{-5}$and 10^{-3} M, that is, in the micromolar to millimolar range. The K_D depends on the Gibbs free energy difference between the free state and the bound state of the involved molecules – including solvent molecules (Eq. (1b)). The binding strength depends on both enthalpic and entropic contributions that make up the Gibbs free energy. Enthalpic contributions include for example electrostatic interactions, hydrogen bonds and van der Waals interactions between the ligand and the protein. Entropic contributions stem for example from constrained diffusion of the ligand upon binding, de-solvation of the ligand and the protein binding pocket and the concomitant release of bound water molecules, as well as from altered internal dynamics of both ligand and protein.

Ligand properties

bound		free
protein	chemical environment	solvent
ω_{bound}	chemical shift	ω_{free}
slow	rotational tumbling	fast
fast	transverse relaxation	slow
strong positive	NOE cross-peaks	weak negative
slow	translational diffusion	fast

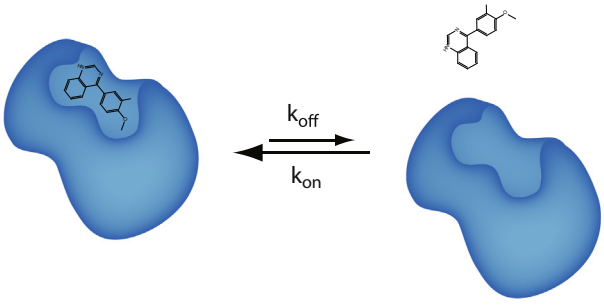

Protein properties

bound		free
ligand	chemical environment	solvent/protein
ω_{bound}	chemical shift	ω_{free}

Fig. 4. Scheme of a prototypical protein-ligand interaction and properties of bound and free states. A protein (blue) and a ligand (chemical structure) associate with their kinetic on-rate constant k_{on}. For a true ligand the dissociation rate (or off-rate) k_{off} is much smaller than the on-rate k_{on}, leading to a significant population of bound complex. Qualitative changes of the ligand between bound and free states are listed in the table, where selected physical effects are shown in blue and NMR parameters in black lettering. (In this review we use the convention given by Levitt [12] that the sign of NOE cross-peaks is defined relative to positive diagonal signals.) A similar table is shown at the bottom for protein properties, where significant changes are detectable in the chemical environment, while overall protein motions are usually barely affected by binding to a small ligand.

1.1.2. Kinetics of ligand binding

In a simple two-state binding model, binding kinetics are described by the on-rate, k_{on}, for complex formation, and the off-rate, k_{off}, for its dissociation. Complex formation is a bi-molecular process, therefore its rate depends on the concentration of the free binding partner (e.g., $k_{on} \times [P]$ for the ligand). The on-rate depends on the number of collisions of the ligand with the protein, of which only a fraction happen in a sterically favorable orientation that can lead to a bound state, i.e., the ligand must hit the binding pocket. The upper limit of the on-rate is the diffusion limit, which is in the order of 10^8 M^{-1} s^{-1}. The on-rate can be further modulated if a conformational change of the protein or the ligand is required for productive binding. The on-rate can therefore be lowered from the diffusion limit down to values of 10^3 M^{-1} s^{-1}, as measured for several marketed drugs [15]. The on-rate is described by the Arrhenius equation, where the pre-exponential factor describes the frequency of collisions in the correct orientation, while the activation energy describes the barrier to be overcome for possible conformational changes, leading to a lowered fraction of binding-competent states (Eq. (2a)). Alternatively, the same process can be described in terms of free energy of activation, which summarizes enthalpic terms describing the activation enthalpy and entropic terms describing probabilities of productive encounters (Eq. (2b)).

The off-rate, k_{off}, reflects the residence time ($\tau_r = 1/k_{off}$) of the ligand on the protein, or the lifetime of the complex [16]. At equilibrium, complex association and dissociation are equally frequent, leading to a stable population of the complex in solution. The equilibrium position depends on K_D, which can be described by $K_D = k_{off}/k_{on}$ (Eq. (1a)). Therefore, the stronger the interaction, the longer the residence time, provided the on-rate is constant (Eq. (3)).

1.1.3. Chemical environment and interactions

When going from a free to a bound state, several physical properties of proteins and ligands change. In the first place, the molecular environment of the ligand and the protein binding site change. For example the ligand will shed its surface water molecules to end up in a possibly hydrophobic cavity in the protein, experiencing different interactions, and probably adopting a different predominant conformation. All of this will induce changes in the shape and local density of the electron clouds of the molecules. For NMR this is relevant because the electrons shield the nuclei from the external magnetic field via diamagnetic and paramagnetic induced currents (Eq. (4)), leading to the observed values of the chemical shift.

1.1.4. Brownian motion: rotational and translational diffusion

The two physico-chemical quantities that will change most dramatically for a small ligand upon binding are translational and rotational diffusion [17,18]. In its free state in solution, the ligand will exhibit fast random rotational motions induced by Brownian

Table 1
Formulas for physical effects and corresponding NMR parameters. On the left column, formulas describing physical effects relevant for ligand binding are listed (Section 1.1). On the right column, formulas for the associated NMR parameters are shown (Section 1.2).

Physical effect	Associated NMR-accessible parameter
Affinity	**Fraction of bound ligand and protein**
$K_D = \frac{[P][L]}{[PL]} = \frac{k_{off}}{k_{on}}$ (1a)	$p_B^L = \frac{[PL]}{[L]_{tot}} = 1 - p_F^L, \quad p_B^P = \frac{[PL]}{[P]_{tot}} = 1 - p_F^P$ (7a, b)
$= e^{-\left(\frac{\Delta H - T\Delta S}{N_A k_B T}\right)}$ (1b)	$[PL] = \frac{[L]_{tot} + [P]_{tot} + K_D - \sqrt{([L]_{tot} + [P]_{tot} + K_D)^2 - 4[L]_{tot}[P]_{tot}}}{2}$ (7c)
Kinetics of binding	**Exchange phenomena**
$k_{on} = Z\rho\, e^{\frac{-Ea}{N_A k_B T}}$ (2a)	Exchange rate $k_{ex}^L = k_{off} + k_{on}[P], \qquad k_{ex}^P = k_{off} + k_{on}[L]$ (8a, b)
$= e^{-\frac{\Delta \ddagger G}{N_A k_B T}}$ (2b)	Fast exchange approximation $(\lvert\omega_F - \omega_B\rvert \ll k_{ex}, \lvert R_F - R_B\rvert \ll k_{ex})$
$k_{off} = \frac{1}{\tau_R} = K_D k_{on}$ (3)	$R_{2,fast} = p_F R_{2,F} + p_B R_{2,B} + \frac{(\omega_F - \omega_B)^2 p_F p_B}{k_{ex}}; \quad \omega_{fast} = p_F\omega_F + p_B\omega_B$ (9a; b)
	Slow exchange approximation $(\lvert\omega_F - \omega_B\rvert \gg k_{ex}, \lvert R_F - R_B\rvert \gg k_{ex})$
	$R_{2,F,slow}^L = R_{2,F} + k_{on}[P] = R_{2,F} + p_B k_{ex}; \quad \omega_{F,slow} = \omega_F$ (10a; b) $R_{2,B,slow} = R_{2,B} + k_{off} = R_{2,B} + p_F k_{ex}; \quad \omega_{B,slow} = \omega_B$ (10c; d)
	Approximation for ligand excess for all time scales $(p_F^L \gg p_B^L)$
	$R_{2,p_F \gg p_B} = p_F R_{2,F} + p_F p_B k_{ex}\left(\frac{R_{2B}(R_{2B} + p_F k_{ex}) + (\omega_F - \omega_B)^2}{(R_{2B} + p_F k_{ex})^2 + (\omega_F - \omega_B)^2}\right)$ (11)
Molecular structure and environment	**Chemical shift and scalar couplings**
$\sigma_{iso} = \sigma_{dia} + \sigma_{para} + \sigma_{rc} \ldots$ (4)	$\omega = -\gamma B_0(1 - \sigma_{iso})$ (12)
Rotational diffusion	**Relaxation**
	Transverse relaxation through dipole-dipole interactions
	$R_{2,DD} = \frac{1}{20}\frac{\hbar^2\mu_0^2\gamma^4}{r^6}\left(5\tau_c + \frac{9\tau_c}{1+\omega_0^2\tau_c^2} + \frac{6\tau_c}{1+4\omega_0^2\tau_c^2}\right)$ (13)
	Transverse relaxation through chemical shift anisotropy
	$R_{2,CSA} = \frac{1}{24}\left(\sigma_{\parallel-\perp}^2 B_0^2\gamma^2\right)\left(4\tau_c + \frac{3\tau_c}{1+\omega_0^2\tau_c^2}\right)$ (14)
$\tau_c = \frac{4\pi\eta r_H^3}{3k_b T}$ (5)	Nuclear Overhauser effect (NOE)
	$R_C^L = \frac{1}{10}\frac{\hbar^2\mu_0^2\gamma^4}{r^6}\left(\tau_c - \frac{6\tau_c}{1+4\omega_0^2\tau_c^2}\right)$ (15)
	Transverse nuclear Overhauser effect (ROE)
	$R_C^T = -\frac{1}{10}\frac{\hbar^2\mu_0^2\gamma^4}{r^6}\left(2\tau_c + \frac{3\tau_c}{1+\omega_0^2\tau_c^2}\right)$ (16)
	Longitudinal relaxation
	$R_{1,DD} = \frac{1}{10}\frac{\hbar^2\mu_0^2\gamma^4}{r^6}\left(\frac{3\tau_c}{1+\omega_0^2\tau_c^2} + \frac{12\tau_c}{1+4\omega_0^2\tau_c^2}\right)$ (17)
	Paramagnetic relaxation
	$R_{2,para} = \frac{1}{20}\frac{\hbar^2\mu_0^2\gamma_n^2\gamma_e^2}{r^6}\left(4\tau_c + \frac{3\tau_c}{1+\omega_0^2\tau_c^2}\right)$ (18)
Translational diffusion	**Diffusion in gradient echoes**
$D = \frac{k_B T}{6\pi\eta r_H}$ (6)	$R_{Diff}^* = -D\gamma^2 g^2\delta^2$ (19)

Expression (7c) is obtained from Eq. (1a), by substituting $[P]$ with $[P_{tot}] - [PL]$ and $[L]$ with $[L_{tot}] - [PL]$, and then solving the resulting quadratic equation in the standard way.
Expressions (13)–(18) for relaxation rates are obtained from the Solomon equations for the homonuclear case ($\gamma_I = \gamma_S$). The classical spectral density function for rigid spherical particles $J(\omega) = \tau_c/(1 + \omega^2\tau_c^2)$ is used, which for the homonuclear case ($\omega_I = \omega_S$) takes the following values: $J(\omega_I - \omega_S) = J(0)$, $J(\omega_I) = J(\omega_S)$ and $J(\omega_I + \omega_S) = J(2\omega)$. For the NOE and ROE, the sign convention for cross-relaxation rate constants R_C is that used by Levitt [12], i.e. the ROE gives negative cross-peaks relative to diagonal peaks in a ROESY spectrum, whereas the NOE gives negative cross-peaks for small molecules and positive cross-peaks for large molecules. The term $(4\pi)^2$ was omitted in the denominator of dipolar terms.
For diffusion in gradient echoes an artificial relaxation rate R^*_{Diff} (19) is formulated, in order to be easily comparable to relaxation effects. Analogous to other relaxation rates, the signal intensity then depends on $\exp(-R_{Diff}{}^*t)$, where t is the time between gradients corrected for gradient duration.
K_D: dissociation constant (M).
$[P]$,$[L]$: concentration of free protein and ligand, respectively (M).
$[PL]$: concentration of protein – ligand complex (M).
$[P]_{tot}$,$[L]_{tot}$: total concentration of protein and ligand, respectively (M).
p_b^P, p_b^L: fraction of bound protein and ligand, respectively.
k_{on}: on-rate ($M^{-1}\,s^{-1}$).
k_{off}: off-rate (s^{-1}).
ΔH: change in enthalpy ($J\,mol^{-1}$).
ΔS: change in entropy ($J\,mol^{-1}$).
N_A: Avogadro constant ($6.023\times10^{23}\,mol^{-1}$).
k_B: Boltzmann constant ($1.38\times10^{-23}\,J\,K^{-1}$).
T: Temperature (K).
Z: collision frequency ($M^{-1}\,s^{-1}$).
ρ: steric factor.
E_a: activation energy ($J\,mol^{-1}$).
$\Delta\ddagger G$: Gibb's free energy change of the transition state ($J\,mol^{-1}$).
τ_R: residence time (s).
k_{ex}: exchange rate (s^{-1}).
$R_{2,F}$, $R_{2,B}$: transverse relaxation rate of free and bound states, respectively (s^{-1}).
ω_F, ω_B: chemical shift of free and bound state, respectively (s^{-1}).
τ_c: rotational correlation time (s).
η: viscosity of solvent ($kg\,m^{-1}\,s^{-1}$).
r_H: hydrodynamic radius of the molecule (m).
r: distance between two nuclei (m).
μ_0: vacuum permeability ($4\pi \times 10^{-7}\,H\,m^{-1}$).
$\hbar$: Planck constant divided by 2π ($1.055 \times 10^{-34}\,J\,s$).
γ: gyromagnetic ratio of nucleus ($T^{-1}\,s^{-1}$).
γ_e: gyromagnetic ratio of electron ($1.76 \times 10^{11}\,T^{-1}\,s^{-1}$).
B_0: magnetic field (T).
σ_{iso}: isotropic chemical shielding.
σ_{dia}, σ_{para}: electron diamagnetic and paramagnetic chemical shielding.
σ_{rc}: chemical shielding from electronic ring-currents.
$\sigma_{\parallel-\perp}$: chemical shift anisotropy = $\sigma_\parallel - \sigma_\perp$.
ω_0: nutation frequency of nucleus (s^{-1}).
D: diffusion coefficient ($m^2\,s^{-1}$).
δ: gradient duration (s).
g: strength of magnetic field gradient ($T\,m^{-1}$).

collisions. These motions are usually described by the rotational correlation time, τ_c, which represents the average lifetime of a given orientation [19]. For a small ligand of 300 Da in aqueous solution, τ_c will be on the order of 0.2 ns. When bound to a 30 kDa protein, it will rotate at the slow pace of the protein with a typical τ_c of roughly 20 ns. Assuming approximately spherical molecules, τ_c is proportional to the third power of the hydrodynamic radius (r_H) of a molecule (Eq. (5)), which in turn is proportional to its molecular weight ($MW \propto r_H^3$).

The translational diffusion of a small molecule will also change upon binding to a protein. However, as evident from the equation for the diffusion coefficient D (see Eq. (6)), diffusion is inversely proportional to the hydrodynamic radius. It is therefore not a strong function of the molecular weight ($r_H \propto MW^{1/3}$). Consequently, the translational diffusion coefficients of a 300 Da ligand and a 30 kDa protein are roughly $D = 5 \times 10^{-6}$ and $9 \times 10^{-7}\,m^{-2}\,s^{-1}$, respectively, a difference of mere factor of 6. Translational diffusion is therefore not a very suitable parameter to identify binding of a ligand to a protein.

1.2. NMR observable parameters associated with basic physical effects

In the following, we shall describe how these physical effects influence parameters that are accessible by NMR.

1.2.1. The "bound fraction" is a consequence of K_D

The equilibrium between bound and free species, characterized by K_D as discussed above, determines the fraction of bound protein and ligand in a given solution. The "bound fraction" (p_B in Eq. (7)) or "occupancy" determines the magnitude of NMR effects in experiments suited for drug discovery that will be discussed in later sections. The bound fraction can be modulated by changing the concentrations of protein and ligand (Eq. (1a)). In typical NMR screening setups, the ligand is present in 10–20-fold excess with respect to the protein, so that the bound fraction of the ligand will always be rather small (<5–10%). Consequently, the NMR effects indicative of binding must be very pronounced in order to result in a significant change of the ligand signal. Compared to other methods, NMR can detect and quantify exceptionally small fractions of bound ligand (down to a few percent), which is why it is the method of choice for the detection of very weak interactions. Additionally, the concentration of ligand $[L]$ and protein $[P]$ can be adjusted in order to maximize the bound fraction, making it possible to measure even weakest affinities (see Section 3.1.1 for detection limits of NMR experiments).

The bound fraction can be derived from NMR experiments in a quantitative way so that K_D can be determined [20,21]. In a typical setting, one of the binding partners, usually the ligand, is titrated into a solution containing the other binding partner. The observed NMR parameter, as a function of the total ligand and protein con-

centrations in the solution, can be fitted to Eq. (7c) in order to determine the K_D of the interaction – provided it fits a simple two-state model. The analysis can be further refined by determining the K_D at different temperatures and assessing the relative contributions of ΔH (temperature-independent) and $T\Delta S$ (temperature dependent) to an interaction (Eq. (1b)). However, in this review we shall focus on a qualitative validation of interactions, which precede further quantitative analysis like the determination of K_D.

1.2.2. Exchange phenomena are a consequence of binding kinetics

After discussing thermodynamics we shall now turn to kinetic effects that leave their marks in NMR spectra. Protein-ligand binding kinetics are governed by on- and off-rates of complex formation and dissociation. This is reflected in NMR by the exchange rate (k_{ex}) between bound and free states (Eq. (8)). The exchange rate will modulate NMR parameters like chemical shifts and relaxation rates and lead to different apparent values. Mathematical descriptions of the resulting values sometimes require complicated expressions. Therefore the problem is usually simplified by treating three limiting cases for time scales of exchange: slow, intermediate and fast. These depend on the frequency difference between the bound and free states compared to the exchange rate. In the fast exchange regime $|\omega_F - \omega_B| \ll k_{ex}$ and $|R_{2F} - R_{2B}| \ll k_{ex}$ must be fulfilled. Under these fast exchange conditions NMR signals will appear at population-weighted averaged chemical shifts and relaxation rates can be described by relatively simple averaged expressions (Eq. (9)). In the limit of slow exchange $|\omega_F - \omega_B| \gg k_{ex}$ and $|R_{2F} - R_{2B}| \gg k_{ex}$, individual signals of bound and free species will appear at their respective chemical shifts, the signal volumes will be nearly proportional to their respective populations, and the apparent relaxation rates for each signal will be modulated by the lifetimes of the respective free and bound states (Fig. 10 and Eq. (10)). In this situation, if the apparent R_2 of the ligand can be observed as a function of protein concentration, k_{on} is experimentally accessible (Eq. (10a)). If K_D is known, the concentration of the free protein can be calculated and R_2 of the free state can be measured separately [20].

As will later be discussed in Fig. 12, drug-like ligands typically exhibit kinetics that are very far within the slow exchange regime ($k_{off} < 10\ s^{-1}$). Conversely, at an early stage of a drug discovery effort, fragments (e.g. compounds with MW ⩽ 250 Da) often have

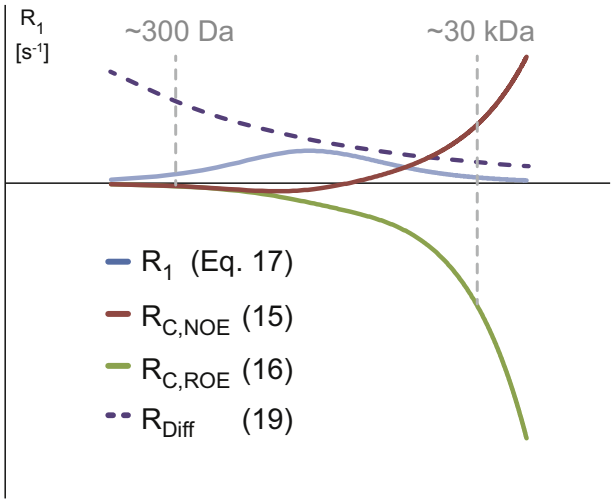

	R_1	R_{NOE}	R_{ROE}	$R_{2,DD}$	$R_{2,CSA}$	R_{Diff}
$\frac{R(\tau_c=0.2\ ns)}{R(\tau_c=20\ ns)}$	0.3	-21	41	26	58	0.2

Fig. 5. Dependence of relaxation rates on molecular size. Longitudinal and transverse relaxation rates are plotted in the upper and lower diagrams, respectively. For symbols and sign conventions see Table 1. Numbers in brackets refer to the equations in Table 1. The vertical grey dashed lines indicate examples of molecular sizes of a ligand (300 Da, $\tau_C \approx 0.2$ ns) and a target protein (30 kDa, $\tau_C \approx 20$ ns). The table at the bottom shows the ratio of relaxation rates for these two different molecular sizes. For diffusion a relaxation rate R_{Diff} is assumed for the sake of comparison. While relaxation rates due to dipolar couplings can be directly compared, CSA-induced R_2 and diffusion are plotted on a somewhat arbitrary scale, as they depend on the magnitude of the CSA, on the gradient strength and the duration of the gradient echo sequence. For ^{19}F, where CSA is most relevant, $R_{2,CSA}$ is approximately 6 times larger than $R_{2,DD}$ at 500 MHz. The curves were calculated using the equations and values in Table 1. Curves are qualitative, as the aim of this plot is to compare relative values for different particle sizes, and some rates are not directly comparable. As a rough guide for the order of magnitude $R_{C,NOE} \approx 10\ s^{-1}$ and $R_{2,DD}$ is about $30\ s^{-1}$ at $\tau_C = 20$ ns (dashed line on right-hand side).

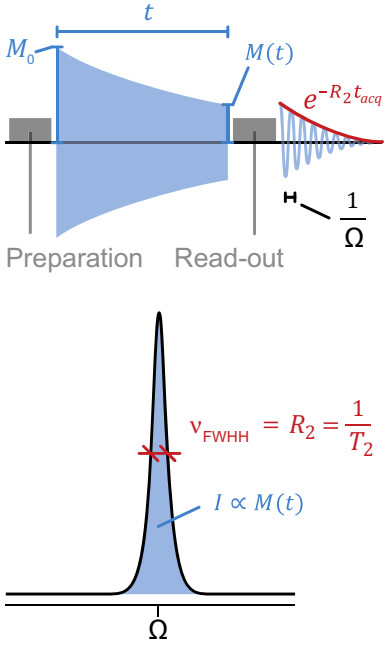

Fig. 6. Experimental parameters that lead to the final NMR signal. In the upper scheme an NMR experiment is sketched. Radio-frequency pulses (grey) are used to prepare a desired magnetization M_0, which relaxes during the relaxation time t (blue). The resulting magnetization $M(t)$ is read out using pulses (grey). The various mathematical expressions of $M(t)$ in different experiments are shown in Table 2. The recorded sinusoidal wave has a given frequency Ω (black), and is attenuated by the transverse relaxation rate R_2 (red, Eqs. (13) and (14)). In the lower panel, an NMR signal in the Fourier-transformed spectrum is depicted. Its intensity I (blue) is represented by the signal integral and depends on the magnetization after the relaxation delay. The decay rate R_2 translates into the width of the signal (FWHH: full width at half height) and the frequency of the signal determines the position of the signal on the frequency axis.

diffusion-limited k_{on} rates and K_D values in the range of $10 < K_D < 1000$ μM, putting them in the fast exchange regime, at least with respect to proton chemical shift differences and to transverse relaxation.

In between these two extreme cases of fast and slow exchange there is the intermediate exchange regime. It includes also mixed exchange regimes, for instance the relatively rare circumstance that exchange is slow/intermediate on the chemical shift timescale but simultaneously fast on the relaxation timescale. It can be described mathematically by large matrices that describe an admixture of kinetic and relaxation terms. Fortunately, in typical screening experiments where ligands are used in large excess ($p_F \gg p_B$), the simplified Swift-Connick equation (Eq. (11)) can be used to approximately describe the relaxation rate throughout all time scales, including intermediate exchange [22]. In Fig. 7 it is apparent that intermediate exchange sometimes exhibits gross line-broadening effects, which can be exploited in drug discovery. Situations of intermediate exchange are typically found when observing ^{19}F NMR for ligand binding experiments, since the very large differences in chemical shifts and relaxation rates between bound and free states are often not averaged out even when the exchange kinetics are rather fast, e.g. $k_{ex} > 10^4$ s^{-1} (Fig. 7).

1.2.3. The chemical shift is a manifestation of changes in the molecular environment

Upon a protein-ligand binding event, the chemical shifts of both binding partners are changed. The chemical shift of a nucleus depends on the local magnetic field that it experiences (Eq. (12)). The local static magnetic field is shielded by the electrons in the immediate environment (σ, Eq. (4)) in a manner that depends on the electron density and the shape of the molecular orbitals, leading to weak diamagnetic and stronger paramagnetic shielding terms. The exact chemical shift value is primarily governed by neighboring atoms. For hydrogen nuclei the chemical shift mainly depends on diamagnetic chemical shielding (σ_{dia}) arising from the electron density of the s-orbitals, leading to a chemical shift range of about 10 ppm for ^{1}H. For heavier nuclei (^{13}C, ^{15}N, ^{19}F, etc.), hybridization of orbitals lead to more important paramagnetic shielding terms (σ_{para}), which translate into a much wider distribution of chemical shifts, typically 200 ppm for ^{13}C and >400 ppm for ^{19}F.

Upon binding, the chemical shifts will change, even if the effect is only due to small changes in the polarization of the electron cloud or small conformational adjustments of the protein or the ligand. These effects usually confer binding-induced chemical shift changes smaller than 0.5 ppm for ^{1}H. However, stronger effects can arise due to the proximity of aromatic rings, which induce large shielding and de-shielding effects through magnetic fields stemming from ring-currents [23]. Also, if ^{1}H nuclei are directly involved in interactions such as hydrogen bonds or ionic bonds, chemical shift changes in the order of 1 ppm or more can occur. Changes in chemical shifts are therefore very reliable indicators of binding; however, in typical screening setups with a large ligand excess, effects on the ligand chemical shift will often not be detectable if the bound fractions are vanishingly small. Nevertheless, if a sufficiently high occupancy can be reached by choosing appropriate protein and ligand concentrations, chemical shift changes are a safe indicator of binding (Sections 2.2.4 and 2.4).

1.2.4. Relaxation rates depend on rotational diffusion

Relaxation effects in NMR depend on molecular motions characterized by the rotational correlation time, τ_c [19,24–27]. In the context of protein-ligand binding, the most pronounced changes in rotational diffusion happen for the ligand, which will typically be slowed down several-fold upon binding to a protein. As discussed above, τ_c is roughly proportional to the molecular weight (very approximately: $\tau_c \approx$ MW × 0.6 ns/kDa). τ_c cannot be measured directly, but it is the main parameter determining relaxation effects. The most useful relaxation effects for identifying ligand binding are therefore those with a strong dependence on τ_c (Fig. 5). These relaxation effects will lead to clear changes in the line width and intensity of the NMR signals (Fig. 6).

Relaxation depends on molecular tumbling in the following way: A nucleus in a molecule "feels" the magnetic field of the nearest neighboring magnetic nuclei. This effect is called the dipolar interaction or dipole-dipole coupling (DD). The shape of these local magnetic fields is identical to that of a familiar dipole magnet. Due to molecular tumbling, a nucleus will rotate through the field lines of the neighboring nuclei, and it will therefore experience a changing magnetic field. Another source for field fluctuations can arise from the electron cloud surrounding the nucleus. If the electrons are not fully symmetrically distributed around the nucleus, the shielding they exert will vary according to the molecular orientation relative to the static magnetic field. This leads to different chemical shifts depending on the molecular orientation, a phenomenon known as chemical shift anisotropy (CSA), and, again, molecular tumbling will lead to fluctuating magnetic fields. Depending on the frequency, these various magnetic field fluctuations can induce transitions between quantum mechanical spin states, which are responsible for relaxation effects. The prevalence of individual frequencies in the magnetic field fluctuations are described by the spectral density function $J(\omega)$. In the equations describing relaxation in Table 1 (Eqs. (13)–(18)), the last term and the pre-factor express the relevant values of the spectral density function. The other term describes either the DD or CSA effect.

Eqs. (13) and (14) describe the two predominant contributions to transverse R_2 relaxation, which lead to line broadening that is proportional to the relevant relaxation rate. For protons, dipole-dipole (DD) relaxation is the dominant line broadening mechanism. Chemical shift anisotropy (CSA) is only important at magnetic fields >800 MHz for protons with asymmetric electronic environments like amide protons. However, for ^{19}F this is the dominating transverse relaxation mechanism even at lower fields, because the ^{19}F nucleus is exposed to a very anisotropic electronic environment due to the high electronegativity of fluorine. CSA-dominated R_2 relaxation will lead to line widths that differ by a factor of about 60 between a small molecule (300 Da, τ_c = 0.2 ns) and a typical protein target (30 kDa with τ_c = 20 ns); DD dependent R_2-relaxation leads to a factor of about 30 (Eqs. (13) and (14) and Fig. 5). The magnitude of these two effects will allow detection of ligand binding through line broadening even if only very small fractions of ligand are bound. In fast exchange (Eq. (9)) a bound fraction of only 3% will lead to doubling of the line width or halving of the signal intensity for ligand protons in a $T_1\rho$ experiment that is typically used to observe these effects (Section 2.2.2). For ^{19}F with CSA-dominated line-broadening, the same effect can already be reached with a bound fraction of 1.5%, ignoring any further line broadening through exchange. R_2-based methods are therefore highly sensitive techniques.

Longitudinal relaxation mechanisms also display a strong dependence on τ_c (Eqs. (15)–(17)). However, simple longitudinal R_1 relaxation only has a small window of utility for drug discovery, because larger proteins may show similar R_1-values as small molecules (Eq. (17) and Fig. 5). This parameter is therefore hardly exploited in ligand binding experiments. Selective R_1 relaxation, where only one nucleus in a molecule is treated, shows a strong dependence on τ_c (Selective R_1 is not shown in Fig. 5, it corresponds to R_{auto} in Levitt's notation, which can be described by $R_1 + R_C$, which are both shown in Fig. 5). However, as will be discussed in Section 2.2.3, selective R_1 is not so easily accessible experimentally, as measurements tend to be long and selective

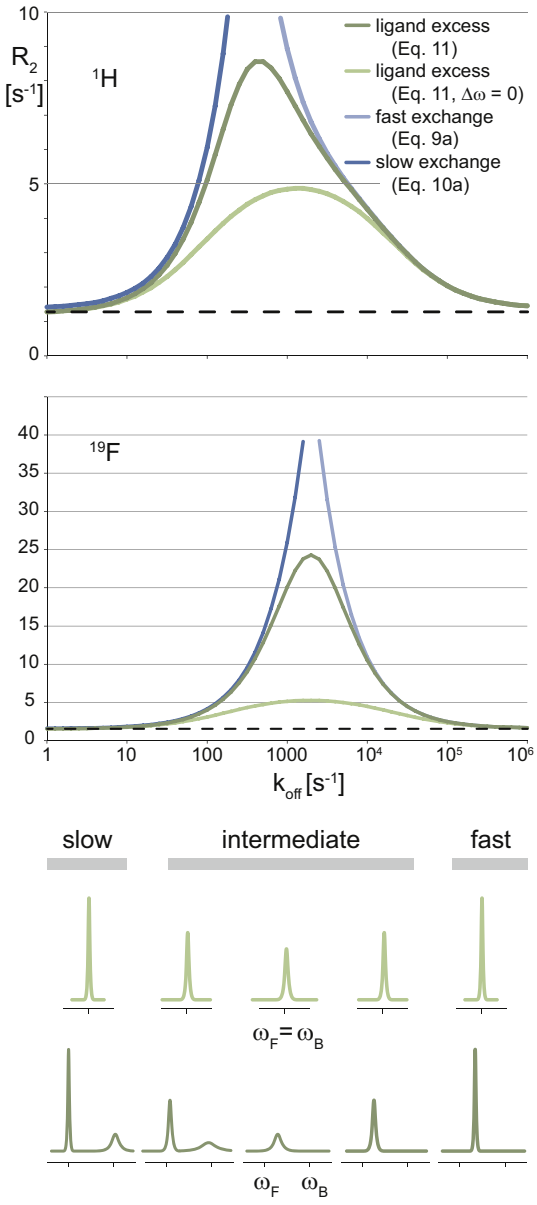

Fig. 7. Apparent relaxation due to exchange effects. The relaxation rates of a ligand are shown for different exchange regimes. The individual traces represent the slow (Eq. (10a)) and fast exchange (Eq. (9)) approximations as well as the Swift-Connick approximation (Eq. (11)) for an excess of ligand and for large or vanishing chemical shift differences (the color code is given in the figure). Typical situations for ^{1}H and ^{19}F are shown in the upper and lower diagrams. Note the different scales of the two diagrams, the effects are much stronger for ^{19}F. Protein and ligand concentrations were 5 and 200 μM and $k_{on} = 10^{8}$ s^{-1} was kept constant at the hypothetical diffusion limit. For ^{1}H, Δω of 300 Hz was used and R_2 rates for free and bound ligand were set to $R_2 = 1.2$ s^{-1} and 30 s^{-1}, respectively. For ^{19}F a linewidth $\Delta\omega/(2\pi) = 2000$ Hz was used and R_2 rates for free and bound ligands were set to $R_2 = 1.3$ s^{-1} and 80 s^{-1}, respectively. Note that the relaxation rates are identical for very strong and very weak binders, i.e., for $k_{off} < 10$ s^{-1} and $k_{off} > 10^{5}$ s^{-1}. As a consequence, binders with slow k_{off} cannot be detected (Fig. 12). The bottom picture illustrates different exchanging signals with chemical shift changes due to binding. The relative populations and relaxation rates are not drawn to scale since the intensities of the signals in the bound state are exaggerated.

excitation of individual resonances is not easily achieved in high-throughput settings.

In contrast, cross-relaxation effects, ROE and NOE, are very sensitive to changes in τ_c, similar to the R_2-based experiments discussed above. In the example of a 300 Da ligand and a 30 kDa globular protein, the cross relaxation rate constant R_C for the ROE will be 40-fold larger and R_C for the NOE will have a 20-fold magnitude (Fig. 5). Additionally, the sign of the NOE changes: small molecules will yield negative NOE cross peaks (relative to the Boltzmann equilibrium magnetization) and large molecules will yield positive NOE cross peaks. (Note that in this text we use conventions for the signs of NOE and ROE cross-relaxation rate constants R_C used by Levitt [12]: R_C (ROE) is negative, as it yields cross-peak signals with signs that are inverted relative to the diagonal signals). The molecular size at which the transition from negative to positive NOE occurs depends on the external magnetic field, but usually is in the order of 1 kDa (Eq. (15)). In terms of measuring NOE and ROE signals, it is important to note that cross relaxation competes with R_1 and R_2, respectively, which are active at the same time (Eq. (21) in Section 1.3 and Table 2). Especially for the ROE, this may result in complete cancellation, as R_2 is of similar magnitude as R_C(ROE), that is, the ROE signal is relaxing away nearly as fast as it is building up. The NOE can be exploited much better, because – especially for large molecules and complexes – the competition of R_1 with of R_C(NOE) is less effective. Additionally, the change of sign of the NOE of a ligand upon binding provides excellent contrast. Therefore the NOE is a highly suited parameter for detection of ligand binding. Popular experiments like STD (saturation transfer difference) and water-LOGSY (water ligand observed via gradient spectroscopy) are based on NOE (Section 2.2.3).

As noted earlier, translational diffusion is not a very sensitive parameter for detection of interactions between proteins and ligands. The diffusion coefficient, D, is directly accessible by NMR experiments using pulsed field gradient echoes of varying length as in diffusion ordered spectroscopy (DOSY, Eq. (19)). But even if the parameter can be directly measured, the difference between bound and free ligands in the example above is only 6-fold [17]. In light of the magnitude of the other effects discussed, which are 5–10-times larger, it is evident that diffusion-based experiments are inferior. They are very rarely used for the purpose of screening protein-ligand interactions. However, the unique feature of DOSY experiments is that attenuation of the ligand signals is uniform across the molecule and the effect is directly proportional to the fraction of bound ligand and therefore to the binding strength (Section 2.2.5). As discussed later, all other binding effects observed by NMR have a very complex dependence on some or all of the following parameters: proton-proton distances, CSA, the chemical environment and exchange rates. In contrast, diffusion effects are the only ones that correlate directly with the strength of the interaction (K_D).

In summary, the most useful relaxation effects for drug discovery experiments are R_2 and the NOE.

1.3. How ligand binding effects influence the NMR signal

The read-out of NMR experiments is based on analyzing the Fourier-transformed NMR signals in terms of their positions, intensities and line-widths. That is why it is worth taking a closer look at these parameters. A Fourier-transformed NMR signal is characterized by its position in the spectrum on the chemical shift axis (Ω), its line width (FWHH) and its intensity (I) (Fig. 6) [12,25]. The phase of the signal is not relevant for this discussion and is assumed to be in absorption.

The chemical shift is directly observable as the position of the signal on the spectral axis. It depends on the precession frequency of the nucleus, which is influenced by the chemical shielding by the electron cloud as discussed in Section 1.2.3.

The width and intensity of the signal depend on relaxation rates. The full width at half height of the signal (FWHH) in Hz is equal to the transverse relaxation rate constant R_2 in s^{-1} ($\nu_{FWHH} = R_2$; or R_2/π if units of rad s^{-1} are used). For a ligand in excess with respect to a protein, R_2 is described by Eq. (11), or by Eqs. (9) and

(10) for the two limiting cases of fast and slow exchange, respectively (see also Fig. 7). This of course only applies in the absence of line broadening caused by inhomogeneities of the static magnetic field or introduced by window functions during processing.

The intensity of the signal depends on relaxation during the pulse sequence. In drug discovery experiments, relaxation delays of duration t are used to emphasize differential relaxation effects. During these relaxation delays, the signal relaxes according to the relaxation rate constants R described in Table 1. The time evolution of the signal during such a delay is described by integrated rate equations, which result in exponential terms of the form e^{-Rt}. Therefore, the intensity of the signal depends on an exponential function of the relaxation rate R and the length of the delay t.

Since the intensity of the signal is the most important observable in popular drug discovery experiments, we will discuss the calculation of the magnetization $M(t)$ in more detail. Since most scientists applying NMR in drug discovery are chemists and biochemists, we chose to express the rate equations using terms like R_1, R_2 and R_{cross}, which are more familiar to practitioners and experimentally more easily accessible than e.g., auto-relaxation. Additionally, as mentioned earlier, we follow the sign conventions of Levitt [12], where R_{cross} for the ROE is negative, for the two reasons he explains in his book: The signs of the rate constants then correspond to the usage in reaction kinetics and they also correspond to the signs of NOE and ROE cross peaks observed in spectra, which is more intuitive to practitioners.

The influence of relaxation on the time evolution of $M(t)$ can be described by the Solomon equations [28]. Eqs. (20a) and (20b) show the Solomon equations for a spin I and a spin S in a two-spin system (re-expressed following the conventions of Levitt [25], where R_{auto} corresponds to ρ and R_{cross} to $-\sigma$ in the original treatment). For a two-spin system the relevant relaxation rate constants are auto-relaxation R_{auto}, which brings the magnetization back to its equilibrium value, and cross-relaxation R_{cross} (abbreviated as R_C), which describes magnetization exchange between the two spins.

$$\frac{dI(t)}{dt} = -R_{auto}(I(t) - I^{eq}) + R_{C,SI}(S(t) - S^{eq}) \tag{20a}$$

$$\frac{dS(t)}{dt} = -R_{auto}(S(t) - S^{eq}) + R_{C,IS}(I(t) - I^{eq}) \tag{20b}$$

For protein-ligand interactions it is convenient to set up a slightly modified version of the classical Solomon equations according to Kalk and Berendsen [7,29] (Eq. (21)). Eq. (20a) can be rearranged (adding $R_C(I(t) - I^{eq})$; assuming $R_C = R_{C,SI} = R_{C,IS}$; using $R_1 = R_{auto} - R_C$, subtracting $R_C(I(t) - I^{eq})$ again and assuming $I^{eq} = S^{eq}$) and substituting I and S for ligand magnetization M_L and protein magnetization M_P yields Eq. (21). This allows one to use longitudinal R_1 and cross relaxation rate constants, which are more familiar to the practical spectroscopist than the auto-relaxation term R_{auto} ($= R_1 + R_C$) that is used in most theoretical treatments. See Table 1 for equations for the relaxation rate constants.

$$\frac{dM_L(t)}{dt} = -R_1(M_L(t) - M_L^{eq}) - R_C(M_L(t) - M_P(t)) \tag{21}$$

This form of the equation is preferred, because it is directly visible that longitudinal relaxation is driven by the difference from equilibrium magnetization and cross relaxation is driven by the difference of magnetization between two nuclei, here between ligand and protein. In more detail, the first term represents relaxation of the ligand magnetization towards its equilibrium value M^{eq} with a rate constant R_1. The second term represents cross relaxation with a rate constant R_C, which will only be active ($\neq 0$) if the magnetizations of the protein and ligand are not equal ($M_L \neq M_P$). From this equation it is therefore directly evident that they must be selectively prepared in different ways in order to observe an NOE. This second term contains the time-dependent magnetization of the protein $M_P(t)$, which is described by an analogous equation for $dM_p(t)/dt$, as was done in Eqs. (20a) and (20b). This system of equations can be solved in a matrix approach. Fortunately, in the classical protein-ligand experiments the time evolution of the protein magnetization is independent of the ligand magnetization and can just be inserted into the rate equation of the ligand. Therefore, the second equation for $dM_p(t)/dt$ is often irrelevant and the time evolution of the ligand magnetization can be easily calculated. (For transverse relaxation a similar equations can be setup, where in the first term the equilibrium value M^{eq} is 0, the relaxation rate constant is R_2, and the cross relaxation rate constant is R_C(ROE).)

However, there are a few gross simplifications in this approach. First of all, protein-ligand systems are rarely two spin systems: There are countless further interactions to spins within the protein, the ligand and the solvent [30–32]. Furthermore, different ligand spins, for example aromatic or methyl protons, may have different R_1 values. This will lead to differences between the populations, and cross-relaxation processes that we have partly ignored will become active. Nevertheless, it is very instructive to use approximate rate equations and protein-ligand experiments in order to compare and understand the experiments in more depth. Eq. (21) will be used to calculate the time evolution of magnetization in different ligand-observed experiments that will be discussed in Section 2.2.6.

2. Part II: Experimental approaches

The following Sections 2.1–2.4 are structured according to the validation cross (Fig. 2). In each section, experiments assessing a field of the validation cross will be discussed. Experimental formats and the theoretical aspects are first introduced and then the practical experimental setup, as well as pitfalls and necessary controls, are listed for each individual experiment.

2.1. Ligand characterization: identity, integrity and concentration

Determination of ligand integrity is represented by the top left field of the validation cross. The idea of "integrity" summarizes several properties: identity of the ligand with its annotated structure, integrity of the ligand in terms of degradation and purity, and finally, solubility and concentration of the ligand in the tested solution. Additionally, it is important to assess whether a ligand tends to self-aggregate. Self-aggregation will lead to false-positive results in several of the ligand binding experiments described in Section 2.2. Although ligand aggregation is relevant for ligand integrity, we will discuss aggregation in Section 2.2, as the same experiments will be used as for ligand binding.

Typically, organic compounds are stored as stock solutions in a mixture of 90% d_6-DMSO and 10% D_2O, usually at 50 or 100 mM. DMSO is regarded as the most universal solvent for organic molecules that is miscible with water and is tolerated by biological systems in concentrations up to a few percent. It is therefore used ubiquitously for stock solutions of substances intended for pharmaceutical assays. Addition of D_2O prevents freezing of the DMSO solution at 4 °C in a fridge and simplifies handling by lowering the viscosity of the solution. The stock solutions are then diluted into the aqueous buffer that will be used for the measurements with the protein. The following quality control experiments should be carried out in the same buffer, if possible. This is not only important for solubility measurements, but also for experiments that assess the integrity of the ligand, because a ligand may for example undergo hydrolysis in an aqueous buffer, which would be missed if quality control was only performed on the DMSO stock solution.

2.1.1. Assessment of ligand integrity and identity

NMR is the gold standard for determining the chemical structure of a ligand [33]. In many cases even a 1D NMR spectrum is sufficient to unambiguously identify the chemical structure of a ligand. In case of doubt, there are many approaches to determine the chemical structure of complicated ligands by 2D NMR methods, which can be complemented by mass spectrometry and optical spectroscopy. There are powerful software packages that can help such analyses. However, it would require a great deal of time to characterize each ligand in depth, bearing in mind that dozens or even hundreds of ligands are to be tested.

In more practical approaches, some compromises have to be taken. Counting the number of signals in the aromatic region of a 1D spectrum and considering their coupling patterns usually allows very quick assessment of ligand identity, with chances of false annotations low enough to be acceptable. Essentially, one must only assess whether the spectrum is compatible with the proposed structure, and there is no need to prove the identity of the compound rigorously.

Impurities or degradation products are easily identified by additional signals in a 1D spectrum that cannot be attributed to alternative conformations like rotamers of double bonds for example. Impurities should not lead per se to disqualification of the ligand, but it is important to annotate them at this stage in order to pay attention in ligand-observed experiments whether it is the actual ligand that is responsible for binding effects, or rather an impurity in the sample.

2.1.2. Determination of ligand concentration

In the context of drug discovery, it is important to have an approximate idea of the concentration of the ligand in a sample. For example, if a ligand is only soluble to 10 μM and induces similar binding effects on a protein as another ligand that is present at 500 μM, then the first ligand is probably a stronger binder. Vice versa, if no binding effects can be detected, lower limits for the K_D can be estimated, which will be very different for the two ligands in this example (see Section 3.1.1 for a more detailed discussion on information content of experiments). For this purpose, solubility measurements only need to be approximate (±30%), and stringent methods to bring the errors below 1% need not be used.

There is a large body of literature describing accurate concentration measurements by NMR [34]. In general, with NMR the absolute concentration cannot be obtained directly, therefore the concentration of a substance is always determined relative to a known reference substance or a synthetic signal [35–37]. NMR signals are proportional to the concentration of a substance in a sample and the number of nuclei giving rise to an individual signal. Therefore simple integration of the signals will reveal their relative concentration. However, signal intensities of different molecules or different chemical groups may deviate from theoretical values due to different relaxation rates. Signal reduction due to transverse relaxation can be avoided by using experiments without intervals where transverse magnetization can decay before acquisition, for instance pre-saturation experiments. However, longitudinal relaxation rates in different chemical groups in a molecule, or between the ligand and the reference, can be very different. Therefore, long relaxation delays between scans should be used so that all nuclei relax back to their Boltzmann equilibrium (Eq. (17)). Considering T_1 values of several seconds for methyl groups in small molecules, the delays should be longer than 10 s, making experiments impractically long. Again, a pragmatic approach is needed in order to be able to efficiently assess the concentration of a ligand and its solubility in aqueous solution.

Experimental setup. In practice, we use DSS as internal reference and compare it with integrals of ligand signals. This compound can be obtained in highly pure form, and stock solutions with accurate concentrations can be prepared. Furthermore, it will be added anyway to the sample. If another compound would be chosen, an additional substance would be present in the sample that could give rise to potential artifacts. DSS contains 9 equivalent methyl protons and is added at a concentration that corresponds to the signal of a single proton of the ligand. For instance, 200/9 = 22.2 mM of DSS is added in order to obtain a proton signal equal to that of 200 mM ligand. The strong methyl signal of DSS at 0 ppm, however, has a rather long longitudinal relaxation time (T_1 = 3.4 s), requiring long relaxation delays. We still suggest using a rather short interscan delay of 3–5 s (including acquisition time) for reasons of time efficiency. At this value the errors due to differential relaxation rates are below 5%, as determined in internal tests with different high-purity compounds.

For the determination of the ligand concentration, essentially only one assigned signal of the ligand with known degeneracy needs to be compared to the reference signal. However, accuracy increases if the average value of several signals is used. In practice, integration of the aromatic region of the spectrum has proved to be most convenient. In this approach the entire aromatic region is integrated, divided by the number of aromatic protons (and other protons with signals in this spectral region) in the ligand and then compared to the reference signal. This approach – which can be automated – yields sufficiently accurate numbers in a short time and does not require any assignment of individual resonances.

The solubility of a ligand is determined by measuring its actual concentration in a sample with high nominal concentration (1 mM). For accurate determination of the solubility, the concentration of the DMSO stock solution also needs to be known. If in a single measurement a concentration lower than nominal is found, it is unclear whether the deviation is due to the solubility limit, or if the stock solution was less concentrated than annotated. This can result from inaccurate weighing of small amounts of powder, or if the powder is contaminated with a salt for example that will increase its weight.

Wrong concentrations could also arise from errors in pipetting. Here, however, the residual DMSO proton signal will help to assess the amount of added stock solution. This provides a highly valuable control to check correct pipetting of the stock solution.

In order to attain the required throughput, a single experiment is used to obtain data on both ligand integrity and concentration. Using a relaxation delay of 3 s, reliable signal areas can be extracted to determine the concentration and confirm the structure.

In theory, the best experiment to obtain data on ligand integrity would be a 1D proton sequence with carefully adjusted pre-saturation of the water resonance in order to obtain a flat baseline. Unlike other water suppression schemes, pre-saturation experiments have no delays after the excitation pulse, which would lead to different intensities of signals due to transverse relaxation and phasing artifacts due to evolution under homonuclear couplings. Unfortunately, this experiment performs very poorly in automation, where several samples are measured sequentially with the same parameters. Especially with cryogenic probes, the water suppression that can be achieved is poor, leading to distorted baselines of the spectra, which strongly hampers accurate integration of signals.

The experiment that we find most suitable is a 1D proton sequence with excitation sculpting for water suppression [38]. It consists of two gradient echoes, where the water signals are selectively de-phased by means of a shaped pulse that cancels the effect of a hard re-focusing pulse on the water resonance. This "soft

watergate" sequence is repeated twice with appropriate gradient strengths and phase cycles, so that artifacts due to pulse imperfections and offset effects are very well suppressed. The experiment is relatively long (on the order of 8 ms), which can lead to small phasing artifacts due to evolution of homonuclear scalar couplings. To suppress these artifacts, a "perfect echo" can be used [39]. This consists of applying a 90° pulse at the center of the evolution period, which has the net effect of exchanging the antiphase terms of the coupling partners and thereby refocusing the scalar coupling effects. Depending on the implementation, the length of the pulse sequence is doubled, leading to slightly less intense signals. If the excitation-sculpting scheme is not symmetric, this can lead to slight baseline distortions. Additionally, signals close to the water resonance are attenuated. Despite of these flaws, in a drug-discovery setup excitation-sculpting is superior to pre-saturation of the water resonance. The excitation sculpting experiment is robust against changes in offset and small miscalibrations of pulse lengths. Radiation damping of the water resonance is negligible in this sequence due to gradient dephasing, and the power of the soft pulses is thus usually very close to the calculated value ($PL_{soft} = -PL_{hard} * (p_{hard}/p_{soft})^2$; where PL: power level in Watt, p: pulse length in μs), provided the amplifiers are highly linear. Pulse sequences relying on hard WATERGATE elements are similarly robust and do not require calibration of a selective shaped pulse for water [40,41]. However, the region with attenuated signals close to the water peak is usually broader, and at periodic intervals, determined by the interpulse delay of the WATERGATE element, there will be additional regions in the spectrum where the signals are attenuated. We therefore suggest the use of excitation sculpting, also because it allows suppressing further strong signals like those of Tris, glycerol or DMSO in the buffer, by using soft pulses with multiple excitation bands.

Practical pitfalls and necessary controls. **Buffer:** Concentration and integrity measurements are only relevant if they are obtained in the same buffer as used for the binding experiments. Ligand integrity and solubility may change depending on pH or additives.

Baseline: For automated integration of signals, it is important that the baseline is flat and has vanishing intensity. In most cases a baseline correction is needed to obtain a zero value for the baseline.

Confirmation of compound addition: The residual ^{1}H signal of DMSO at 2.66 ppm serves as an indicator of the addition of compound stock solution. Its presence and magnitude can be used for checking the amount of compound stock solution that was added, and indeed if it was added at all.

Slow R_1 relaxation may lead to wrong concentrations: One should be aware about limitations due to the short recovery delay of 3 s that is usually chosen. For very small compounds and compounds with highly mobile groups false results may be obtained.

Solubility of single compounds may be different in mixtures: Keep in mind that solubility of individual ligands may be different in mixtures. Therefore, a reference spectrum of a compound mixture should be recorded, just to confirm that each compound is present at the expected concentration.

2.2. Ligand binding effects

2.2.1. Ligand observation format with ligand in excess

In principle, in order to observe the strongest effects on ligands, one would add protein in excess. However, since relatively high amounts (>100 μM) of ligand are needed to observe its NMR signals in a few minutes, and since proteins are usually very expensive reagents, this is impractical – especially if many compounds are supposed to be tested. Thanks to the sensitivity of relaxation-based methods to binding events, the opposite experimental strategy is actually useful, that is, a ligand in 10–20-fold excess over protein is chosen in general. When choosing 200 μM as the ligand concentration, 1D spectra with a signal-to-noise ratio >10 can easily be recorded within 5 min, thus enabling relatively high throughput. In the typical setup, only 10 μM of expensive protein needs to be employed. Even if the maximal bound fraction of ligand, p_B^L, is only 5% in this setup, relaxation-based methods allow detection of ligands as weak as K_D = 10 mM.

The basis for this sensitivity is the averaging of effects experienced by the bound ligand and the free ligand via fast exchange between free and bound states. This is often called the "transfer" of effects from bound to free ligand using the following simplified concept: strong relaxation effects are imprinted on the ligand during its visit to the protein, and are then read out on the free ligand after it dissociates from the protein. According to this concept the experiment is dissected into individual steps. A ligand binds to the protein and experiences strong relaxation. Unfortunately, the signals of the bound ligands will probably be undetectable by direct observation: they will be strongly broadened and – since there is little (10 μM) protein in the solution – their intensity is vanishingly low. However, the ligands will be released from the protein, with strong relaxation effects imprinted on them. Free ligand signals can easily be detected, because they are sharp. Even with ligands in large excess, most ligand molecules will visit a protein several times and accumulate effects due to relaxation in the bound state. The final signal is then observed on the signals of the 200 μM free ligands, yielding high signal-to-noise but containing encoded binding effects: hence the notion of "transferred" effects. Of course, in reality ligands continuously exchange between free and bound states and averaged effects are measured (Eqs. (9) and (11)); the key point is that, for a low-molecular-weight ligand present in excess, averaging of its relaxation properties is dominated by what happens in the bound state, whereas averaging of its lineshapes is dominated by the sharp signals of the free state. "Transferred" effects are established terms to describe this, and there are experiments to measure transferred NOEs [42] or transferred residual dipolar couplings [43,44] or transferred cross-correlated relaxation [45,46], all on ligand signals.

In summary, the experimental format with ligands in 10–20-fold excess over protein is a fast and economic approach yielding good signal-to-noise and high sensitivity to binding events.

2.2.2. Transverse relaxation-based approaches

Transverse relaxation effects can be most easily exploited, because no complicated pulse sequences are needed. Essentially, the linewidths of the ligand in the presence or absence of protein can be compared in simple 1D experiments. The line width is proportional to R_2 (Fig. 6), which is several times higher for the ligand in the bound state than in the free state (Fig. 5, Eqs. (13) and (14)).

In order to transform line widths into signal intensities (which are more easily analyzed), experiments with a relaxation delay of 100–300 ms are typically used, which will lead to a significant reduction of the signal intensities (Fig. 6, Eq. (23)). Such a signal reduction is very easy to identify as a sign of binding, and thus hundreds of spectra can be analyzed quite efficiently.

The basic ligand-observed experiment: ^{1}H-$T_1\rho$.

Experimental setup. In theory, a long spin echo can simply be used to observe the effects of R_2-relaxation. For ^{1}H spectroscopy, however, homonuclear couplings will evolve during a long transverse relaxation delay, leading to phase-distorted peak shapes. Therefore, the spins are subjected to a spin-lock field that suppresses homonuclear couplings. The resulting experiment is the well-known $T_1\rho$ pulse sequence [47]. Here, on-resonance signals relax according to T_2, while with increasing offsets, T_1 effects creep in, leading to mixed relaxation due to R_1 and R_2 (Eq. (24) in Table 2

at the end of the section). While this is interesting for other dynamic studies, as discussed earlier R_1 is not a parameter of high interest in drug discovery, as it may not differ at all between protein and ligand. Therefore, in the drug discovery version of the $T_1\rho$ experiment, the carrier is set to the center of the spectrum and high spin lock power is applied in order to minimize off-resonance effects. Relaxation of protons is then dominated by transverse relaxation through dipole-dipole interactions (R_2(DD), Eq. (13)), and offset-dependent R_1 and ROE effects are neglected.

The spin lock field can lead to sample heating and some signals may shift in a temperature-dependent manner. When comparing two different lengths of the spin lock duration, it is advisable to insert a compensation spin-lock interval just after acquisition, so that the total spin lock duration per scan is the same in the two experiments. The duration of the spin lock time can be lengthened in order to obtain discriminating effects between binding and non-binding ligands even for small proteins or low protein concentrations. In Fig. 9 it can be seen that the highest contrast between a bound and a free ligand is obtained at very long spin-lock times, e.g. >2 s. Unfortunately, the signals are so strongly attenuated after such a long spin-lock time, that a reliable analysis is not possible. At the same time, the spin-lock duration represents another limitation of this experiment. Due to power restrictions of the probe and heating of the sample, the maximum spin-lock time is on the order of 200 ms for conventional probes and 500 ms for cryoprobes. Historically, 200 ms is the typical relaxation time used in these experiments. With modern equipment 400–500 ms seems to be possible. Compared to NOE-based techniques, where the relaxation period can be longer than 1 s, here relaxation effects – which are actually stronger – can only act during typically 200 ms. This results in reduced contrast: Signals are less attenuated and the difference between signals of free and bound ligands is often not obvious for very weakly binding ligands, or relatively small protein targets.

For small proteins, protein signals may be present in spectra with short spin-lock intervals, hampering analysis of the ligand signals. In this situation, a blank protein spectrum can be recorded and subtracted from the protein-ligand spectrum – with due regard for potential subtraction artifacts associated with difference spectroscopy.

Practical pitfalls and necessary controls. **Comparison of two relaxation times using ratios of ratios:** The $T_1\rho$ experiment is carried out once with protein and once without. Compounds may self-aggregate and therefore it is necessary to record the experiment of the free compound in the protein buffer. Additionally, the analysis of the $T_1\rho$ experiment should be carried out in the "ratio of ratios" format. That is, two spectra with different relaxation periods, for example 10 and 200 ms, are recorded on a single sample. In general, comparing two measurements from the same sample is always superior to comparing single measurements from two samples. For the $T_1\rho$ experiment, two spectra are recorded for the free ligand and another two for the ligand in presence of protein. This format protects from trivial artifacts like pipetting errors or spectrometer shortcomings like bad shimming, which could lead to reduced signal intensity in the sample containing protein and therefore result in false-positive results. Conveniently, a relaxation factor f is defined as the signal intensity after a 200 ms relaxation period, divided by the signal intensity after a 10 ms relaxation period. A rapid decrease in signal intensity ($f \ll 1$)corresponds to fast relaxation (binding), whereas a slow decrease in signal intensity ($f \approx 1$) corresponds to slow relaxation (non-binding). Typically, a ligand in the absence of protein shows a factor f = 0.8–0.9, whereas upon binding to protein, the factor decreases to 0.5 or less. A cutoff criterium for binding is generally if the factor f in the presence of protein is at least 0.2 units smaller than in the absence of protein.

The signal reduction can be a very rough indication of the relative affinity of different ligands, as it depends on the fraction of bound ligand. However, the signal reduction under dipolar relaxation depends strongly on the distance between protons (r^{-6}, Eq. (13)). Since the chemical environment of protons in different ligands, especially in the context of a protein-ligand complex, is not identical, an affinity in terms of K_D cannot be derived from a single $T_1\rho$ experiment. It is possible that a ligand featuring a modest signal reduction is more potent than one with a large signal reduction, simply because of different distances between protons. Additionally, exchange phenomena in the intermediate exchange regime may lead to strongly-enhanced apparent transverse relaxation rates (Fig. 7). They depend mainly on the chemical shift differences between the free and bound states of a ligand, which is not a good measure of the binding affinity (Eq. (11)).

Protein homogeneity: If several batches or aliquots of protein are used for measuring a series of samples, all protein samples should be mixed in order to obtain a single homogeneous stock solution of protein. Slight batch-to-batch variations in protein may lead to inconsistent results. This applies to all ligand observed experiments.

Exploiting enhanced relaxation properties of fluorine: ^{19}F-T_2. The use of fluorinated ligands may sound a bit exotic initially, but fluorine is actually very widely used in medicinal chemistry. 25% of current drugs contain fluorine and the archives of pharmaceutical companies have a similar abundance of fluorine containing molecules.

^{19}F is a highly attractive nuclear probe for NMR applications in drug discovery. In essence, effects of binding are much more pronounced for ^{19}F than for ^{1}H; furthermore, ^{19}F has a sensitivity of 83% ($0.94^{5/2}$) compared to ^{1}H ($\gamma_F = 0.94 \times \gamma_H$). The reason for the more pronounced binding effects lies mainly in the much larger chemical shift anisotropy (CSA) of ^{19}F and in a much bigger differences in chemical shift between the free and bound states [48,49].

The large CSA of ^{19}F stems from the high electronegativity of fluorine, which leads to strongly polarized bonds and asymmetric electron orbitals, which result in strongly different shielding effects depending on the orientation of the molecule. The CSA is described by using a cylindrical chemical shielding tensor and by taking the difference of the minimal and maximal shielding values. The CSA of a fluorine moiety can be as large as 400 ppm, even up to 1000 ppm in exceptional cases [50], while typical values of proton CSA are typically in the range of 5–15 ppm. Therefore, CSA dominates the transverse relaxation for ^{19}F, as opposed to ^{1}H, where dipolar interactions are the prevalent mechanism. Transverse relaxation by CSA has a stronger dependence on τ_c: the $R_{2,CSA}$ values of a 300 Da ligand and a 30 kDa protein have a ratio of about 60, as opposed to a ratio of about 30 for the case of $R_{2,DD}$ (Fig. 5). As apparent from Eq. (14), CSA-dependent relaxation is proportional to the square of the magnetic field and the square of the CSA. In a static magnetic field of 600 MHz, CSA relaxation is nearly 10 times faster for ^{19}F than dipolar relaxation. This actually often leads to line broadening of the bound state beyond detection.

There is a second factor that can enormously amplify binding effects for ^{19}F. Due to large chemical shift differences between the free and bound states, exchange effects can lead to large apparent R_2 values, even for small fractions of bound ligand (Eq. (11) and Fig. 7).

Of course, the magnitude of the exchange contribution depends on the chemical shift difference and the exchange rate, which will be different for every ligand and therefore cannot be predicted. However, chemical shift differences are very often large for ^{19}F and therefore most ligands will be experience exchange line broadening. In favorable cases, this allows one to reduce the protein concentration to below 1 μM while still obtaining significant line broadening for the ligand [49]. Typically, about 5-fold less protein

can be employed for ^{19}F than for ^{1}H spectroscopy, that is 2 μM protein and 25–50 μM ligand.

The use of fluorinated ligands may sound a bit exotic at first glance, but fluorine is actually very widely used in medicinal chemistry. 25% of current drugs contain fluorine and the archives of pharmaceutical companies have a similar fraction of fluorine containing molecules.

Recently, the sensitivity of ^{19}F-detected experiments was further increased by the use of dissolution dynamic nuclear polarization (dissolution DNP). Using hyperpolarized ligands, it was possible to identify binding effects on ligands at concentrations as low as 1 μM [51]. This has several advantages: first, the ligands do not need to be very soluble; therefore the coverage of ligands that can be studied is larger than with other methods. Second, proteins can be employed at equal concentrations as the ligands, turning the method into an equimolar experiment (Section 2.2.7). Consequently, there is no lower limit on the exchange rate and high-affinity ligands become accessible (Fig. 12). Since the range of accessible concentrations is larger, a wider range of K_D can be determined.

The following paragraph is dedicated to a short explanation of hyperpolarization [52]. Afterwards, we shall resume our discussion of conventional experiments. In NMR, the signal magnitude is determined by the population difference of spin-up and spin-down states. For nuclear spins in a typical 14 T magnetic field (600 MHz for protons), the energy levels are so close in energy that the Boltzmann equilibrium of 10^4 spins at room temperature results in about 1 more spin in the lower than in the higher energy level. In DNP, advantage is taken of the high gyromagnetic ratio of electrons ($\gamma_e = 658 \times \gamma_H$), which leads to larger differences in the populations of the energy levels and therefore a higher resulting polarization. Furthermore, by lowering the temperature, the polarization can be further increased. In fact, for electrons it is possible to achieve essentially full polarization – >99.9% of the electrons are at the lower energy level – even at moderate magnetic fields (e.g., $B_0 = 3.4$ T) and a temperature of 1.2 K, which is technically relatively easy to achieve. This polarization can be transferred to nuclei like ^{1}H, ^{13}C, and ^{19}F by irradiating with microwaves tuned to the difference in frequency between nuclei and electrons. In practice, a mixture of ligands (nuclei) and radicals (electrons) are frozen and put in a magnet. Then microwaves are irradiated for tens of minutes to build up hyperpolarization on the ligand nuclei. Up to 70% polarization can be achieved, that is a 10,000-fold enhancement over Boltzmann equilibrium magnetization at room temperature for ^{1}H and ^{19}F, and close to 100,000-fold enhancement for ^{13}C. For the actual NMR experiment, the frozen ligand is dissolved with superheated buffer and transferred to a sample containing the target protein that is waiting in an NMR magnet. After mixing, NMR experiments are recorded. The entire process of dissolution, transfer and measurement needs to be very fast, because the magnetization of the hyperpolarized ligand decays with R_1 as soon as it is in the liquid state. Therefore, for ^{1}H or ^{19}F the entire process needs to be run within seconds.

Experimental setup. For fluorine T_2-experiments, Carr-Purcell-Meiboom-Gill (CPMG) sequences are best suited, because – unlike proton spectroscopy – no homonuclear scalar couplings need to be suppressed by a spin lock [49]. There rarely is more than one non-equivalent fluorine atom in a ligand, so that scalar couplings between fluorine nuclei are not an issue and scalar couplings to protons can be suppressed by decoupling – provided the probe supports proton decoupling during ^{19}F acquisition.

In the CPMG sequence, a rather long delay between refocusing pulses should be used, typically $t_{CPMG} = 20$ ms, in order not to attenuate the effects of exchange. Actually, for characterizing protein and protein-ligand dynamics, CPMG sequences are usually employed with high pulse repetition rates for the purpose of modulating the apparent exchange effects to facilitate extracting the exchange rates (Eq. (25)). In contrast, for drug discovery applications, exchange effects are desirable to bring as much additional line broadening as possible. The length of the delay between the refocusing pulses of the CPMG sequence is only limited by the inhomogeneity of the magnetic field, which will lead to signal attenuation through diffusion of the molecules.

Typically, two experiments are recorded, one with a very short T_2-relaxation delay of 20 ms and one with 100–400 ms (shorter for molecules containing ^{19}F with large CSA, and longer for CF_3-containing molecules). The signal intensities are then compared in the same "ratio-of-ratios" format as described for $T_1\rho$ experiments above. To save measurement time, the two experiments can actually be concatenated in a slightly modified version of the pulse sequence [53].

The major challenge in ^{19}F spectroscopy is the enormous chemical shift dispersion, which spans >300 ppm for organic molecules, actually 400 ppm if more exotic substituents are also considered. This means that mixtures of compounds employed in screening may need spectral widths of the same order of magnitude. This spectral width is impossible to cover with regular pulses, since a 90° pulse length of about 1 μs would be needed. When measuring individual compounds, the resonance offset can be centered at the resonance frequency of the fluorine nucleus under study. When working with mixtures, for example in fragment based screening, it is important to design the mixtures in a way that signals of all compounds in the mixture can be recorded at high quality in one single spectrum, meaning that the signals in a mixture should not span more than about 40 ppm. In order to achieve proper refocusing of widely dispersed fluorine signals, adiabatic refocusing pulses could be used or Hadamard spectroscopy could be run on all resonance frequencies of the ligands in a mixture. With the advent of numerically optimized pulses based on optimal control theory, much larger refocusing bandwidths are possible [54,55], as shown for ^{1}H and ^{13}C nuclei. Whether this approach can be applied for the large spectral width of ^{19}F still needs to be fully explored (Frank et al., personal communication).

On the flip side, the large chemical shift dispersion of ^{19}F is a huge advantage, as it allows measuring mixtures of 30 or even 50 compounds. Because each compound usually only yields a single singlet signal, there is practically no overlap and large libraries can be screened very efficiently.

Practical pitfalls and necessary controls. In general, fluorine-based experiments are quite delicate and need careful setup in order to provide reproducible results. Therefore, the following points need careful consideration.

Sample homogeneity: Fluorine signals are much more sensitive to sample inhomogeneity than are proton signals. One important point is therefore to mix the samples thoroughly, especially after addition of viscous solutions of DMSO, glycerol or D_2O. In our experience, sometimes the DSS proton signal linewidth can be shimmed to below 1 Hz, but under the same shimming fluorine signals show several shoulders, which only disappear upon thorough mixing.

Temperature stability: Temperature needs to be tightly controlled and samples need to be well equilibrated. Fluorine signals are very sensitive to temperature changes as well as imperfect shims. Therefore, if samples are not equilibrated for long enough before shimming, the homogeneity might not be good enough to yield sharp lines. A rough guide for equilibration time is the sample diameter, that is a 5 mm tube should be equilibrated for 5 min, a 3 mm tube for 3 min. Additionally, proton decoupling during acquisition may heat the sample. Therefore, many dummy scans are needed (say, 64) and ideally, an internal temperature control should be used, such as an NMR thermometer [56,57].

Insufficient bandwidth of refocusing pulses: Negative control experiments are needed for two very different reasons. First, self-aggregation of compounds can be detected in this way. Second, due to the extreme chemical shift dispersion of fluorine signals, the refocusing of signals at the edges of the excitation bandwidth of the CPMG sequence may lead to artificial reduction of the signal intensity, which could result in false positive interpretation. One way to mitigate this problem is to design mixtures of compounds with similar fluorine chemical shifts (within 40 ppm) and then to adjust the offset of the experiment for each mixture.

Exceeding power input in proton decoupled experiments: For experiments with ^{1}H-decoupling during acquisition it is important to monitor the duration of acquisition. Especially, when manipulating the width of the spectral window in reporter experiments, acquisition times of >1 s may occur, which can lead to spectral artifacts or even to serious damage of the probe. Depending on the probe, acquisition times of 0.5–0.75 s should not be exceeded.

Enhanced relaxations with spin labels: SLAPSTIC. SLAPSTIC (Spin Labels Attached to Protein Side chains as a Tool to identify Interacting Compounds) is an even more sensitive method to detect ligand binding [58]. It relies on labeling the target protein with a paramagnetic spin label, and thereby introducing an unpaired electron. This can be achieved by covalently modifying a natural or engineered cysteine residue close to the binding pocket with a nitroxide label like TEMPO or a lanthanide chelator. Alternatively, a ligand binding tightly to a pocket in close proximity can be derivatized with a spin label. The power of this method comes from the 658-fold higher magnetic moment of the electron compared to the proton. Paramagnetic relaxation depends on the squares of the gyromagnetic ratios (γ) of the two involved microscopic magnets. In the first terms of Eqs. (11) and (13)–(15) describing nuclear dipolar interaction, the γ of both nuclei are the same, yielding $\gamma^2 \times \gamma^2 = \gamma^4$ in the equation. For the paramagnetic dipole-dipole interaction this pre-factor takes the form of $\gamma_\varepsilon^2 \times \gamma_H^2$ resulting in a 658^2 = 432,964-fold enhancement over proton dipolar relaxation (Eq. (18)). The huge factor of 430,000 in enhanced dipolar interaction compared to proton-proton interaction cannot be fully realized because the spin label will be farther away than the closest proton relevant for proton dipolar relaxation. That is mainly because the spin label needs to be attached on an amino acid close to the binding site, but without perturbing the binding site. Therefore, this distance is usually 10–12 Å, which is typically 5-fold farther than the distance to the closest proton. Due to the r^{-6} dependence of the paramagnetic relaxation rate, the relaxation effect is reduced. In practice, this still allows detection of much lower fractions of bound ligand than with conventional methods, therefore the protein concentration can be lowered about 50-fold to 0.2 μM. It also allows study of small target proteins, for which other τ_c-dependent relaxations effects are weak.

2.2.3. NOE-based approaches

Observing magnetization transfer between ligand and protein represents a very attractive way of demonstrating a protein-ligand interaction. Interestingly, observing NOEs on the ligand itself already can give a strong indication of binding. The NOE for a fast tumbling small ligand free in solution yields a negative cross-peaks in a NOESY spectrum (assuming the diagonal peaks are positive), whereas cross-peaks for a bound ligand that tumbles as slowly as the protein are positive relative to the diagonal, and additionally are about 20-fold stronger in our standard example (Fig. 5). Therefore, if a 2D ^{1}H,^{1}H-NOESY of the ligand is recorded and the bound fraction is >5%, positive intra-ligand NOE cross-peaks will be visible. Of course, here also fast exchange between bound and free state is assumed. This so-called transferred NOE (tr-NOE) therefore will indicate ligand binding to the protein [42,59]. Just to clarify, a transferred NOE is not an NOE from the protein to the ligand, it is an intra-ligand NOE that built up on the ligand during the time that it visited the protein – i.e. the NOEs reflect the protein-bound state of the ligand. However, several experiments have been devised which measure an intermolecular NOE between protein and ligand. A prerequisite for such an intermolecular magnetization transfer to happen is a difference in magnetization between protein and ligand (second term in Eq. (21) $\neq$ 0). For isotope labeled proteins, filtering and editing methods can be used to prepare labeled protein and unlabeled ligand differentially [60]. However, such half-filter experiments are rather insensitive and take typically a day or more to record, depending on sample concentrations. Additionally, unlabeled protein is preferred on grounds of cost. Other approaches have been devised in order to select protein or ligand magnetization, based on differential translational and rotational diffusion of protein and ligand. In "NOE pumping" experiments, ligand signals are attenuated using diffusion filters before the NOE mixing time, resulting in a net transfer of magnetization from protein to ligand. A more efficient approach is "reverse NOE pumping", in which protein signals are attenuated using transverse relaxation filters before the NOE mixing time. This is more efficient since the difference between the protein and ligand in their transverse relaxation properties is several folds larger than the difference in diffusion properties. NOE pumping experiments are already very sensitive compared to 2D NOESY experiments, but their limitation stems from the usually relatively low amount of protein. The magnetization on the protein can be "turned over" once per scan and then a long relaxation delay is needed before the next scan.

In practice, therefore, the two experiments that have found the most widespread applications use long lasting magnetization reservoirs that allow continuous turn-over of ligands for NOE-mixing times longer than a second. These are the 1D ^{1}H experiments termed STD and waterLOGSY, which will be discussed in the following two sections.

Saturation transfer between protein and ligand via NOEs: STD. The saturation transfer difference (STD) experiment relies on magnetization transfer between the protein and the ligand [61]. To this end, signals of the protein are selectively saturated, with the result that bound ligands will also be saturated as a result of nuclear Overhauser effects between the protein and ligand. In contrast, free ligands in solution do not experience any change in their magnetization during the same experiment (Fig. 8). What makes this approach so sensitive is that many ligand molecules can visit the protein and be affected during one experimental scan. Because the protein is constantly irradiated it acts as a magnetization sink; the mixing time can be longer than second, allowing ligands to acquire saturation from the protein over and over again on successive visits. The limit to the length of the mixing time is the T_1 of the ligands, with which ligands will relax back to equilibrium magnetization and thereby lose the imprinted effects of their visit to the protein (Eq. (28)). With this comes also a requirement on the exchange rate, which needs to be in the intermediate to fast regime in order for several ligands to be affected by each protein and therefore amplifying the response.

The limitation from R_1 relaxation, which counteracts the effect of saturation, can be alleviated by preparing the sample in D_2O instead of H_2O. In this setup, the protein and the ligand are surrounded by a kind of insulating solvent, where the microscopic processes leading to R_1 relaxation – namely dipole-dipole relaxation – are strongly attenuated. Therefore, pictorially, there is much less leakage of the magnetization to the solvent, and the STD effect can be boosted several-fold. Mathematically, this is easily seen in Eq. (28). For long relaxation times t, the magnetiza-

tion asymptotically approaches a value of $1 - R_C/(R_1 + R_C)$ (set $t = \infty$). The smaller is R_1, the larger the reduction in signal intensity therefore will be.

In the original version of the experiment [61], isolated saturation of the protein is achieved by irradiating at a frequency where only protein nuclei will resonate, typically in the far upfield region around zero ppm. These extreme chemical shifts usually only occur due to ring current shifts in the context of folded proteins, meaning that no compound signals will be saturated directly by irradiation at −0.5 ppm (for example). Saturation is then transferred within the protein by spin diffusion. The efficiency of this process depends on the proton density and rotational correlation time of the biomolecule. This means that for example RNA, with its intrinsically low proton density, is not an ideal target molecule for STD experiments. On the other hand, large proteins will enable extremely efficient STD experiments. The STD effect can be maximized by immobilizing the protein and performing the experiments in a solid-state NMR setup under magic angle spinning [62,63]. However, one then gives up the distinct advantage that solution NMR offers, namely, measuring protein-ligand interactions in solution.

At a practical level, STD is an experiment that measures the difference between spectra acquired with protein saturation and without saturation in two sub-experiments. For ligands free in solution there will be essentially no difference between these two sub-experiments, and if the signals are subtracted from each other that will result in no signal from the free ligands. For bound ligands, in the sub-experiment without protein saturation, a signal with high intensity will be recorded, while this signal will be attenuated by magnetization transfer to the saturated protein in the second sub-experiment. When subtracting now the latter from the first, a residual signal will remain – indicating binding of the ligand (Fig. 9).

The difference procedure has an interesting consequence, in that the signal of the free state of a ligand does not contribute to the final spectrum. This makes this experiment unique among those based on ligand observation: One can in principle go to very high ligand-to-protein ratios, and still obtain effects. When acquiring more and more scans the binding signal will just increase allowing accessing even very low fractions of bound ligand. For other experiments, there is always the competition of the signal of the free ligand, making it progressively more difficult to analyze subtle changes in signal intensity.

Experimental setup. Selective saturation in STD experiments is typically achieved by means of soft pulses with excitation centered at −0.5 ppm and 30 ppm for the on- and off-resonance saturation of the protein, respectively. Usually a Gauss or REBURP shape is used with duration of 50 ms and low power in the order of $\gamma B_1 \leqslant 100$ Hz. The pulse is repeated during a 1–2 s period. An overview of the influence of different parameters has been compiled by Rowe et al. [64]. In order to obtain more uniform and more complete saturation of the protein, several irradiation frequencies can be used, but this increases the risk of hitting a resonance of the ligand, leading to saturation of this particular resonance. However, for a non-binding compound such saturation will not be transferred to other ligand signals, and a signal enhancement rather than a signal decrease will occur, unless the compound is aggregated. Ligand irradiation can easily be identified by recording the same STD spectra of free ligands and subtracting these signals from the STD spectra in presence of protein: this approach is called STDD for saturation transfer double difference.

Another way of applying STDD is when complex samples – like cell extracts – yield crowded spectra. Here, an STD spectrum of the sample without ligand can be subtracted from the one with ligand, yielding a spectrum with ligand only [65].

If the protein is rather small, a $T_1\rho$ filter may be necessary to suppress protein signals.

The on- and off-resonance spectra are either subtracted directly by phase cycling of alternate scans, or the two spectra are recorded separately and only compared in the subsequent analysis. The first approach has the advantage of minimizing subtraction artifacts as both spectra are recorded at the same time. The latter approach with two different spectra allows observing all ligands in a mixture and confirms their presence and integrity, and is advisable if subtraction artifacts are particularly strong.

Practical pitfalls and necessary controls. **Compound or protein aggregation:** Conceptually, self-aggregation of compound should not lead to false positives in STD, because effects should only arise from saturation transfer from protein. However, resonance signals of aggregated compounds can sometimes be so broad that they will be saturated by the soft pulses, especially if several irradiation frequencies are used. Negative controls on free compounds need to be performed, which, unfortunately, can only identify a subset of the troublesome compounds. In practice, aggregation usually involves co-aggregation with protein, leading to strong false positive STD effects. Protein aggregation alone can also lead to non-specific binding of compounds to protein aggregates, which leads to a false positive STD signal. Therefore, a protein-observed follow-up experiment is always necessary.

Subtraction artifacts: Depending on the stability of the NMR system, severe subtraction artifacts can hamper analysis. In this case, either lock parameters can be optimized or two separate spectra are recorded corresponding to on- and off-resonance irradiation. The analysis then is based on comparing signal intensities in these two spectra.

Direct irradiation of ligand signals: The STD effect can be increased significantly by irradiation at 0.5 or 1 ppm and higher power ($\gamma B_1 > 50$ Hz), since more protein resonances will be affected by irradiation in this region. In such cases a reference spectrum of the ligand alone needs to be recorded in order to detect direct saturation of ligand signals that would lead to false positive interpretation.

Water mediated NOEs to identify binders: waterLOGSY. Similar to STD, waterLOGSY (water Ligand-Observed by Gradient SpectroscopY) takes advantage of a long-lasting reservoir of magnetization, which can be continuously tapped to imprint properties of the bound state onto many ligands even at very low fractions of bound ligand [66,67]. In the waterLOGSY experiment, the reservoir used to boost the sensitivity compared to a regular NOESY or trNOE experiment is the water magnetization: it is very abundant and normally has a T_1 of more than two seconds, which typically allows for many visits of ligands to a protein. Essentially, what is measured is just an NOE between water and the ligand. If an NOE evolves between water and a fast-tumbling free ligand, a small negative net effect will result (i.e. negative relative to the starting magnetization on the water). Conversely, if a water-to-ligand NOE evolves on the slowly tumbling bound ligand; this will result in a positive effect (Fig. 8). In the resulting spectra, compounds that bind to a protein will therefore show positive signals and compounds that do not bind will show negative signals (Fig. 9). This is a very clear read-out to distinguish binders from non-binders enabling a swift analysis.

Mathematically, the experiment is best understood when looking at the relevant rate equations, which give rise to Eqs. (31) and (32). The initial rates are $-R_1 - R_C$ and $-R_1 + R_C$ for scan 1 and 2, respectively (with $t = 0$ and using the given initial conditions). When subtracting scan 1 from scan 2, relaxation effects are cancelled (terms in R_1 disappear) and cross-relaxation effects dominate ($2 \times R_C$).

In addition to the rotational correlation time (τ_c) of the particle, the measured NOE is also influenced by the residence time of water molecules on the protein (τ_r) (Eq. (34)). For fast exchanging water

molecules, τ_r may become smaller than τ_c, and NOEs may be negative. In most cases this will rather enhance the contrast, as fast exchanging water will be the dominant situation for the free ligand whereas slow exchanging water will prevail on the protein complex.

The magnetization transfer from water to bound ligand does not only occur via bound water in the binding pocket; the contribution from indirect relayed spin diffusion can be significant as well. In this case, water magnetization enters the protein via chemical exchange at labile positions such as hydroxyl groups or amines. On large proteins, spin diffusion is efficient enough to reach the ligand-binding pocket, where the magnetization transfer to the ligand will take place – with the same sign as the original water magnetization (Fig. 8). However, the waterLOGSY experiment does not rely solely on spin diffusion on the target in the way that STD does. Magnetization transfer from water in the binding pocket allows one to study relatively small targets, as well as targets with low proton density such as RNA, where spin diffusion is inefficient [66].

Recently, a hyperpolarized version of the waterLOGSY experiment has been published [68]. Here, water is hyperpolarized in an external polarizer (see end of Section 2.2.2 for a short introduction to hyperpolarization). After mixing with hot D_2O, the hyperpolarized water is injected into a solution with protein and ligand that is waiting in an NMR magnet. Strong waterLOGSY effects can then be read out in just a few seconds. There are a few interesting aspects to this version of the experiment: Firstly, the pulse sequence is highly simplified, since the sizes of the protein and ligand magnetizations are miniscule compared to the size of the hyperpolarized water magnetization. Secondly – and this is of practical importance – only water is hyperpolarized. If ligands were to be directly polarized, the resulting polarizations would vary tremendously due to different polarizability and relaxation of individual ligands. Additionally, many ligands tend to aggregate at elevated concentrations and could clog the transfer line from the polarizer to the magnet. Therefore, polarizing the water enhances the robustness and reproducibility of the method considerably. Thirdly, magnetization from water is not only transferred to the ligand, but also very efficiently to the protein. This allows observation of protein signals, enabling one to assess the protein integrity in the same experiment.

Experimental setup. The first step in the waterLOGSY experiment is to prepare the system by quenching coherent magnetization on ligands and protein, leaving only the water magnetization conserved along the z-axis. This can be done by means of soft pulses, WATERGATE pulse trains or by taking advantage of selective radiation damping of water [67,69,70]. Next, NOEs are allowed to evolve and transferred magnetization to build up during a mixing period of typically 0.8–1.2 s, after which the ligand signals are read by a 90° pulse and appropriate water handling. Interestingly, if the water magnetization is conserved by means of a flip-back scheme, there is no need for a relaxation delay before the next scan, as practically the same water magnetization is available after the scan as before it. A second scan with inverted starting magnetization, which is needed in order to subtract artifacts, can therefore be run directly after the first one, in a kind of double scan experiment. Only after this second, inverted, scan is a relaxation delay needed. In this way the waterLOGSY can be run in a time efficient way, that is in 5–10 min, spectra with sufficient signal-to-noise can be acquired [69].

Practical pitfalls and necessary controls. **Exchangeable protons:** As with all other experiments, negative control experiments with the free ligand are needed, not only to detect self-aggregation of the compounds but also to identify positive signal from protons exchanging with water, which lead to strong positive signals.

Buffer signals: Buffer and DSS signals provide a handy control for detecting general micelle formation or compound aggregation. These signals should always be negative; if they become weak or even positive, this is a strong indication that some type of aggregation is occurring in the sample.

NOEs between ligands: ILOE and INPHARMA. There is yet another class of NOE-based ligand-observed experiments: Inter-ligand NOEs (ILOE) and inter-ligand NOE for pharmacophore mapping (INPHARMA). We consider these to be experiments for characterization of ligand binding modes rather than experiments for validation of protein ligand interactions, which is why they lie at the limit of the scope of this review and are not discussed in depth.

In these experiments, an NOE between a previously well-characterized ligand and test ligands is measured. Such an NOE between two ligands can occur essentially in two ways: (i) A second ligand binds in close proximity to the first, i.e. they bind simultaneously to different sub-pockets of a large binding site (ILOE) [71]. (ii) Both ligands bind sequentially to the same pocket and magnetization transfer is mediated via the protein. The first ligand transfers magnetization to protein nuclei in the binding pocket. Once the first ligand has left and been replaced by the second ligand at the same binding site, magnetization from the protein is then transferred to the second ligand. This leads to an apparent NOE from the first to the second ligand (INPHARMA) [72–74].

Both experiments yield information on the binding mode of the second ligand, if the binding mode of the first ligand is known. The ILOE experiment is reasonably sensitive; it is similar to a transferred NOE experiment, but intensities are attenuated if the occupancy of the first (known) ligand is below 100%. An additional limitation is that the two ligands need to approach each other to within less than 5 Å. The ILOE experiment has been used for screening large mixtures of compounds (up to a hundred), even without a known ligand in the mixture [75]. Compounds binding to the protein in close proximity of the first ligand will obtain a transferred NOE from the first ligand and can thereby be identified. The INPHARMA experiment is less sensitive, as the NOE between the ligands is indirect and behaves in a similar way as spin diffusion [73]. Additionally, both ligands need to bind in fast exchange and the relative concentrations of each should be adjusted in order to obtain similar occupancy (p_B) of the binding site for both. Hyperpolarization has been used as means to improve sensitivity of the method [76]. In summary, these two experiments each have their "niche" for applications, and can yield highly valuable information on the binding mode of a ligand in the right circumstances, but they do not represent general methods for screening or validation.

2.2.4. Chemical shift-based approaches

Direct observation of chemical shift changes on the ligand. The chemical shift is an exquisitely sensitive probe for specific binding as it depends on the chemical environment of a ligand (Fig. 4). It is a parameter that is complementary to the relaxation effects that are exploited by the other ligand-observed experiments discussed up to this point. It has no dependence on the size of the protein or its proton density, and it therefore enables studies of small proteins as well as RNA or exotic targets that are not biomolecules.

However, in the setting of a large ligand excess, the ligand chemical shift becomes a rather insensitive probe of binding. Depending on the interaction, chemical shift changes can be quite subtle: consider a case where the free and bound states differ by 0.1 ppm, that is, 60 Hz on a 600 MHz spectrometer. In fast exchange the resulting measured chemical shift will be a population-weighted average (Eq. (8b)). In a typical experimental setup where there is a 20-fold excess of ligand over protein, the population of the bound state will always be below 5%, so that the resulting change in chemical shift will be smaller than 3 Hz.

This might seem trivial to detect, but in practice many false positives will result from an analysis of such small chemical shift changes, which may also arise, for instance, from slight changes in pH or temperature. Therefore, for chemical shift based detection of ligand binding, the fraction of bound ligand should be increased, inevitably leading to a requirement for more protein or longer measurement times. Direct observation of chemical shifts is best applied in equimolar mixtures as discussed further below (Section 2.2.7). Recently, however, an indirect method was brought forward that translates chemical shift changes into prominent changes in the spectra. This is based on using long-lived states.

Amplifying the response to chemical shift changes using long-lived states. Using appropriate spin state manipulations, it is possible to create very slowly relaxing spin populations. These so-called long-lived states (LLS) can have relaxation times up to hundreds of seconds [77,78]. A long-lived state can be achieved by creating equivalence between two coupled spins by continuous irradiation at a frequency exactly at the center between the two resonance frequencies of the nuclei involved. As long as this condition is fulfilled, a long-lived state can exist. If an LLS is created on a ligand in its free state, it will yield a strong signal, even after a long relaxation delay, because if the proper rf-irradiation is maintained, it will relax only very slowly. If the same ligand now binds to a protein, the chemical shifts of the nuclei change. This means the rf-irradation is no longer centered between the two chemical shifts, and the long-lived state breaks down, leading to normal, much faster relaxation of the ligand. In the resulting spectra, signals of the binding ligands will disappear or be strongly attenuated [79,80]. The sensitivity of this experiment can be further enhanced by coupling it with hyperpolarization [81].

Molecules suited for experiments exploiting LLS should therefore contain two coupled spins, which have similar chemical shifts, in order that equivalence can be achieved by a spin-lock at their center frequency. In practice, geminal aliphatic protons and ortho-related aromatic protons have been used for creating LLS.

LLS can be used to strongly enhance the response to a binding event. However, the underlying mechanism is still the chemical shift change of the ligand upon binding to a protein, which is not among the strongest effects of binding. Therefore, the amplified response makes it easier to identify a binder, but the binding assay is not more sensitive in terms of required protein concentrations. Ideal applications may therefore be in computer-based analysis of spectra, where clear-cut effects simplify analysis by computer algorithms.

In principle, chemical shift changes can also be enhanced by labeling the protein with a lanthanide with anisotropic paramagnetic properties. These metals act as pseudocontact shift (PCS) inducing agents, and, interestingly, this effect depends on r^{-3} [82–84]. Therefore, it is a long range effect and has no dependence on the tumbling time of the molecule, as distinct from the SLAPSTIC method, potentially enabling studies of even small peptides as targets.

Practical pitfalls and necessary controls. **pH changes:** General pitfalls of chemical-shift based methods are changes in pH and temperature, which can lead to chemical shift changes that are erroneously attributed to binding effects. Changes in pH can be avoided by using well-buffered solutions (20–50 mM buffer within 0.5 pH units of its pK_a). Additionally, it is possible to monitor pH in the NMR tube, by using substances with pH-sensitive resonance lines like imidazole or Tris. If a change in the pH-sensor resonance

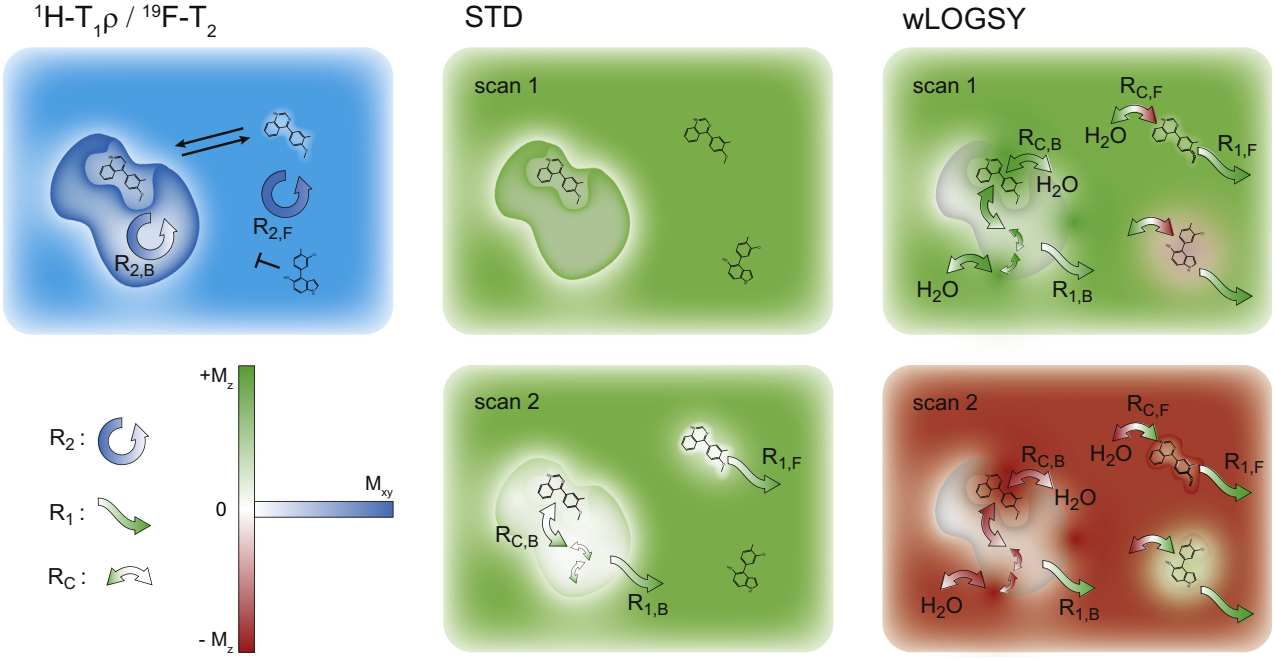

Fig. 8. Schematic drawings of relaxation mechanisms relevant for different ligand-observed experiments. All schemes follow the architecture explained on the upper left panel. On the left hand side, a protein is depicted with a bound compound. The compound is in exchange with its free state in the upper right, as indicated by double arrows. A second compound is shown on the lower right, which does not interact with the protein, as indicated by the blocked line. Proteins and compounds are surrounded by water. The colors of the proteins, compounds and water represent their – idealized – magnetization after the relaxation period in each experiment. The color scale for each experiment is shown on the bars on lower left, where the colors encode longitudinal (+M_z green, −M_z red) and transverse magnetization M_{xy} (blue), respectively. Relaxation leads to changes in magnetization. The different relaxation processes are shown by filled arrows: thus transverse relaxation (R_2) leads to the attenuation of transverse magnetization (blue to white), cross-relaxation (R_C) can lead to exchange or enhancement depending on whether it occurs in the bound or free states. Only the most relevant relaxation pathways are shown, and the effects are exaggerated. Thus ^{1}H-T$_1\rho$ and ^{19}F-T$_2$ result in the binding compound carrying less transverse magnetization than the non-binding compound. In the other two experiments, the differences in longitudinal magnetization are obvious. For a more quantitative description of relaxation processes see Fig. 9.

Table 2
Rate equations, initial conditions and time evolution of magnetization in different ligand-observed experiments. The basic rate equation for the magnetization is shown again on top of the table (Eq. (21)) [29]. For its derivation see Section 1.3. Rate equations for the individual experiments are derived by inserting the initial conditions and appropriate relaxation rate constants into Eq. (21). Integration of the rate equations yields the time evolution of the magnetization. The relaxation rate constants that are relevant for each experiment are given in the last column (see Table 1 for their exact form). In the lower part of the table, formulas for NOE-based experiments are shown.

$$\frac{dM_L(t)}{dt} = -R_L\left(M_L(t) - M_L^{eq}\right) - R_C(M_L(t) - M_P(t)) \quad (21)$$

Experiment	Initial conditions	Rate equation	Time evolution		Relaxation rates		
T_1	$M_{z,L}(0) = 0$ $M_{z,P}(0) = 0$	$\frac{dM_L(t)}{dt} = -R_{1,L}(M_L(t) - M_L^{eq})$	$M_{z,L}(t) = M_{z,L}^{eq}(1 - e^{-R_1 t})$	(22)	$R_{1,avg} = p_F R_{1,F} + p_B R_{1,B}$		
T_2 $T_1\rho$ CPMG	$M_{xy,L}(0) = M_z^{eq}$ $M_{xy,P}(0) = M_z^{eq}$	$\frac{dM_L(t)}{dt} = -R_{2,L}(M_L(t) - M_L^{eq})$	$M_{xy,L}(t) = M_{xy,L}(0)e^{-R_2 t}$	(23)	$R_{1\rho}^{SL} = R_{2,avg} + \frac{(\omega_F - \omega_B)^2 p_F p_B}{k_{ex}} \times (\sin\Theta_{rf})^2 \frac{k_{ex}}{k_{ex}^2 + \Omega_{SL}^2}$ $R_2^{CPMG} = R_{2,avg} + \frac{(\omega_F - \omega_B)^2 p_F p_B}{k_{ex}} \times \left(1 - \frac{2\tanh\left(\frac{k_{ex} t_{CPMG}}{2}\right)}{k_{ex} t_{CPMG}}\right)$	(24) (25)	
Diffusion	$M_{xy,L}(0) = M_z^{eq}$ $M_{xy,P}(0) = M_z^{eq}$	$\frac{dM_L(t)}{dt} = -R_{Diff}(M_L^{eq})$	$M_{z,L}(t) = M_{xy,L}(0)e^{-(R_{Diff} t_D)}$	(26)	$R_{Diff,avg} = p_F R_{Diff,F} + p_B R_{Diff,B}$	$t_D = t - \frac{\delta}{3}$	(27)

Experiment	Initial conditions	Rate equation	Time evolution		Relaxation rates	
STD scan 1	$M_{z,P}(t) = 0$ $M_{z,L}(0) = M_z^{eq}$	$\frac{dM_L(t)}{dt} = -R_{1,L}(M_L(t) - M^{eq}) - R_C(M_L(t))$	$M_{z,L}(t) = M_{z,L}^{eq} - M^{eq}\frac{R_c}{(R_1 + R_c)}(1 - e^{-(R_1+R_C)t})$	(28)		
scan 2	$M_{z,P}(t) = M_z^{eq}$ $M_{z,L}(0) = M_z^{eq}$	$\frac{dM_L(t)}{dt} = 0$	$M_{z,L}(t) = M_{z,L}^{eq}$	(29)	$R_1 = p_F R_{1,F} + p_B R_{1,B}$ $R_C = p_B R_{C,B}$	(30)
wLOGSY scan 1	$M_{z,H_2O}(t) = M_z^{eq}$ $M_{z,L}(0) = 0$ $M_{z,H_2O}(0) = M_z^{eq}$	$\frac{dM_L(t)}{dt} = -R_{1,L}(M_L(t) - M^{eq}) - R_C(M_L(t) - M^{eq})$	$M_{z,L}(t) = M_{z,L}^{eq}(1 - e^{-(R_1+R_C)t})$	(31)	$R_1 = p_F R_{1,F} + p_B R_{1,B}$ $R_C = p_F R_{C,F} + p_B R_{C,B}$	(33)
scan 2	$M_{z,H_2O}(t) = M^{eq} - 2M^{eq}e^{-R_{1,H_2O}t}$ $M_{z,L}(0) = 0$ $M_{z,H_2O}(0) = -M_z^{eq}$	$\frac{dM_L(t)}{dt} = -R_{1,L}(M_L(t) - M^{eq})e - R_C(M_L(t) - M^{eq} + 2M^{eq}e^{-R_{1,H2O}t})$	$M_{z,L}(t) = M_{z,L}^{eq}\left(1 - \frac{R_1 - R_C - R_{1,H_2O}}{R_1 + R_C - R_{1,H_2O}}e^{-(R_1+R_C)t} - \frac{2R_C}{R_1 + R_C - R_{1,H_2O}}e^{-R_{1,H_2O}t}\right)$	(32)	$\tau_{c,eff} = \frac{\tau_c \tau_r}{\tau_c + \tau_r}$	(34)

R_{avg}: Average relaxation rate ($p_F R_F + p_B R_B$)(s^{-1}).
R_C: Eq. (15).
R_2: Eqs. (13) and (14).
t: Relaxation time (s).
M_L, M_P: Ligand and protein magnetization, respectively.
M_{xy}, M_z: Transverse and longitudinal magnetization, respectively.
M_{H_2O}: Magnetization of water.
τ_r: residence time of water (s).
R_1: Table 1, Eq. (17).

is observed, chemical shift changes on the ligand need to be interpreted with considerable caution [85].

Temperature changes: There are also currently several solutions for temperature monitoring within the sample. They are based on temperature-sensitive resonance lines of labile protons, as for example in water or in the traditional temperature calibration substances methanol and glycerol. These particular resonances have a strong dependence on temperature, which can be revealed by comparison to temperature-insensitive signals from aliphatic methyl groups like in the DSS reference signal. However, it is not always practical either to add such a substance or to analyze the difference in chemical shift between signals in order to monitor the temperature. For protein-ligand samples there is an elegant automated way of controlling temperature using the deuterium lock-channel. In typical samples there is 10% ^2H_2O as well as 0.5–2% $^2H_6$-DMSO. Of these, ^2H_2O shows a strong temperature dependence and the methyl groups of DMSO are practically insensitive to temperature changes. The difference between these two signals can therefore be used to determine accurately the temperature in the sample [56,57]. An automated procedure for calibration and monitoring of temperature based on these substances is implemented on some modern spectrometers (“NMR Thermometer”, Bruker).

2.2.5. Diffusion based approaches

A ligand that interacts with a protein will experience reduced translational diffusion. The diffusion coefficient D (Eq. (6)) depends on the third root of the mass, therefore a 300 Da ligand will have a roughly 6-fold higher diffusion coefficient compared to a 30 kDa protein. In fast exchange binding, the resulting diffusion coefficient will be a population-weighted average. As noted in Section 1.2, diffusion is therefore not as sensitive to binding events as the other

relaxation effects described so far (Fig. 5), meaning that relatively large amounts of protein are needed to induce clear effects on a ligand. For example, for an interaction having a K_D of 100 μM, in order to induce a 2-fold change in (apparent) relaxation rate when using 200 μM ligand, the approximate protein concentrations would need to be 10 μM for NOE-based experiments and 40 μM for diffusion based experiments.

Interestingly, while NOE or other relaxation effects are different for each nucleus in a molecule, diffusion is the same for all. Translational diffusion is therefore the only effect where there is a straightforward correlation between binding strength and the size of the observed effect.

Diffusion is measured in NMR by spatial encoding of the position of a molecule in the sample by means of local changes in the magnetic field, which after a given time are reversed. Molecules that stay at the same location will have refocused signals with full intensity after the experiment. Molecules that diffuse away from their original position will not experience the same field after application of the reversed gradient, so their signals will only be partially refocused, leading to reduced signal intensity (Eq. (26)). In practice, this is achieved by applying magnetic field gradients, typically along the z-axis, followed after a delay by application of a second gradient with the same strength and duration as the first but with inverted sign. The extent to which the signal is reduced will depend on the strength of the gradients and the delay between them, in addition to rate of solute diffusion. For comparison with the relaxation effects described above, an artificial relaxation rate can be formulated, which depends on gradient strength (Eq. (19)).

Experimental setup. Experiments suited for diffusion measurements are 1D pulsed field gradients – stimulated echo (PFG-STE) sequences [86]. For determining ligand binding, a reference spectrum of the free ligand is first recorded, followed by protein-ligand spectra at two different delay times between gradients. In contrast to all other experiments discussed, here, an increase in signal is expected upon binding to the protein, as the bound ligand will diffuse more slowly, therefore staying closer to its original position where it will experience a full refocusing gradient. On the other hand, transverse relaxation effects during gradients and during water suppression schemes will act against the signal increase. Unfortunately, transverse relaxation is enhanced for binding ligands, leading to broad signals of low intensity somewhat compromising the effects. Additionally, while line broadening in the intermediate exchange regime is a welcome enhancement for R_2-based methods, here it is unfavorable for the experiment. Therefore, 1D PFG-STE experiments are further limited to fast exchange kinetics ($k_{ex} > 10^4\ s^{-1}$).

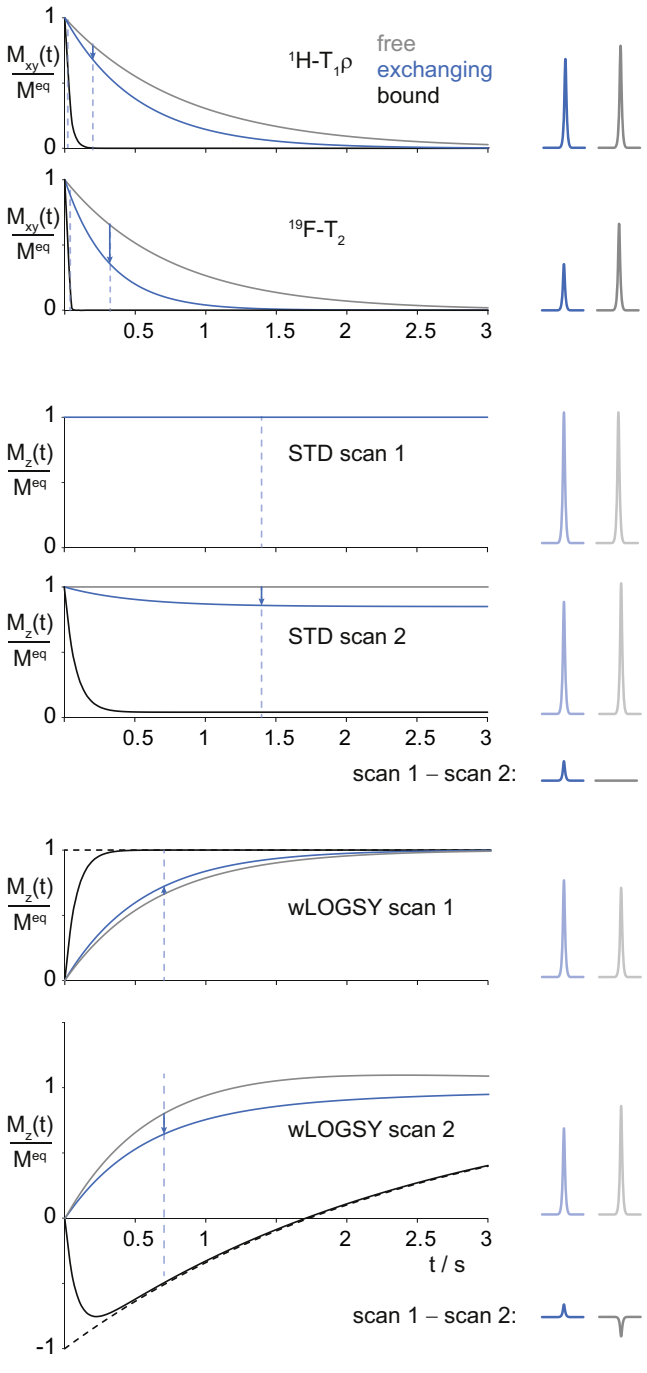

Fig. 9. Time evolution of ligand signals in different ligand-observed experiments. Equations from Table 2 were used to calculate the time evolution of free and fully bound ligands (grey and black lines, respectively). The blue line represents the magnetization of a fast-exchanging ligand with a K_D = 200 μM. In this setup the fraction of bound ligand is 2.5%. Simple population-weighted averages were used for the relaxation rates, without considering exchange effects. The vertical blue arrows depict the magnitude of the "binding effect" compared to free ligands. They are placed at typical durations of the relaxation delay. For the waterLOGSY scheme, the dashed black line represents the time course of the water magnetization. On the right, theoretical signals of the individual scans are shown for non-binding (grey) and binding (blue) ligands. The signals are observed at the time indicated by the grey dashed line in the diagrams. To assess binding effects, signals at short and long relaxation times are compared for R_2-based experiments: 10 and 200 ms for ^{1}H-T$_1\rho$, 20 and 320 ms for ^{19}F-T$_2$. For the NOE-based STD and wLOGSY experiments the differences of two scans are used to assess binding. The following experimental conditions were assumed: 200 μM of a 300 Da ligand, 10 μM of a 30 kDa protein, and K_D = 200 μM. The following relaxation rates were used: R_2(DD) free = 1.2 s^{-1}, bound = 31 s^{-1}; R_2(CSA) free = 1.3 s^{-1}, bound = 77 s^{-1}; R_1 free = 1.7 s^{-1}, bound = 0.5 s^{-1}; R_C free = −0.6 s^{-1}, bound = 12 s^{-1}; $R_{1,H2O}$ = 0.4 s^{-1}; $\tau_{r,H2O}$ = 0.1 ns. A number of simplifications were used: only the relaxation during the relaxation delay is considered. Thus R_2 is neglected during handling and preparation of the magnetization of water, while complete relaxation is assumed between scans. For T$_1\rho$ and ^{19}F-T$_2$, the traces represent the minimal relaxation effect because exchange effects are neglected. If exchange effects are considered, stronger relaxation with a stronger concomitant signal reduction is expected for binding ligands. For STD experiments, full saturation of the protein is assumed, leading to calculated effects that are stronger than would be observed in practice. On the other hand, if measurements are carried out in D_2O, R_1 of the free state and of the protein will be lower, therefore the calculated effects are weaker than would be observed in practice. For waterLOGSY, an arbitrarily long residence time of water molecules associated with the protein is assumed, while for the free state, a residence time of water on the ligand of 0.1 ns is used. This leads to a overestimation of R_C (bound). The same distance to the closest proton was assumed for all dipolar relaxation mechanisms. However, for T$_1\rho$ the nearest proton is usually on the same molecule, while for STD and waterLOGSY, the relevant nearest proton is on the protein and water, which on average will be further away.

A way around the complications due to transverse relaxation is offered by two-dimensional DOSY experiments, where the diffusion coefficient is encoded in the indirect dimension [87]. However, 2D DOSY experiments require much longer measurement times. Taken together with the relatively high protein requirement, DOSY experiments are therefore not suited to be used as high-throughput assays for screening.

Practical pitfalls and necessary controls. **Temperature homogeneity:** For DOSY-type experiments it is essential that the temperature is highly homogenous along the entire sample volume. If there is a temperature gradient, molecules at the top and the bottom of the tube may have different diffusion coefficients, and, even worse, a temperature gradient may lead to convection. Therefore, equilibration of the sample is an essential pre-requisite for such measurements. As a rule of thumb, equilibration time in minutes should equal the sample diameter in millimeters; a 5 mm tube should be equilibrated for 5 min before DOSY experiments are started.

Constant delays: T_1 and T_2 relaxation during PFG-STE experiments can theoretically be accounted for using proper formulas [87]. In practice, however, it is advisable to keep delays constant and increase gradient strength according to a pre-defined scheme.

2.2.6. Summary of ligand-observed experiments

Ligand-observed experiments rely on different relaxation mechanisms. In Fig. 8, the relevant relaxation mechanisms for the most popular experiments are shown. How these relaxation rates give rise to the signal intensity is mathematically described in Table 2. Finally, the time course of magnetization in these selected ligand-observed experiments is shown in the diagrams of Fig. 9.

2.2.7. Equimolar format

In order to obtain the largest possible effects on a ligand, the protein should actually be used in stoichiometric amounts or even in excess. In this way the fraction of bound ligand (p_B) is maximized, and hence so also are the observed binding effects. Since proteins are usually the most expensive components, this format is not used for screening of many ligands. However, such an "equimolar format" – that is, using equimolar amounts of protein and ligand – is much more versatile. It can reveal very weak as well as very strong interactions even on small targets (MW < 15 kDa), regardless of the binding kinetics, and therefore overcomes the shortcomings of the methods described above based on using large excess of ligand. The range of application and limitations of experiments are discussed more deeply in Section 3.1.

In principle, the methods described for use with excess ligand can all be applied in equimolar format, however, in terms of sensitivity and typical fields of application, only chemical shift and transverse relaxation based experiments are usually employed, using excitation sculpting or $T_1\rho$ pulse sequences.

An additional advantage of equimolar experiments is that usually protein signals are detectable due to the long measurement times. This allows assessment of protein integrity and sometimes even binding effects on the protein can be observed.

Chemical shift based approach. In the equimolar format, the fraction of bound ligand is high enough for chemical shift based assays to be sufficiently sensitive to detect even weak ligands with K_D - $\geqslant$ 1 mM. Additionally, there is no lower size limitation or special requirement for the target biomolecule and there is no strong constraint on ligand solubility. This experiment is thus the most generally applicable ligand-observed NMR assay. It comes, however, with relatively high requirements for measurement time (typically 20 min to 1 h per sample) and slightly higher protein consumption than experiments based on excess ligand. An additional complication comes from the presence of intense protein signals, especially for small proteins, as the protein is present in equimolar amounts (typically 20 μM). By subtracting a reference spectrum of the protein alone in the same buffer, usually a good interpretation of ligand signals is possible; however, the usual subtraction artifacts can appear, although fortunately these are less pronounced on broad protein signals than on sharp ligand signals.

Transverse-relaxation based approach. In addition to changes in chemical shift, relaxation effects will also be accentuated in equimolar experiments, relative to those with ligand in excess. Therefore, much weaker binders can in principle be detected. On the other hand, for large proteins (MW $\geqslant$ 30 kDa), signals are difficult to interpret in the context of a non-ideal baseline after subtraction of the protein reference spectrum.

However, in the case of slow exchange this results in a spectrum, which essentially shows only unbound ligand, since bound ligand has much broader resonances. The signal intensity from unbound ligand in this spectrum can then be compared to the signal intensity of ligand in the absence of protein. If this intensity significantly decreases in the presence of protein, the ligand is binding to the protein. Since in slow exchange the signal of the free ligand directly reflects the fraction of free ligand, $p_{L,F}$, this is a very powerful technique for ranking high-affinity ligands [88].

Practical pitfalls and necessary controls. **Subtraction artifacts:** Perfect subtraction of protein signals can be difficult. Experimentally, it is sometimes possible to quench fast relaxing protein signals by using $T_1\rho$-type experiments. However, this will also significantly reduce ligand signal intensity. Therefore, in most cases subtraction of protein signals will be the preferred option. In order to reduce subtraction artifacts to a minimum, a single protein stock solution should be prepared, which is used without further dilution for the protein reference spectrum and all subsequent protein-ligand spectra. The same amount of DMSO needs to be added to the protein reference spectrum as will be present in the protein-ligand spectra. All measurement parameters between different samples should be identical or as similar as possible, including equilibration times before measurements. It is additionally advisable to control temperature as tightly as possible, by using for example in situ temperature-sensitive lock substances (NMR thermometer, Bruker).

Precise ligand concentration: When reductions of ligand signals are monitored, it is essential that samples of ligand alone and ligand in the presence of protein contain exactly the same amount of ligand. This can be monitored by comparing the intensity of the residual DMSO proton signal from the compound stock solution in the two samples. Alternatively, ligand solutions in buffer can be prepared that are divided and protein or buffer is added to them. This will come at the expense of subtraction artifacts in the protein spectra, but will ensure more accurate determination of ligand binding. This is especially important in the context of ranking of different high-affinity ligands [88].

Protein concentration: Equally, the protein concentration must be precisely known, especially for ranking experiments. The protein concentration should be equal to or slightly above the ligand concentration. For mixtures of ligands the protein concentration should be equal to or above the sum of ligand concentrations. For methods on how to determine protein concentrations, see Section 2.3.1.

Disappearance of signals: If signals are broadened beyond detection, it is only safe to interpret this as implying binding if the reference sample and the sample with protein were prepared by splitting the same mother solution of compound in buffer and then protein was added to only one of the samples.

2.2.8. Competition formats

A great deal of additional information can be gained when using known ligands of the protein in competition with unknown (target) ligands. Two main formats of such experiments can be distinguished. In the first one, the "competitor" format, a known *strong* binder is added to a protein-ligand mixture with the aim of displacing the ligand under study. In this format the target ligand signals are observed and one looks for reversed binding effects, that is, released free target ligand. The competitor does not necessarily need to be detected. In the "reporter" format, a known *weak* binder is used, with the aim that the target ligand will displace the reporter. Here, one looks for reduced binding effects on the reporter. The signals of the target ligand do not need to be observed, therefore labeled reporter ligands are often employed in order to obtain simplified spectra.

Competitor/Displacement experiments. A competitor is usually a well-characterized specific binder that will saturate a protein binding site at rather low concentrations. It can be an organic molecule, or a peptide, protein or other biomolecule.

The traditional ligand-observed experiments are run with three samples. A reference spectrum of the ligand alone, a "binding" spectrum with protein and ligand and finally the competition experiment after addition of the competitor molecule. If ligand signals show binding effects in the presence of protein, and if these are abolished or reduced after addition of the competitor, this is a strong indication of specific binding at the same site as the competitor.

Competition in equimolar format. Competition experiments in the equimolar format do have an additional advantage as they enable relative ranking of the binding strength of tight binding ligands, which are very difficult to rank with other NMR assays. Ligands with $k_{off} < 10\ s^{-1}$ cannot be observed with traditional ligand-observed techniques (Fig. 12), and in protein-observed experiments the potency of ligands with K_Ds much below the assayed protein concentration cannot be discriminated. In equimolar assays, two compounds can be added in stoichiometric amounts to the protein, so that the concentrations of the two compounds and the protein are all the same, for example 20 μM. The ligand with the larger fraction of displacement is then identified as the weaker one.

Reporter assays. NMR reporter screening refers to NMR-based competition assays using a weakly binding competitor ligand [89,90]. Rather than directly observing binding of the target ligand, the ability of the target ligand to displace a known, low-affinity "reporter ligand" is monitored. By using reporter screening, strong binding of a target ligand can be detected (by strong displacement of the reporter ligand) which could not be detected by ligand observation methods (Fig. 12).

Reporter screening not only confirms or disproves binding of a target ligand, but also yields its quantitative binding affinity relative to the reporter ligand: Strongly binding ligands lead to large or full displacement of the reporter ligand, whereas weakly binding ligands will only partially displace the reporter ligand [89].

With reporters the most sensitive NMR experiments can be exploited, which usually require some kind of label on the ligand. For example, fluorinated molecules are among the most popular reporters, offering the possibility of employing very low protein concentrations in ^{19}F-T_2 experiments. Also reporters with a ^{13}C label or less commonly with ^{15}N labels are used. ^{13}C is often easily introduced into a molecule using the readily available reagents $^{13}CH_3I$ or ^{13}CHO. Additionally, the more recently introduced concept of LLS may provide excellent reporter assays. Here, a molecule with a suitable group of coupled protons is needed. Another area where the reporter format can exploit very high sensitivity is in combination with DNP. Here, it is always the same reporter ligand that is hyperpolarized, leading to reproducible and comparable results. In the case of fluorinated reporter ligands, where the spectra consist of a single fluorine resonance, a T_2 decay of the fluorine signal can easily be directly measured, allowing indirect assessment of the affinity of the test ligand. In this way, the information content of the experiment is increased [91].

Practical pitfalls and necessary controls. **Presence of competitor:** The competitor format provides a very robust experiment. Only the presence of the competitor in the sample needs to be confirmed in some way, either by observation of its signals or by increase of the residual DMSO proton signal after addition of the competitor stock solution. The exact amount of competitor is less important, provided it saturates the protein binding site. If the competitor is a large biomolecule, an additional control needs to be run in order to exclude competitor binding to the target ligand.

Reproducible reporter concentration: Reporter experiments require much more careful set up. Since reporter signal intensities will be interpreted, it is essential to have exactly the same concentration of reporter in each sample. Therefore, a large stock solution of protein and reporter is prepared and distributed into individual tubes. The ligands to be studied are only added afterwards. Only in this way are samples properly comparable.

Positive and negative controls for reporter experiments: It is further important to include positive and negative controls at the beginning and end of an experimental series. A negative control consists of reporter and protein with DMSO and shows maximal binding effects on the reporter. In the positive control a potent competitor is added to obtain a significant displacement of the reporter. If many samples are screened, it is advisable to run a positive and negative control after every 10th sample or so. This defines the range of expected signal intensities for binders and non-binders and provides some statistics on the variability of the experiment. Most importantly, the negative controls, which should always show binding of the reporter, are very informative by indirectly monitoring protein integrity.

Further controls depend on the experiment that is chosen for the reporter or competition assay, as described in the respective sections above.

Solubility of competitors and reporters: By adding a further component to the sample, there are additional risks of co-aggregation of either ligand or protein with the competitor or reporter. Therefore competitors and in particular reporter molecules need to have favorable solubility and should be added at concentrations well below their solubility limit, in order not to precipitate readily, even in highly crowded protein-ligand solutions.

Site specificity: In general, competition formats have the weakness of only probing one binding site, or allosterically connected binding sites on a protein. This need to be kept in mind when analyzing these experiments and drawing conclusions: the lack of displacement of a reporter ligand does not necessarily mean that the test compound does not bind at all.

Protein denaturation: Compounds that denature the protein can release the reporter ligand by this mechanism, which could be wrongly interpreted as displacement by binding.

2.3. Protein characterization: Identity, Integrity and Concentration

2.3.1. Determination of protein concentration

Protein concentration could in principle be measured ab initio by NMR using methods like pulcon [35]. In practice, however, it is much more convenient to use ultraviolet (UV) spectroscopy for initial concentration determination of a protein stock solution

and then compare NMR spectra to a reference spectrum of a solution of known concentration.

Proteins have several UV-absorbing groups, aromatic side chains with absorption maxima at 276 nm and the backbone amides with maximal absorption at 215 nm. The extinction coefficient at 276 nm can be calculated for each protein and depends on the number of individual aromatic amino acids. This extinction coefficient is however only valid for the unfolded state of the protein. On the other hand, absorption at 215 nm only depends on the number of amide bonds and extinction coefficients are identical for all proteins. To measure concentration, absorption is compared to a reference protein of precisely known concentration, usually bovine serum albumin (Sigma-Aldrich Cat.-No. P0914) in the same buffer. For measurements at 276 nm, the different extinction coefficients of target protein and reference are factored in.

Therefore, for proper measurement of UV absorption, the protein needs to be denatured and contaminants need to be removed or subtracted by measuring blank spectra. The best-suited technical setup for this is reversed phase high-pressure liquid chromatography coupled with a UV detector (RP-HPLC-UV). In this setting, the protein is denatured by a low pH water-acetonitrile mixture containing tri-fluoro-acetic acid (TFA). Additionally, the chromatography column is heated to 80 °C. The protein is eluted from the column using a gradient towards higher acetonitrile content. Thereby, conveniently, contaminants and impurities are separated from the protein of interest and a clean UV chromatogram is obtained where the protein peak can be integrated. Using the value obtained from the reference protein, the protein concentration can be calculated accurately. At the same time the purity of the protein can easily be assessed from additional signals in the chromatogram.

Practical pitfalls and necessary controls. **Limited linearity of detectors:** UV detectors are linear only in a certain range. Therefore, the linear range needs to be determined initially by titration with a reference protein of known concentration. The protein of interest then needs to be diluted in order that the concentration is in the range where the response of the UV detector is linear.

Incomplete denaturation: Some proteins do not fully denature in the short time they are exposed to the HPLC solution. If a protein is known to be highly stable, pre-incubation with 6 M guanidine and 100 mM dithiothreitol or TCEP is advisable. The denaturant and reducing agent will be separated from the protein on the column and will not contribute to the protein peak in the chromatogram.

Cleaning of system: An injection of the same guanidine/DTT solution is used to clean the column from non-eluted traces of protein that could contaminate the next run.

2.3.2. Identification of the protein

Initially, the identity of a protein needs to be determined after purification by mass spectrometry (MS). After unambiguous identification of the protein construct, NMR spectra serve as reference due to the unique "fingerprint" of the resonances.

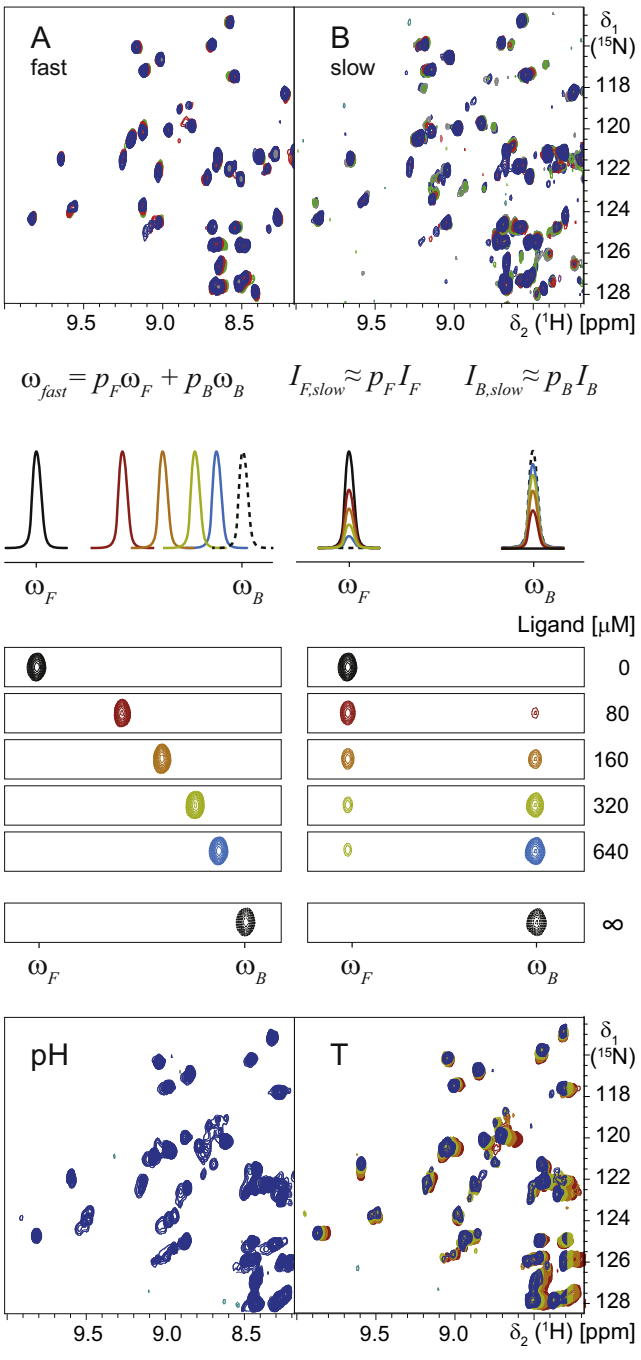

Fig. 10. Changes of protein spectra upon ligand addition in fast and slow exchange, as well as pH- and temperature-induced changes. In A, a ligand binding in fast exchange is added to the protein with increasing concentrations, leading to a subset of signals that are shifting towards the chemical shifts of the bound state. If the signals follow a curved rather than a straight line between ω_F and ω_B, this is an indication of binding to an additional secondary site [21,95]. In B a ligand binding in slow exchange is added at different concentrations, leading to a subset of signals with decreasing intensity, and new signals appearing at the chemical shift of the bound state. Here, yet an additional set of signals would appear, if the ligand binds to a second site. Below each spectrum schematic representations of a 1D trace of a protein signal and an excerpt of a 2D spectrum are shown for increasing concentrations of a ligand with a K_D of 100 μM. For the 2D signal, the chemical shift in the second dimension is set to be the same for bound and free protein. In the fast exchange case a single averaged signal is visible. Its chemical shift gradually changes from the chemical shift of the free state (ω_F) to the bound state (ω_B), according to Eq. (9b), which is reproduced here. The ligand concentration affects the bound fraction (p_B). From the position of the signal between ω_F and ω_B, the bound fraction p_B can be extracted, and K_D can be calculated (Eqs. (7b) and (7c)). The fully bound state of the protein (at arbitrarily high ligand concentration, dashed line) is experimentally not accessible in most cases, as ligands in fast exchange are typically rather weak. In the slow exchange case, two separate signals are visible at the chemical shifts of the free state (ω_F) and the bound state (ω_B). Here the intensity of the signals reflects the free and bound fractions. If the binding kinetics approach the intermediate exchange regime, the lines will be broadened according to the lifetime of the free and bound states (Eqs. (10a) and (10c)), and intensities no longer exactly reflect p_B and p_F. In the panels labeled "pH" and "*T*" at the bottom, shifts of signals induced by pH changes (pH 6.2, 6.8 and 7.4) and temperature (296–310 K) are shown, respectively. This is to emphasize that effects that are very similar to those of binding can be induced by pH and temperature changes.

Currently, most mass spectrometry setups consist of chromatography coupled to an electrospray ionization (ESI) chamber, from where ionized particles are accelerated through the mass spectrometer. This arrangement delivers good results in most cases.

Practical pitfalls and necessary controls. **Non-covalent modifications:** There are special cases where the concomitant denaturation of the protein represents a problem, for example if the protein carries a non-covalent prosthetic group. In that case matrix assisted laser desorption ionization (MALDI) may be a viable alternative, as here native proteins can be ionized and non-covalent complexes survive the treatment in most cases.

Inhomogeneous samples: Sometimes, inhomogeneous modifications of the protein can impair MS studies. This is often the case for multiply glycosylated proteins produced in eukaryotic expression systems. Here, the problem can be alleviated by digestion of the poly-glycans using enzymes like endoglycosydases on the partially denatured protein (PNGase treatment). In the most difficult cases, amino acid sequencing will be the technique of last resort in order to determine the identity of a protein.

2.3.3. Assessment of protein integrity

Once the concentration of a protein stock solution is determined and the identity of the protein confirmed, a reference spectrum is recorded. This protein reference spectrum will be used for comparison in order to confirm presence of the protein, its concentration and integrity in protein-ligand samples used for detection of interactions. For the purpose of assessing protein quality, 1D NMR experiments often yield sufficient information. Of course 2D experiments are superior. They are not considered at this stage but will be discussed in the section on protein binding effects below (Section 2.4.1).

The basis for assessing protein quality is the unique pattern of resonance signals that each folded protein displays. Even if only the lateral regions upfield of 0.5 ppm and downfield of 9 ppm are interpretable, due to often excessive overlap in the central parts of the spectrum, the identity, concentration and integrity of the protein can be assessed. Identity is confirmed by comparing the location of the resonance lines and the spectrum envelope to a reference spectrum. Concentration is reflected in the intensity of the signals. Broadening or disappearance of the signals can reveal aggregation. Finally, if regions of random coil chemical shifts are highly populated this is likely to be indicative of denaturation of the protein.

Experimental setup. There are again several 1D NMR experiments that are suited for recording spectra of the protein. For reasons of simplicity, the same experiment as for small molecules is used, that is the 1D ^{1}H experiment with excitation sculpting for suppression of the water resonance. It performs robustly in automation and several solvent signals (H_2O and DMSO) can easily be suppressed simultaneously. However, on must be aware of the compromises taken by choosing this experiment for proteins. The excitation sculpting scheme is relatively long (about 8 ms when using 2 ms soft pulses and 1 ms gradient pulses, and leaving away the perfect echo element, Fig. 18). For larger proteins this already leads to significant reduction in signal intensity due to transverse relaxation. A pre-saturation experiment would be best from the point of view of transverse relaxation, but saturated water protons exchange into the protein at labile positions and lead to saturation of the protein through NOEs and spin diffusion. Furthermore, pre-saturation is difficult to use in automation as it is very sensitive to small changes between samples. WATERGATE-type experiments are attractive because the delays during which magnetization is transverse are shorter, water is not saturated to the same extent as in pre-saturation experiments and they need still fewer parameters to be optimized (no soft pulse needs to be calibrated). However, we still prefer excitation sculpting-based experiments, because WATERGATE experiments do have broader suppression regions, a second solvent cannot easily be suppressed and in order to obtain a flat baseline the WATERGATE elements also need to be carried out twice using an excitation sculpting gradient and phase cycling scheme.

2.4. Protein binding effects

The ability to observe binding effects directly on the protein is one of the main strong points of NMR.

Binding is detected by chemical shift changes of the protein resonances induced by interactions with the ligand. These chemical shift changes originate from changes in the molecular microenvironment of nuclei, for example slight differences in the electron density, induced by polarization or deformation of molecular orbitals upon binding. This will already happen simply if water in a binding pocket is exchanged for a ligand. Conformational changes of the polypeptide can also lead to chemical shift changes, in particular if aromatic side chains of the protein are re-oriented. The latter cause changed magnetic fields over substantial distances, induced by ring currents in aromatic rings, and can cause very prominent changes in the chemical shift. A particularly important case of chemical shift change caused by protein-ligand interactions arises from insertion of an aromatic ring of the ligand into a binding pocket of the protein, leading to strongly distorted chemical shifts on the protein. Such ring-current shifts can be used to determine the orientation of the compound in the binding pocket, provided the compound ring-current effects can be separated from other chemical shift changes [92,93].

If assignments of resonances are available, the ligand-binding site of the protein can be approximately located. Also here, it is essential to be able to separate chemical shift changes stemming from direct interaction from those induced by allosteric conformational changes of the protein, which may happen far away from the actual ligand-binding site. For isolating direct from allosteric effects of ligand binding, cross-saturation experiments can be useful [94].

However, for the purpose of identifying and validating protein-ligand interactions – the scope of this review – no resonance assignments are needed. In practice, ligand binding is revealed by comparing a reference spectrum to a spectrum in presence of ligand. If there are changes in the resonance positions of a subset of protein signals, this is interpreted as binding (Fig. 10).

One complication arises from the kinetics of binding. In fast exchange, ligand binding to a protein will result in shifting of the resonances to a chemical shift value between those for fully bound and free protein; the number of protein signals stays constant, some signals just shift to new positions. Since the effective chemical shift position in fast exchange is a population weighted average (Eq. (9b)), the position between fully bound and free chemical shifts represent the fraction of bound protein (Fig. 10). In slow exchange, two populations of protein signals will emerge, one at the chemical shifts of the free protein and one at the chemical shifts of the bound protein (Eqs. (10b) and (10d)). The relative intensities of the two sets of signals will approximately represent the fraction of free and bound protein (Fig. 10).

The great advantage of protein-observed experiments is that protein integrity is revealed in the same spectrum as binding, and thus many false positives can be excluded from the start, without additional control experiments.

2.4.1. Experimental formats and isotope labeling

The general format of protein-observed experiments is to use a large excess of ligand over protein, in order to maximize binding effects; in other words the fraction of bound protein is maximized. Since proteins need to be employed at typically 20–50 μM in order to obtain sufficient signal-to-noise, ligands are added at concentrations of 200–500 μM (Fig. 13). This already illustrates an important weakness of the method: it is limited by ligand solubility, which often is below these values.

The protein signal can be recorded using simple 1D ^{1}H experiments in many cases. However, for larger proteins, the spectra become very crowded and only a few well-dispersed signals in the spectrum can be analyzed. If the protein can be produced with ^{15}N or ^{13}C isotopes incorporated either uniformly or at specific sites, that is usually the preferred option. The main factors influencing the choice of the isotope labeling pattern are protein size, expression system, available budget and prior structural knowledge of the protein.

Expression systems and available labeling patterns. The expression system is the main factor that determines which labeling patterns are available.

Nowadays, labeling protocols are available for the most important expression systems for structural biology, namely bacteria (species: *E. coli*, cell line: BL21), insect cells (*Spodoptera frugiperda*, sf9 and sf21; trichoplusa ni, Hi5; *Drosophila melanogaster*, S2), yeast (*Pichia pastoris*) and mammalian cells (*Cricetulus griseus*, CHO; *Homo sapiens*, HEK293), to give just a few examples [96,97]. However, with increasing complexity of the expression host, fewer options for isotope labeling patterns are available. In bacteria, an impressive wealth of labeling patterns are possible, starting from amino acid type specific labeling through uniform labeling with ^{15}N, ^{13}C and ^{2}H to various extents, to specific protonation of methyl groups on deuterated backgrounds, thus enabling studies in favorable cases of proteins ranging up to a size of 1 MDa [98,99].

In the special situation of drug discovery, most protein targets are of human origin and no bacterial homologs can be used as surrogates, and these complex human proteins often need to be expressed in eukaryotic cells. Typically, cytosolic proteins are expressed in insect cells and secreted ones in mammalian cells, whereas for membrane proteins both systems seem to work to a similar extent. This limits the available isotope labeling patterns somewhat.

Amino acid type specific labeling is possible in all these cell lines, thanks to vendors offering amino acid "drop-out media", where the original medium can be ordered with just one or several amino acids missing. The missing amino acids can then be replaced by labeled ones [100]. In general, amino acid type specific labeling works well for amino acids without roles in central metabolism. Asparagine, glutamine, aspartic acid and glutamic acid on the other hand are in general metabolized strongly; when these amino acid types are supplied to the cells in labeled form, the isotopes from them are distributed to other amino acids (label scrambling) and unlabeled forms of the amino acids are steadily synthesized by the cells leading to reduced incorporation (label dilution). Most other amino acids can be labeled without much scrambling, and if scrambling occurs it is mainly to just one other amino acid and at low intensity. In any case, often the goal is to put just some type of heteronuclear label onto the protein in order to be able to record 2D spectra, in which case scrambling is not an issue.

For uniform labeling, recently protocols have been published bringing down the cost per liter of medium to a few hundred USD for ^{15}N-labeling in insect cells [101–103]. Also, uniform ^{13}C and ^{2}H labeling are possible at roughly double that price. While incorporation levels of 80–90% can be reached for ^{15}N and ^{13}C, for ^{2}H incorporation is lower, rather in the range of 70% [100]. Still such a deuteration level has a strong impact on the spectrum, enabling studies of proteins much larger than 30 kDa [104]. Probably similar protocols are applicable to mammalian cells, implying that uniform labeling in eukaryotic cells will be a viable option in the near future.

Choice of labeling pattern. If the protein can be expressed in *E. coli*, usually uniform labeling is chosen, because it is less work-intensive than amino-acid type specific labeling. Then protein size will determine which labeling pattern should be used. For proteins <25 kDa, uniform ^{15}N and ^{13}C labeling have different advantages and disadvantages. U-^{15}N labeling is the least expensive labeling pattern and resonance assignments are more often available for ^{15}N than for ^{13}C nuclei. Additionally, ^{15}N labeled proteins are conveniently expressed in auto-inducing media [105–107]. In *E. coli* U-^{13}C labeling is approximately 10-fold more expensive. However, methyl groups labeled in this way provide exquisitely sensitive NMR probes. Protein consumption can often be lowered 4-fold compared to U-^{15}N labeled samples, and high quality spectra of methyl groups are easily obtained [108]. Furthermore, while spectral quality of backbone amide ^{15}N,^{1}H correlations decays strongly for proteins >30 kDa, methyl groups can yield excellent spectra even for large proteins up to 100 kDa. For proteins that are larger than these respective size limits for ^{15}N and ^{13}C detection, deuteration is necessary in order to obtain high quality spectra [109].

For eukaryotic cells it is usually easier to produce amino acid type selective labeled samples. Here, the price of individual isotope labeled amino acids can vary greatly. One of the most affordable labeled amino acids is methionine with a ^{13}C-labeled methyl group. This methyl group of methionine is ideally suited as an NMR probe, because it has very favorable relaxation properties and there are no scalar couplings to other carbons present. High-resolution spectra of ^{13}Cmethyl-methionine can thus easily be obtained even for large proteins with molecular weights approaching 100 kDa. Furthermore, the chemical shift of ^{13}C$^{\varepsilon}$-methionine methyl groups is very sensitive to ligand binding or conformational changes. The main caveat when using this labeling pattern for drug discovery is of course the need for at least one methionine to be close enough to the binding pocket of interest that its chemical shift is perturbed by ligand binding. However, in >20 target proteins, we have only once had a case that methionines were insensitive to ligand binding, and that was in a protein containing only two methionine residues.

Depending on prior structural knowledge of the target protein, other amino acid types may be chosen for use as isotope labeled NMR probes. If one particular pocket is targeted, if protein resonance assignments are not known it is convenient to assign individual amino acids by either mutagenesis or by dual labeling of a unique couple of amino acids [110]. Additionally, a different approach is offered by post-translational chemical labeling of reactive amino acid side chains like cysteine, lysine or even tyrosine. By using mutagenesis, a single site can then be labeled and used as a probe.

For RNA and DNA targets also, several labeling techniques have been established; for instance, solid phase chemical synthesis, in vitro translation using recombinant polymerases and in vivo expression of tRNA fusion constructs or DNA plasmids, from which the target nucleic acid sequence is excised using appropriate enzymes [96].

Experimental formats. For non-isotope labeled samples, only proton spectra can be recorded. In lucky cases, 1D spectra show isolated signals that can be interpreted. More time consuming is recording of 2D NOESY spectra, which however provide excellent fingerprints and coverage of the entire protein resonances. The

same is true for 2D TOCSY spectra, which are widely used in work with RNA as a target. In terms of throughput and coverage of the protein, we focus here on heteronuclear 2D correlation spectra for labeled proteins, which have high information content and are very time efficient.

There are dozens of NMR experiments for recording 2D heteronuclear correlations, each with individual advantages and disadvantages. In order to reduce complexity of the NMR setup, it is advisable to try to identify the smallest set of experiments that can yield high quality spectra with the majority of protein samples, with regards to their size and labeling pattern. The ALSOFAST-HMQC represents a good compromise because of its very broad range of applicability [111]. It offers higher sensitivity than conventional HSQC experiments and there are additional advantages for amino-acid selectively labeled samples. The experiment takes advantage of what has become known as the BEST or SOFAST effect [112]. Conventional HSQC experiments rely on R_1 relaxation to bring back the magnetization close to its equilibrium value between two scans. Since especially for large proteins R_1 is rather small, this is not efficient, as recovery to 90% of equilibrium magnetization can take up to four seconds for a 30 kDa protein. However, if nuclei in close proximity to the nucleus that is recorded are at equilibrium magnetization, cross relaxation will additionally become active; Eq. (21) describes this phenomenon (replace ligand and protein spins with two spins I and S of the protein, where I is the detected spin and S is kept at equilibrium along the +z-axis). The second term in Eq. (21) with R_C will become active because $M_{Iz} - M_{Sz}$ is no longer zero, as M_{Iz} will essentially be zero after acquisition and M_{Sz} will be at equilibrium. In large molecules, cross-relaxation is a much faster process than longitudinal relaxation; R_1 (Eq. (17)) and R_C (Eq. (15)) rates can be compared in Fig. 5. Therefore, equilibrium magnetization will be restored much faster if only a selected subset of nuclei is observed, and the magnetization of the rest of the protein and solvent nuclei is kept close to equilibrium.

To achieve this in SOFAST experiments, care is taken not to saturate protein resonances that are not observed, for example in a $^{15}N,^{1}H$ correlation spectrum, all protons that are not bound to nitrogen will be kept along the z-axis. In traditional SOFAST experiments this is achieved with soft pulses which selectively only excite the region between 6 and 10 ppm, where amide signals are expected. This has two slight disadvantages, in that signals close to the water line or far downfield are more difficult to observe, and because in selectively labeled samples, a considerable fraction of protein resonances are saturated even if only a few protons are observed; for example only 10 selectively labeled valine amides. The ALSOFAST-HMQC uses a spin state selection scheme with hard pulses for selection of the protons bound to the desired heteronucleus. This is achieved by simply changing the phase of the last pulse in the first INEPT step to x instead of y. This experiment is equally applicable to small or large proteins, and can be used to obtain either complete spectra of uniformly ^{15}N and ^{13}C labeled proteins, or of amino acid specifically labeled proteins – all with high sensitivity. Additionally, RNA imino signals that exchange strongly with the water give good signals, since water is not saturated. Therefore, with a $^{15}N,^{1}H$ and a $^{13}C,^{1}H$ version of the ALSOFAST-HMQC nearly all practical situations are covered.

However, for recording $^{15}N,^{1}H$ correlations of deuterated proteins with molecular weight above 30 kDa, a different experiment is preferable – the famous TROSY experiment. Against a deuterated background this experiment is more sensitive than the ALSOFAST-HMQC. The TROSY effect is discussed in great detail in several excellent reviews [12,113–115]. In short, narrow resonance lines can be obtained even for large proteins because the effects of

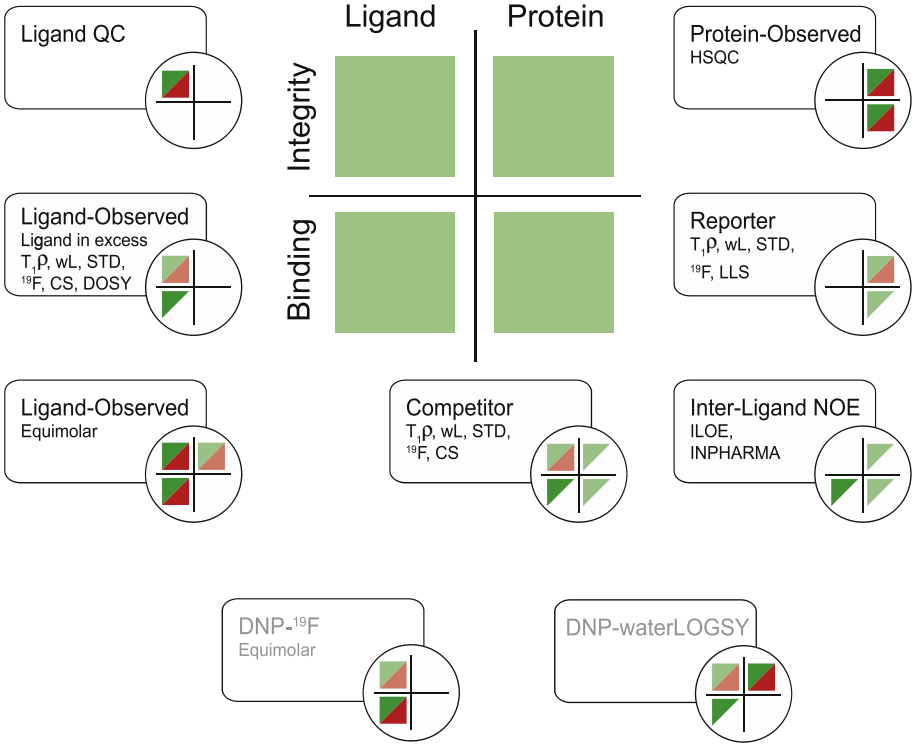

Fig. 11. Information content of individual NMR experiments depicted by "Validation Operators". An experiment can give information on a number of aspects of an interaction. For example a protein-observed experiment will reveal positive or negative binding effects on the protein, hence the experiment can define the color of the "protein binding" field as being dark green or red. At the same time, protein integrity is revealed in this experiment and thus it will also define the color of the "protein integrity" field. On the other hand, no information on the ligand integrity or on ligand binding effects is gained. Therefore, the color of the corresponding fields will not be defined by such experiments. For the detailed color code of the validation operators see Fig. 2.

two relaxation mechanism mutually cancel in this experiment. When considering a nitrogen in an amide of the protein backbone, there will be two dominant relaxation effects: It will have a strong R_2(CSA) term (Eq. (14)) due to the asymmetric binding pattern, which results in asymmetric electron density around the nitrogen nucleus, and in addition it will experience the magnetic field of the amide proton, which is at only 1 Å distance leading to an R_2(DD) contribution (Eq. (13)). With molecular tumbling, these two effects will fluctuate as a function of the different orientations that the molecule adopts. Depending on whether the proton spin is "up" or "down", the CSA and DD effects will either reinforce or oppose each other, respectively. Since the CSA is dependent on the square of the magnetic field strength (Eq. (14)), at a given magnetic field the CSA and DD effects will be of same magnitude, and can fully cancel for the amides where the proton spin is "down". In the TROSY experiment, those amides with proton spin "down" are selected, which in practice means selecting the downfield component of the doublet from scalar coupling. The same is done for the proton (for which, co-incidentally, roughly the same magnetic field is optimal for TROSY), leading to a signal, which is narrow because CSA and DD effects are partially cancelled out both for the nitrogen and proton signals of the amide.

When setting up the experiment, care should be taken not to saturate the water resonance. As in waterLOGSY, water protons can exchange into the protein at labile sites or influence protein spins via cross relaxation. If water is saturated, this saturation will be spread through the protein by means of spin diffusion, even if the protein is deuterated. Therefore, water flip-up pulses are used to keep the water magnetization along the z-axis close to its equilibrium value. With this treatment, water will only contribute to faster apparent T_1 relaxation and increase signal in the next scan similar as in the ALSOFAST experiment.

The TROSY experiment therefore enables one to obtain ^{15}N,^{1}H correlation spectra for proteins with molecular weights beyond 100 kDa.

Potential pitfalls and necessary controls. **Temperature and pH changes:** There are a number of factors that lead to chemical shift changes in protein observed spectra that can be mistakenly interpreted as binding effects. These particularly include changes in pH and temperature that were already discussed in Section 2.2.4. In order to identify pH or temperature induced shifts quickly, a series of protein spectra at different pH values and different temperatures can be measured. In this way the pH and temperature sensitive groups are identified. When experiments are performed at physiological pH, the titrating groups are usually amides in proximity to histidine side chains. Temperature sensitive signals are usually amides or other signals that exchange with water, since the water resonance is strongly affected by temperature changes. Actually, such a temperature titration can reveal involvement of amides in hydrogen bonds, which protect protons from exchange with bulk water [116]. In summary, if a similar pattern of shift changes is induced by a compound as with pH or temperature changes, then care should be taken to exclude the possibility that one of these two effects are the real cause of the observed shifts. Alternatively, statistical analysis methods have been proposed to identify spectral changes due to changes in sample conditions as opposed to changes due to ligand binding [117,118]

Excluding DMSO effects: Usually, compound stock solutions are prepared at 50 mM concentration in 90% d_6-DMSO/10% D_2O. When adding 500 μM compound to a protein solution, about 1% of DMSO is thereby added to the protein. In many cases such DMSO concentrations may induce small chemical shift changes on the protein signals. Therefore, reference spectra always need to be recorded for samples having the same DMSO content as the samples following addition of the compounds.

3. Part III: Validation of protein-ligand interactions. Information content of individual experiments and their usage in validation workflows

3.1. Information content of NMR experiments; general considerations

The experiments described in Section 2 have widely varying information content, as is described in this section. Possible experimental outcomes and their interpretation are used to explain the information that can be drawn from experiments. The aspects discussed here include: the meaning of presence or absence of signals and binding effects, whether binding specificity can be assessed, and whether binding effects can be compared among different ligands in order to rank their affinity. Among these aspects, the "detection limit" of an experiment and the notion of "specific binding" need some further explanation, which forms the topic of the next two Sections 3.1.1 and 3.1.2.

The information content of these experiments can also be illustrated in a compact notation by using the validation cross as though it were an operator, using red and green colors in the different fields. This helps to categorize experiments quickly and visually, and simplifies the process of selecting the right experiment for a given question (Fig. 11).

As a reminder, the fields of the validation cross can take solid red or green colors, indicating positive or negative experimental evidence for integrity or binding, which has been directly observed. They can also be transparent, which indicates indirect observation of effects, that is, information that is only inferred from the directly measured experimental effects. If a number is written into a field, in integrity fields it shows the solubility and in binding fields it shows the K_D.

3.1.1. Detection limits for affinity of individual experiments

The detection limit of an experiment in terms of the weakest affinity (K_D) that can reliably be observed depends on several factors: the concentrations of protein and ligand, the signal-to-noise ratio of the experiment and the difference of the signals of bound and unbound ligands in terms of relaxation and chemical shift. It is therefore important to note that a given experiment doesn't have a fixed, intrinsic detection limit – to the contrary, the detection limit will depend on all the factors listed above. As a first example, with long measurement times the signal-to-noise ratio in a ligand-observed experiment can become high enough to detect a 1% change in signal, leading to a different detection limit than for a typical 10-min experiment that would have lower sensitivity. As a second example, in protein-observed experiments, the ligand concentration can be increased in order to enlarge effects. An extreme case from our work is that we sometimes detect binding of DMSO to proteins, although its role should just be to solubilize the ligands. Since the sample can contain as much as 2% DMSO, the K_D of the DMSO-protein interaction may be in the hundreds of millimolar and it would still be detectable – though biologically irrelevant. On the other hand, many ligands are not very soluble and can for example only be assayed at 10 μM. For such a ligand, the detection limit may be around K_D = 50 μM, depending of course also on all the parameters discussed above. A mathematical description of the detection limit of a given experiment will thus in general contain several imprecise assumptions leading to a lengthy expression, which is of little practical value in day to day work. A much simplified expression for the maximal detectable K_D is $K_{D,max} \sim \varepsilon \times [L]$, where $[L]$ is the ligand concentration and ε is an empirical experimental factor, which encompasses protein size, concentration and experiment-dependent parameters like signal-to-noise ratio and strength of binding effects. For chemical shift based experiments in the slow exchange case, newly appear-

ing signals at 10–20% intensity are usually detectable, setting ε at about 3. That is, a ligand assayed at 200 μM without showing effect will have a K_D higher than ~600 μM. In the fast exchange case, these considerations are somewhat more complicated, because the magnitude of the maximal chemical shift change is unknown, but one can assume that there usually are a few signals shifting by ~0.5 ppm at full saturation, while the limit of significance can be represented by half the peak width at half height, which will typically be about 20 Hz. On a 600 MHz spectrometer the reliable detection limit will therefore be ~0.03 ppm, or a tenth part of the maximum expected chemical shift. ε may therefore be in the order of 3 in these experiments. For chemical shift based experiments, ε will not depend strongly on protein size. Larger protein size will however affect the signal-to-noise ratio and increase peak width, therefore lowering the detection limit of the experiments.

Empirically, the above formula for estimating the detection limit of an experiment can be applied for ligand-observed experiments based on τ_c, although with some important reservations. In our exemplary setting that we're using throughout this review (10 μM of a 30 kDa protein, 200 μM of 300 Da ligand), ε is in the order of 5–10 for STD and waterLOGSY experiments recorded in 10 min. That is, a ligand assayed at 200 μM without showing effect will have a K_D which is larger than ~2 mM. For a low soluble ligand assayed at 20 μM, the K_D would therefore be 200 μM. Here, a reservation applies: Of course, for a ligand assayed at low concentration the bound fraction will be potentially much higher enabling detection of weaker interactions. However, at the same time the signal-to-noise of this ligand is 10-fold lower, counteracting the advantage from the higher bound fraction. However, this effect is not linear, therefore the ε-factor should be used with much caution. For equimolar experiments, where higher signal-to-noise is typically acquired with longer measurement times, ε is approximately 10. For $T_1\rho$, ε may be around 5 and for ^{19}F-T_2 around 20.

The above ε-factors are somewhat "hand-waving" approximations; however, the sensitivity can be ranked as T_1-ρ < waterLOGSY ≈ STD < ^{19}F-T_2 < SLAPSTIC following theoretical considerations. Although $T_1\rho$ takes advantage of T_2 relaxation, which is a steeper function of τ_c than the NOE exploited in STD and waterLOGSY, it usually is less sensitive. This is due to the shorter relaxation period that is used in the experiment, for which mainly limitations in the hardware are responsible. This in turn means that the magnitude of the relaxation effect, which is proportional to e^{-Rt}, is less pronounced for relatively short relaxation periods t as employed in $T_1\rho$ (200 ms) vs. waterLOGSY (0.8–1.5 s) and STD (1–2 s) (Fig. 9). WaterLOGSY and STD have similar sensitivities in our experience, although at first glance waterLOGSY might be expected to be more sensitive. In waterLOGSY both scans contribute to the final NOE signal, while in STD a population difference between ligand and protein is created only in the scan that drives the NOE. The second scan is needed only to allow subtraction of the reference spectrum. However, longer relaxation times in STD, short lifetimes of bound water molecules in waterLOGSY and maybe higher density of saturated protons versus selectively excited water protons in the binding pocket may account for the effects leading to similar overall sensitivity with respect to binding events. Fluorine T_2 experiments are even more sensitive, due to the combination of a large dependence of $R_{2,CSA}$ on τ_c, the significant exchange contributions and relaxation times of up to 400 ms.

Clearly, the formula given above using the oversimplified ε-factor is by no means exact, especially not for ligand-observed experiments. However, these approximate considerations should help when comparing results from different experiments in order to see whether they are roughly in agreement or not.

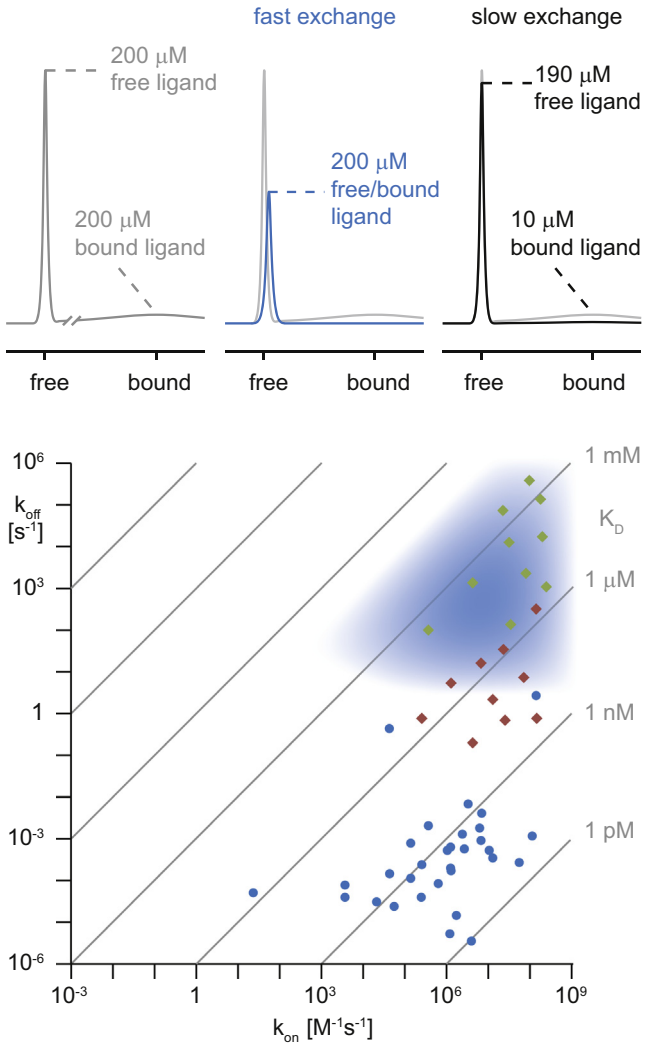

Fig. 12. Limitations of ligand-observed experiments with large ligand excess. In the top panel, hypothetical signals of 200 μM of free and fully bound ligand are shown in grey, with the chemical shift of free and bound states indicated below. Spectra of a ligand in the limiting cases of fast exchange (blue) and slow exchange (black) of a mixture of 200 μM ligand and 10 μM protein are shown superimposed on the grey reference spectra. In the case of fast exchange, (blue) signals with averaged relaxation rates (Eq. (9a)) and averaged resonance frequencies (Eq. (9b)) are obtained. Binding effects are clearly evident. A spectrum in the slow exchange regime is shown in black. It results in a narrow line with nearly the same intensity as the free ligand and a very weak bound signal of the small bound population. The bound signal will not be detectable for typical signal-to-noise ratios obtained in screening experiments. This spectrum might be mistakenly interpreted as evidence for non-binding, even if the K_D of the interaction may be in the nM range. In the lower panel, a kinetic plot for binding is shown. The blue area indicates the approximate range of applicability of experiments based on ligand excess in the situation of limited signal-to-noise, for fast and intermediate exchange regimes. For comparison, kinetic parameters of putative fragment hits (green diamonds), putative HTS hits (red diamonds) and selected marketed drugs are shown (blue dots, data from [15]). On the other hand, for NMR experiments where the observed species is present in lower concentration than the binding partner (e.g., equimolar ligand-observed experiments or protein observed experiments) there are no kinetic limitations.

3.1.2. On the notion of specific binding

Specific binding has two components: binding stoichiometry, which should be a low integer number; and binding site specificity, that is, whether a ligand binds specifically to a protein in a well-defined binding site. There may be more than one specific binding site per protein or protein complex, but the stoichiometry should still be described by low integer numbers [119]. In addition, a

specifically binding ligand does not require the presence of another ligand molecule to bind to the protein. This definition therefore excludes ligands that induce micelle formation or protein aggregation.

3.2. Information content and range of application of individual experiments

3.2.1. Ligand solubility

(The ligand alone is measured in buffer. The signal intensities are interpreted to assess the solubility of the ligand, Section 2.1.2.)

Information content.

- Presence of ligand signals: the intensities of ligand signals relative to that of the DSS internal standard signal reveal the ligand concentrations in the solution. If the concentration is below the nominally added value, than the concentration represents the ligand solubility (provided that the DMSO stock solution concentration is correct and the intended amount of stock solution was added, as can be checked by the intensity of the residual ^{1}H-DMSO signal). If the ligand concentration is as expected from the nominally added amount of stock solution, the solubility is equal to or greater than the nominal concentration. Occasionally the measured ligand concentration can be larger than the expected maximum concentration, as a consequence of an incorrect DMSO stock solution concentration. In this case the condition that the solubility $\geqslant [L]$ applies as well.
- Absence of ligand signals: this shows the solubility of the ligand is below the detection limit of the experiment, which is typically 5 μM. The statement applies only if the residual ^{1}H-DMSO signal is visible, which demonstrates addition of ligand stock solution, and if the ligand has been confirmed to be present in the DMSO stock solution.

3.2.2. Ligand integrity

(The ligand is measured in buffer, alone or with protein. The coupling patterns and signal intensities are interpreted to assess the identity and integrity of the ligand, Section 2.1.1.)

Information content.

- Number of signals, their chemical shifts and coupling patterns match the expected spectrum: the spectrum is compatible with chemical structure.
- There are additional signals in addition to the expected ones: impurities or degradation products are present, which may be quantified (e.g. 20% impurity present).
- The number of signals, and their chemical shifts and coupling patterns are not compatible with the expected spectrum: the ligand is not the expected one.

3.2.3. Ligand-observed experiments with ligand excess

(The ligand is present in 10–20-fold excess over protein. One looks for changes of the ligand signals, due to changed relaxation properties induced by slower rotational motions upon binding to the larger protein, Sections 2.2.1–2.2.6.)

Ligand-observed experiments based on ligand excess are the basis for the success of NMR in drug discovery. Through amplification effects they make it possible to overcome the inherently limited sensitivity of NMR and allow detection of very weak interactions with dissociation constants up to 10 mM. This upper limit for detectable affinities was discussed in Section 3.1.1. However, these considerations only hold for the fast and intermediate exchange regimes. In addition to the detection limit of weak binding there is a detection limit imposed by slow exchange kinetics, which actually prevents detection of binding of strong ligands (Fig. 12).

The effect can be easily explained with the example of an R_2-based experiment such as $T_1\rho$ with a ligand in slow exchange. One can assume a very strong interaction, which fully saturates the protein. In the case of the standard setup with ligand and protein present at 200 and 10 μM concentrations, 5% of the ligand will be bound. This will lead to a strongly broadened signal of the bound ligand (Eq. (9b)). The remaining free ligands will however yield non-broadened signal. The observed total signal will actually be nearly indistinguishable from that of the free ligand. Its intensity will be 95%, and there will be no line broadening, because there is no contribution from the slowly exchanging bound state. A signal reduction from 100% to 95% will not be qualified as a binding effect; usually a reduction to 70% is chosen as a typical threshold for binding. In other words, even with careful analysis, binders in slow exchange will not be detected because, firstly, 5% lies well below the reproducibility tolerance for such experiments and, secondly, the signal-to-noise ratio is usually not sufficient to see such a small effect. The limit for detection of ligands binding with slow kinetics depends on the individual experiment and will be discussed there. Assuming that in such experiments the signal-to-noise ratio is deliberately limited to less than 10 in order to attain the desired throughput, the limit of $k_{off} = 10\ s^{-1}$ as shown in Fig. 12 seems generally realistic.

Therefore all experiments based on ligand observation under ligand excess (Section 2.2.1) are limited to fast kinetics, and strong binders will not be detected. Nevertheless, these experiments are highly valuable and represent the basis of the success of NMR in drug discovery. It is just important to bear in mind that there is an upper as well as a lower limit of detection.

Information content. The considerations below apply only if the required negative controls are carried out as described for each experiment in part II.

- Direct observation of binding effects: The ligand is interacting with another particle. K_D is smaller than the ligand concentration present in the experiment or more precisely: $K_D \leqslant \varepsilon \times [L]$, (see precaution in Section 3.1.1). Protein-observed experiments are required in order to distinguish binding to the target protein from artifactual binding to protein aggregates or other particles.
- No binding effects are observed: The compound could still bind with slow kinetics. In order to investigate this possibility, equimolar experiments or reporter displacement can be considered. (No conclusive interpretation can be derived from this result. For ligands with fast or intermediate exchange kinetics ($k_{off} > 10\ s^{-1}$) the K_D must be larger than the ligand concentration present in the experiment ($K_D \geqslant \varepsilon \times [L]$). It may, however, be binding with slow kinetics.)
- Ligand integrity: If resonance lines are not broadened excessively due to binding effects, the ligand is easily identified based on its pattern of resonance lines.
- Binding specificity: Binding specificity can be assessed by using appropriate reporter or competitor molecules. Ligand-observed experiments can in principle also discriminate between specific and unspecific binding, that is, binding of the ligand in a (integer) stoichiometric fashion and in a defined orientation to defined binding sites of the protein. The idea behind this is that for specific binders, the binding effects will be different for individual resonances, because different parts of the ligands will experience different environments in the protein [95]. This is true for dipolar interactions and most prominently for NOE based experiments. Since differences in signal intensity may also arise from different R_1 relaxation of individual groups in the free state of the ligand, it is important to investigate differential relaxation of the free and bound states of the ligand.

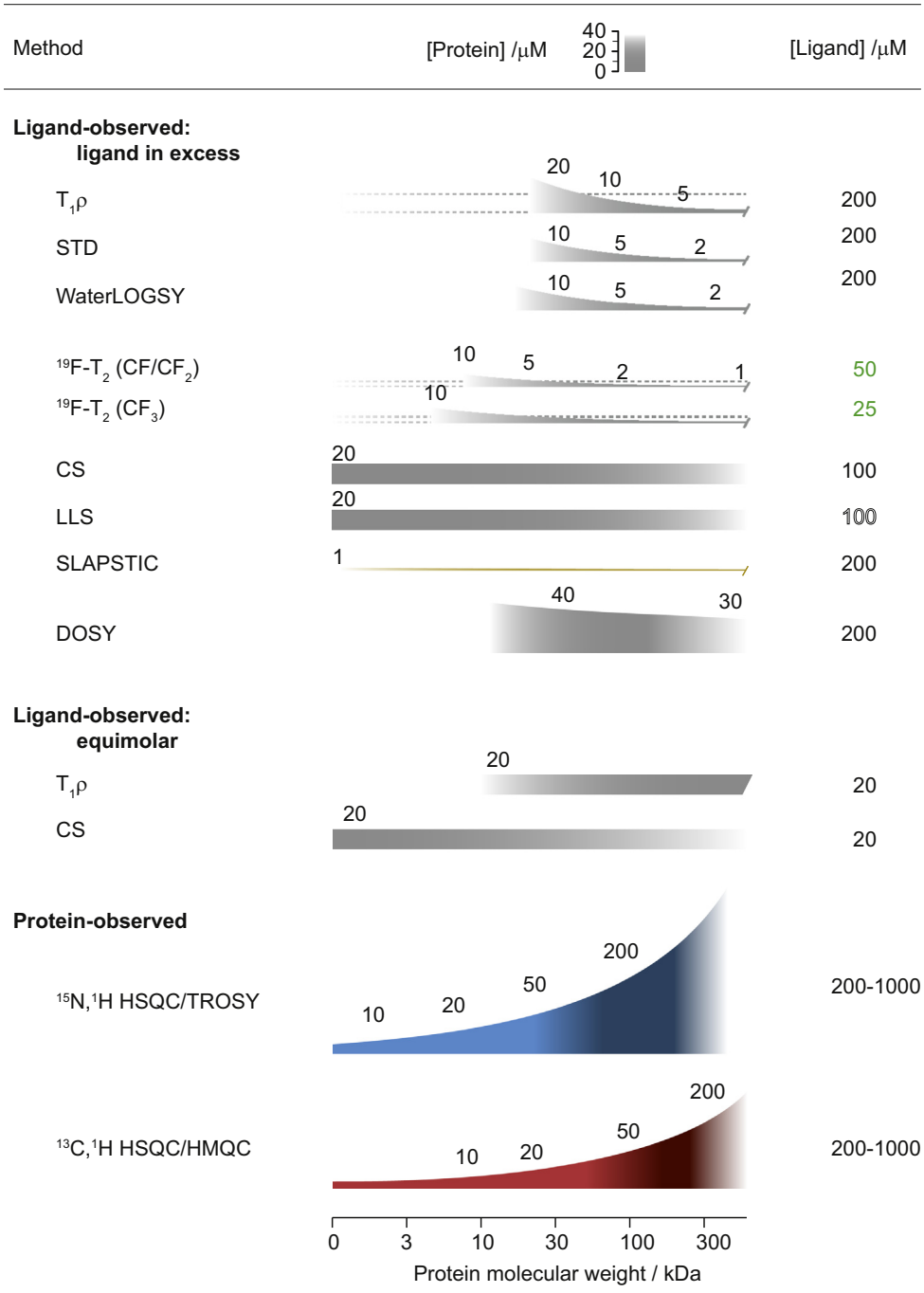

Fig. 13. Summary of protein and ligand concentrations used in practice for NMR experiments to detect ligand binding. On the left, the names of NMR experiments are given. In the center, protein concentrations are indicated as area graphs of concentration (vertical axis, scale at top of figure) against protein molecular weight (horizontal axis, scale at bottom of figure). Typical ligand concentrations are indicated as numbers in the right column. Black or grey-scale shadings indicate non-labeled proteins and ligands, colors indicate labeling of molecules. For proteins: spin label within 10–15 Å of the binding pocket (yellow, in SLAPSTIC), ^{15}N-labeling, either without or with perdeuteration of the protein (blue and dark blue, respectively), ^{13}C-methyl labeling, either without or with perdeuteration of the protein (red and dark red, respectively). For ligands: presence of ^{19}F (green), presence of two coupled spins suitable to sustain a long-lived state (outlined). The area graphs represent the application range of experiments. For example the $T_1\rho$ experiment (at the top) can be applied with target proteins of a range of sizes. The minimal molecular weight is about 20 kDa and there is no upper limitation, indicated by the cut end. Since the relaxation effects observed in $T_1\rho$ depend on the target protein size, smaller target proteins need to be employed at higher concentrations in order to obtain similar effects as larger proteins, as indicated by the varying height of the area. The lower limit is not strict, which is indicated by a fading color. The dashed lines for protein concentration in ^{19}F and $T_1\rho$ experiments indicate the detection of exchange effects (e.g. line broadening by chemical shift changes in intermediate exchange), which are independent of protein size. Therefore, interactions with a strong exchange component can be detected even for very small targets. Chemical shift changes don't depend on protein size, therefore this results in continuous bars for the graphs for protein concentration towards low molecular weight. The upper limit is imposed by faster relaxation of binding ligands, leading to disappearance of their signals at the target protein concentrations needed to induce chemical shift changes.

- Relative binding affinity: Although the magnitude of effects observed for different ligands in ligand observed experiments depends on p_B, there is no direct correlation between affinity (K_D) and the observed effects, except for DOSY-type experiments: ^{1}H-$T_1\rho$, STD, waterLOGSY and NOE pumping experiments are based on dipolar interactions which strongly depend on the distance between nuclei (r^{-6}), which are not known and are different for each signal and each protein-ligand complex. ^{19}F-T_2 experiments are based on CSA relaxation, for which the CSA tensor asymmetry is normally not known. For $T_1\rho$ and CPMG experiments, the contribution from chemical shift exchange is usually not suppressed fully, and the exchange rate (k_{ex}) and the value of the bound chemical shift (ω_B) are not known. Only diffusion experiments directly depend on the bound fraction the magnitude of the effect – here the shift in the DOSY dimension – can be used to rank compounds according to their affinity. For all other ligand-observed experiments, the relative binding affinity of ligands can be deduced from competition experiments.

Usage and range of application.

- Ideal for fragment based screening (FBS): Ligand-observed experiments have high throughput because mixtures of compounds can be measured, they use minimal amounts of protein and are highly sensitive to binding events. FBS libraries are selected for high solubility (>200 μM) and one expects weak binding (K_D > 1 μM) in fast or intermediate exchange (k_{ex} > 10 - s^{-1}) for fragment-sized ligands.
- Ideal when a strong reference ligand (competitor) is available to mitigate vulnerability to unspecific binding to protein aggregates.
- Depending on experimental format, (lower) size limitations for the target apply (Fig. 13).
- The ligand must be much smaller than the target, ideally well below 1 kDa, and highly soluble (detection limit ≈ 10–20 μM, preferably >100 μM).
- Binding kinetics must be in the fast or intermediate exchange regimes (k_{ex} > 10 s^{-1}).
- Diffusion-based experiments require more protein and have lower throughput than the other ligand-observed experiments; there is no obvious advantage for screening and validation. However, these experiments allow direct assessment of relative affinities for compounds in fast exchange. If no reporter has been established, this is the preferred option.

3.2.4. Ligand-observed: Equimolar

(The ligand and protein are present in stoichiometric amounts, e.g. 20 μM each. One looks for changes of the ligand signals, due to changed chemical shift or changed relaxation properties induced by slower rotational motions upon binding to the larger protein, Section 2.2.7.)

Information content.

- Direct observation of effects: The ligand is interacting with another particle.
- No effects are observed: The ligand is not interacting with another particle. This experiment is probably the safest experiment to rule out binding, as it does not depend on kinetics and the ligand is observed directly.
- Protein integrity: If the protein is not excessively large (>50 kDa), the envelope of protein signals is visible in the 1D spectrum, revealing protein integrity.
- Ligand integrity: If resonance lines are not broadened excessively due to binding effects, the ligand is easily identified based on its pattern of resonance lines.
- Binding specificity: Binding specificity can be assessed by using appropriate reporter or competitor molecules. In cases of slow-exchange binding, the stoichiometry of the interaction can be determined by titration.
- Relative binding affinity: In cases of slow-exchange binding, relative binding strengths of two ligands can be determined by comparing the remaining free fraction of each ligand.

Usage and range of application.

- This is the most generally applicable ligand-observed experiment for validation: For equimolar experiments there are no restrictions on the target nor on ligand except for solubility, which must be >10–20 μM. With DNP that limit may further be reduced.
- This is probably safest experiment to rule out binding of a ligand.
- It can be used to rank ligands that are in slow exchange according to affinity [88].

3.2.5. Ligand-observed: Reporter

(A known ligand with weak affinity, a reporter, is present in a mixture containing target ligands and protein. Using ligand-observed experiments, one looks for changes of the signals of the reporter indicating displacement of the reporter, Section 2.2.8.)

Information content.

- Observation of reporter displacement: In general, it can be inferred that the ligand bound to the target with higher occupancy than the reporter, and that the target protein is intact. However, in odd cases, it is also possible that the ligand induced protein denaturation. Since the ligand is not visible in reporter experiments, it is not clear whether it is present at the intended concentration or even whether it is intact.
- No displacement is observed: The ligand is not binding competitively at the same binding site (or an allosteric site) as the reporter, or it is binding there but with weaker affinity. In odd cases, the reporter could bind to the ligand (e.g. if the ligand is peptidic) and lead to a false negative result. In cases of large ligands, their direct binding to the reporter should be ruled out in a control experiment.
- Binding specificity: If the reporter is displaced and ligand-induced protein aggregation can be ruled out, the ligand is binding specifically. (Additionally, it may still be that there is an secondary unspecific binding mode of the ligand.)
- Relative binding affinity: Displacement effects on the reporter are related to binding strength of the individual ligands. Ligands can therefore be ranked according to their K_D.

Usage and range of application.

- Generally applicable experiment for validation and screening, if a suitable reporter ligand is available.
- There are no limitations on ligand solubility or size, provided proper controls are in place.
- Lower limits on protein size depend on the chosen experimental format.

3.2.6. Ligand-observed: Displacer-Competitor

(A known ligand with high affinity, a displacer, is present in a mixture containing target ligands and protein. Using ligand-observed experiments, one looks for changes of the signals of the target ligands indicating displacement of the target ligands, Section 2.2.8.)

Information content.

- Observation of ligand displacement: The competitor is displacing the ligand. It can be inferred that the ligand is binding specifically to the protein and that the protein is intact. Observation of ligand signals allows assessment of ligand integrity.
- No displacement is observed: The ligand is not binding at the same site as the competitor (or an allosterically related site). Binding to a different site on the protein cannot be ruled out.
- Partial displacement is observed: The ligand binds to the protein, but either binding of the competitor is not much stronger than that of the target ligand, or the target ligand has another – maybe unspecific – binding site.
- Binding specificity: If protein aggregation can be ruled out, the ligand is binding specifically. (Incomplete displacement may indicate an additional unspecific binding mode.)
- Relative binding affinity: Usually the competitor molecule is chosen to bind much more strongly to the protein than the ligands under study, so that there is always full displacement observed. Incomplete displacement of the ligand cannot be used for ranking of different ligands, as it may be dominated by unspecific secondary interactions.

Usage and range of application.

- Ideal as a complementary experiment to simple ligand-observed screening, if a strong competitor is available.
- Ligand, target size and solubility limitations of individual experimental formats apply.

3.2.7. Protein-observed: Integrity

(The protein is measured alone or in presence of a ligand. Using protein-observed experiments, one analyzes the chemical shift and the intensity of signals to assess the integrity of the protein, Section 2.4.)

Information content.

- Signal intensity of protein signals corresponds with intensity of protein reference spectrum without ligand: this indicates an intact protein.
- Appearance of new signals while most of the protein signals remain unchanged: this indicates altered dynamic behavior of regions of the protein. Newly appearing signals may also stem from natural abundance nuclei of the ligand if it was added at high concentration. Of course, ligand binding in slow exchange will also lead to additional protein signals.
- Reduction of signal intensity or disappearance of signals: line broadening indicates oligomerization or even complete aggregation of the protein. In odd cases a ligand can induce unfolding of the protein, which can be detected by narrow dispersion of the resonances around random coil chemical shifts.

Usage and range of application.

- Ideal for isotope-labeled small and medium-sized proteins (<30 kDa for ^{15}N labeling, <100 kDa for ^{13}C-methyl labeled proteins) or for larger proteins with ^{2}H-labeling.
- Useful also for unlabeled proteins <30–50 kDa if ^{1}H spectra show well-resolved signals.

3.2.8. Protein-observed: Binding

(The ligand is present in 10–20-fold excess over protein. Using protein-observed experiments, one looks for changes of the protein signals indicating binding of the ligand, Section 2.4.)

Information content.

- Chemical shift changes are observed: The protein is interacting with another particle. In general this will be the added ligand, but for rigorous validation, a ligand observed experiment is needed to identify the ligand, as binding to a contaminant in the ligand solution cannot be ruled out. Chemical shift changes in a protein observed spectrum are generally the "gold standard" for ligand validation.
- If a subset of resonances disappears, and no new resonances appear, the interaction may take place with intermediate exchange kinetics. Such a situation may also hint at binding of a ligand with multiple binding modes.
- No effects are observed: The protein is not interacting with another particle ($K_D > \varepsilon \times [L]$, $\varepsilon \approx 3$). However, information is limited to the observable region of a protein, depending on construct, labeling pattern and non-observable signals due to overlap or unfavorable dynamics.
- Binding specificity: Effects on a defined subset of signals are indicative of specific binding. Often more amino acids are affected than just those in close proximity of the ligand binding site, caused by allosteric effects in cases of rearrangements of the protein. Therefore, a large number of affected chemical shifts is not per se an indication of unspecific binding. If a known ligand is available, coincidence of affected resonances upon ligand binding indicates a similar binding mode. Cross-saturation methods are indicated for mapping protein binding sites without allosteric effects [94]. If a titration is performed and the chemical shift changes are not linear between the positions of free and bound states, but instead a curved pattern is observed, this is indicative of one or multiple additional binding modes.
- Relative binding affinity: The magnitude of chemical shift changes does not directly correlate with the binding strength. It is strongly dependent on the chemical nature of the ligand, which may bring aromatic rings inducing strong ring current shifts into proximity of certain residues. Binding may also affect the orientation of aromatic side chains of the protein, leading to strong chemical shift changes, which are not directly related with the magnitude of the bound fraction.

Usage and range of application.

- Ideal for isotope-labeled small and medium-sized proteins (<30 kDa for ^{15}N labeling, <100 kDa for ^{13}C-methyl labeled proteins) or for larger proteins with ^{2}H-labeling.
- Useful also for unlabeled proteins <30–50 kDa if ^{1}H spectra show well-resolved signals.
- In order to obtain significant effects, ligand solubility should be similar to or higher than the concentration of the target protein. $[L] \geqslant [P]/\varepsilon$, ($\varepsilon \approx 3$).

3.3. Recommended usage of experiments

3.3.1. Range of application depending on size and concentration of proteins and ligands

The applicability of each type of NMR experiment depends on the target protein size and the protein and ligand concentrations; these dependencies and the consecutive limitations were discussed in the sections on individual experiments. For the following discussions on which experiment to choose at a given stage of a validation workflow, typical values for protein and ligand concentrations are summarized in Fig. 13. These values are empirical and may differ from ideal values for best performance of individual experiments.

3.3.2. Throughput and cost of screening and validation experiments

In Fig. 14, we try to give a simplified overview of the throughput and cost of individual experiments. For the purpose of screening,

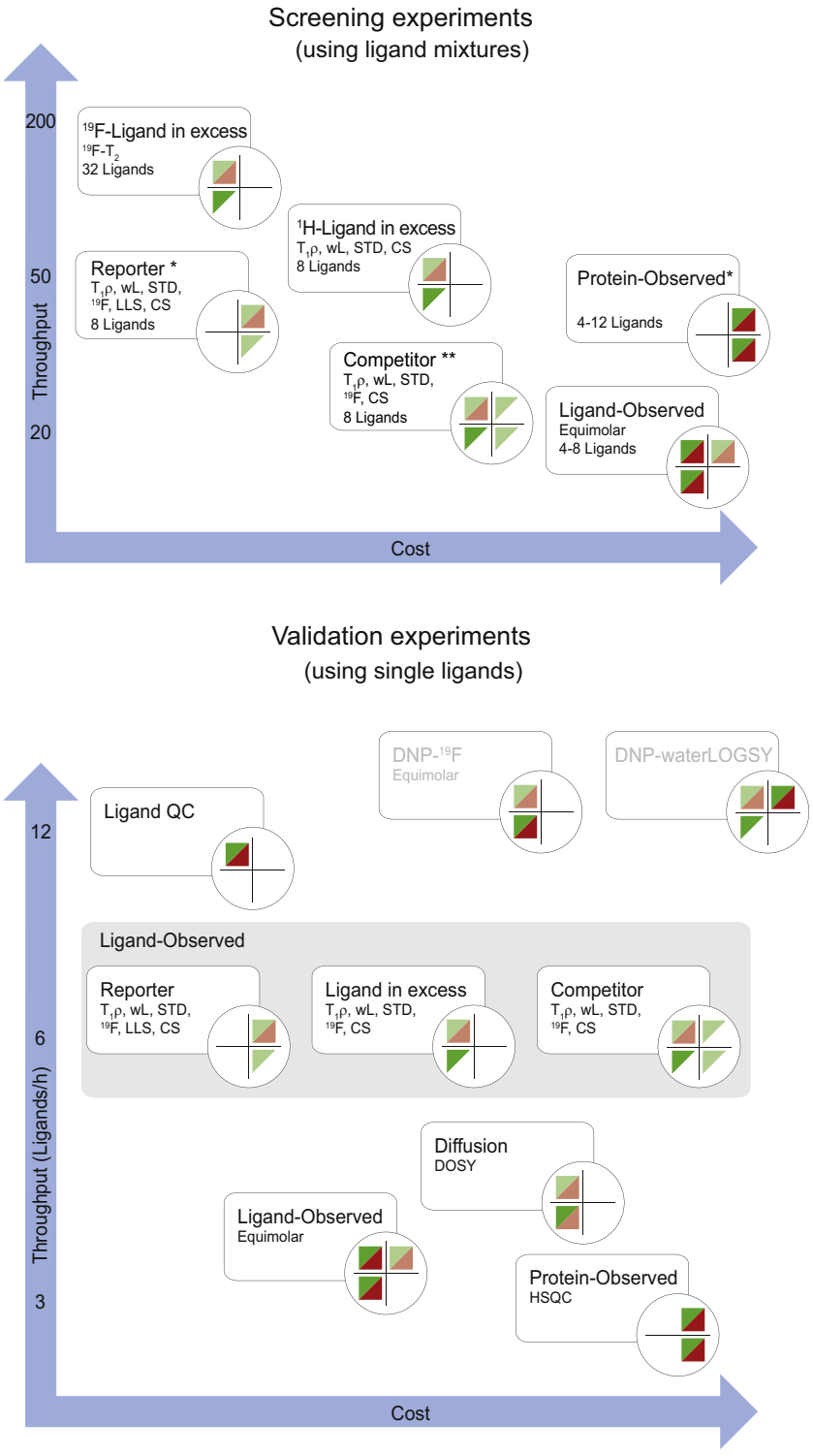

Fig. 14. Throughput and cost of individual experiments: NMR experiments are placed in a plane where the vertical and horizontal axes represent throughput and approximate cost, respectively. For the vertical axis an approximate throughput in ligands per hour is given. The positioning along the axes depends on the cost of protein production and is therefore very crude. Interestingly, information content and cost roughly correlate. When designing validation workflows, usually one employs less expensive experiments with higher throughput first, in order to bring down the numbers of compounds that need to be tested in more informative but more costly low-throughput assays later. In the screening experiments, protein-observed and reporter experiments are marked with an asterisk (*) because even if large mixtures allow high throughput, the binding ligand cannot be identified immediately. Therefore the throughput is somewhat overestimated in these experiments. (**) Competition-based screening can only be applied in conjunction with another ligand-observed screening method, therefore it cannot be used on its own. DNP-based experiments are shown in grey, as they are not yet established at this time but represent a promise for potentially higher throughput in the future.

most NMR experiments can be multiplexed by measuring compound mixtures. The advantage of NMR here is that binding ligands in a mixture can immediately be identified in ligand-observed experiments. The number of ligands in a mixture is limited by two parameters: overlap of signals and amount of DMSO. Signal overlap in 1D ^{1}H spectra typically limits the number of

ligands to 8. ^{19}F has an advantage in this respect, because most ligands only show one signal, allowing mixtures of 32 without overlap. Here, the amount of DMSO added to the protein sample is the limiting factor. For protein-observed experiments there is no issue with overlapping ligand signals. However, because the binding ligand(s) in a mixture need to be subsequently identified, a recommended number of ligands per mixture are 8–12. Because ligands are added at relatively high concentration in protein-observed experiments, DMSO amounts quickly become limiting. In principle, when multiplexing equimolar experiments, the amount of protein that needs to be added to the sample increases linearly with the number of compounds in the mixture. However,

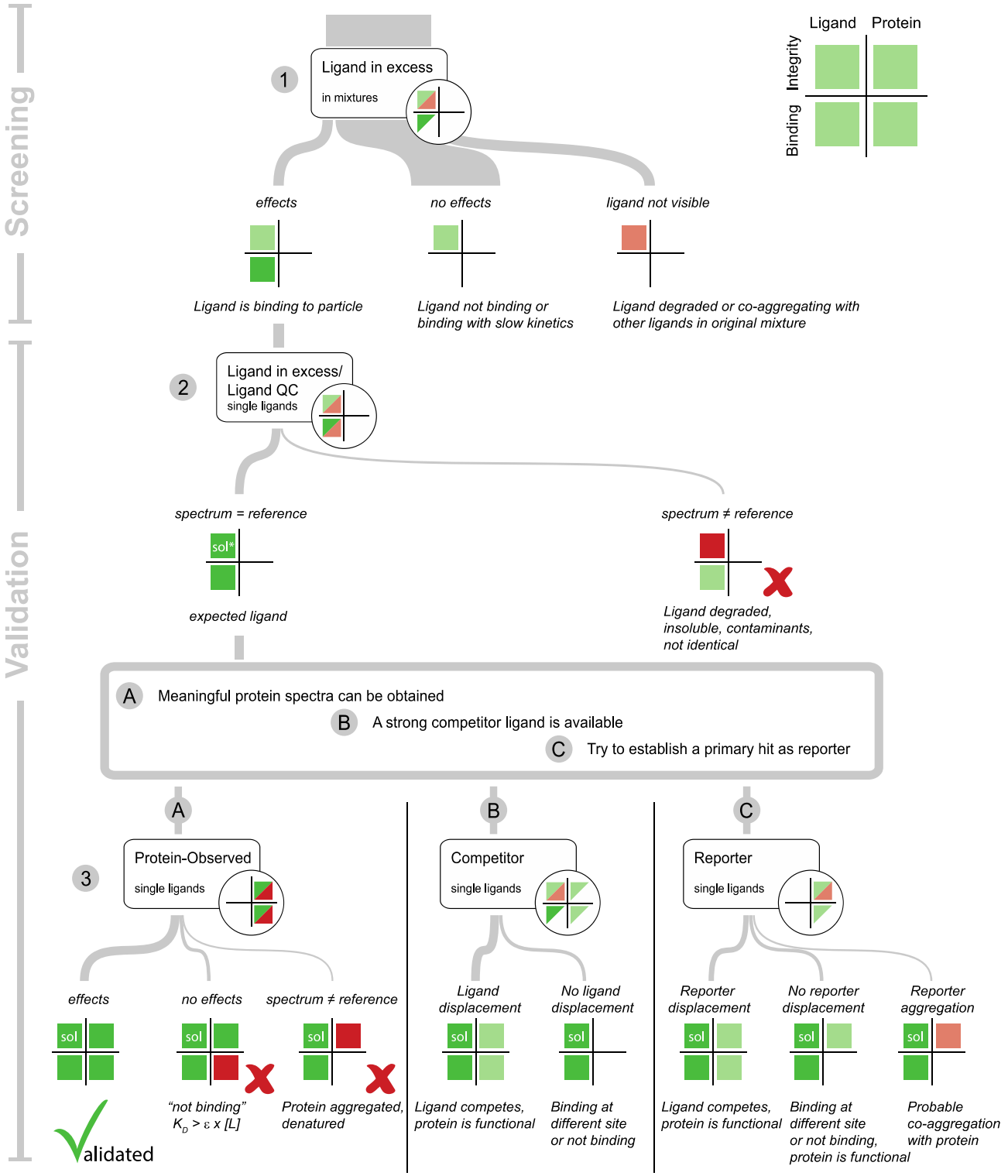

Fig. 15. Validation workflow for ligand-observed FBS. At the beginning, thousands of fragments, indicated by the thick grey line, are screened with ligand-observed experiments (box with rounded corners). Depending on the observed effects, each ligand will lead to a pattern in its validation cross. A few positive ligands will be taken to the next experiment, as indicated by a narrow grey line. Further experimental steps are added in order to obtain fully validated ligands (validation cross with all fields in dark green), or at least a partially validated ligand (validation cross with as many filled fields as possible). A detailed explanation of the workflow is given in the main text.

the NMR measurement time stays constant and therefore throughput is increased. Alternatively, the protein concentration can be kept at the concentration of individual ligands (e.g. 20 μM protein and 8 ligands at 20 μM); however, if a ligand binds in slow exchange it may saturate the protein and make it unavailable for the other ligands in the mixture. In this case the remaining ligands of the mixture would need to be re-tested in order to exclude binding.

3.4. Validation and de-validation of protein-ligand interactions

We can use the validation cross to define what is meant by a validated interaction. A validated protein-ligand interaction is simply represented by four solid green squares in the quadrants of the cross. This means that binding effects have been directly observed both on the ligand and on the protein. Additionally, there is direct experimental data demonstrating the integrity of protein and ligand in the sample used for the interaction measurement (Fig. 3).

Obtaining direct data on all four aspects will eliminate artifacts from false-positive and false-negative interpretations of individual experiments. A validated true-positive protein-ligand interaction will likely be worth investing the many resources required in a lead optimization effort, including further biophysical and structural methods as well as chemistry and biology.

In practice, a validation cross where all fields result in solid green, is only one of many possible experimental outcomes.

The other well-defined situation is that of a de-validated interaction. De-validation of an interaction must be treated as stringently as validation. Absence of direct binding effects per se is not sufficient for de-validation of an interaction; this conclusion is only valid if the integrity of protein and ligand have been determined. Demonstration of protein aggregation or ligand degradation on the other hand are sufficient in order to de-validate a ligand. Therefore, there are four patterns in the validation cross that will lead to de-validation of a ligand (Fig. 3).

In this stringent scheme for evaluation, all patterns not falling into the validated or de-validated category essentially need to be annotated as "inconclusive". However, the pattern of green and red fields will allow ranking of such partially validated hits, according to the annotation derived from different experiments.

In practice, it requires a great deal of time and effort to obtain a fully validated ligand, in terms of the stringent requirements defined here. More pragmatically, it makes sense to truly validate only one representative of a ligand class. Structurally similar ligands can then be assessed with simpler experiments based on the prior knowledge of the relevant compound class that minimizes the risk of artifactual interpretation of results.

3.5. Examples of validation workflows

In this section a few examples of workflows are presented. These workflows aim to provide validated ligands with the minimal number of experiments. Three scenarios are shown. Two are pure NMR workflows based on screening fragment libraries, one based on a ligand-observed FBS, the other on a protein-observed FBS. The third validation workflow starts with a biochemical high-throughput screen (HTS) of a library of a million compounds. These different primary screens demand different approaches to validation.

3.5.1. Workflow for a ligand-observed FBS

In an FBS workflow the focus lies on selecting ligands that bind to a target protein from a library of thousands of highly diverse ligands, which have been selected for high solubility and chemical integrity [120]. The workflow is focused on selecting ligands showing positive effects and there is little emphasis on de-validation of hits, which is a more demanding process.

Deliberately, the possibility of ligands binding in slow exchange is ignored (Fig. 12). This is a pragmatic decision, since in most cases it is unlikely that a fragment has a high affinity that leads to a slow off-rate. However, if binding involves a slow activation step, such as a conformational change of the protein, ligands will not be detected at all by this approach. Nevertheless, it represents the most economic and efficient workflow for FBS by NMR (Fig. 14); no labeled protein is needed for the screening step, required protein amounts are low and ligands are immediately identified from the mixture. The only additional restriction is a minimal target size of about 20 kDa (Fig. 9). Therefore, ligand-observed FBS is the most widely used approach.

Ligand screening in mixtures. Step 1 in Fig. 15: For the initial step, any of the popular ligand observed methods is suitable, that is ^{1}H-$T_1\rho$, STD or waterLOGSY. We suggest running a combination of a transverse relaxation- and NOE-based experiment. For example ^{1}H-$T_1\rho$ and waterLOGSY can be run on the same sample in order to have two data points per ligand. For these experiments, mixtures of eight ligands are typically used. If a fluorinated fragment library is available, the initial screen can be run with ^{19}F-T_2 experiments, making the throughput potentially much higher as mixtures of up to 32 fragments can be measured at once.

There are three potential outcomes of this first step: (i) the ligand is not visible or degraded, (ii) there are no binding effects or (iii) there are binding effects. The first two outcomes are negative and these compounds are then not followed up further. Theoretically, however, such compounds could still be valid ligands, for example if they bind in slow exchange. Also, a strong ligand may compete with all other ligands in a mixture, making their results appear negative, even if they were valid but weak binders. As it is completely impractical to rescue all these ligands, and since in a fragment based screen weak ligands binding with fast kinetics are actually expected, it is very improbable that important ligands are missed by only following up those that showed binding effects.

Confirmation of individual ligands and quality control. Step 2 in Fig. 15: In order to exclude artifacts arising from the fact that ligands were measured in mixtures, each initial hit is confirmed in essentially the same experiment but as single compound. In the same experiment, the ligand integrity can be assessed. In principle, ligands in a fragment library have been quality controlled beforehand when the library was assembled, but it may still be possible that the ligand degraded since the initial production of the stock solution.

Protein observation of single ligands. Step 3A in Fig. 15: The ligands that passed the test of step 2, are thereby identified and known to bind to a larger particle. Whether this particle is the functional target protein, or an artificial aggregate needs to be determined using a protein-observed experiment. Here, ideally, experiments are recorded on isotope labeled protein; however, if ^{1}H spectra (e.g. 1D, 2D NOESY for proteins or 2D TOCSY for RNA) are of sufficient quality and one can be sure that isolated signals allow enough coverage of the protein, then these may be sufficient at this point. Using a protein-observed experiment will address the remaining two fields of the validation cross and enable proper validation of the ligands (Step 3A). Ligands leading to observable binding effects on the intact protein can thereby be classified as fully validated ligands. For ligands for which no binding effects can be observed, the K_D must be at least 3-fold higher than the assayed ligand concentration, which is typically 500 μM for fragments (recall that ε is in the order of 3 for chemical shift based experiments, see Section 3.1.1).

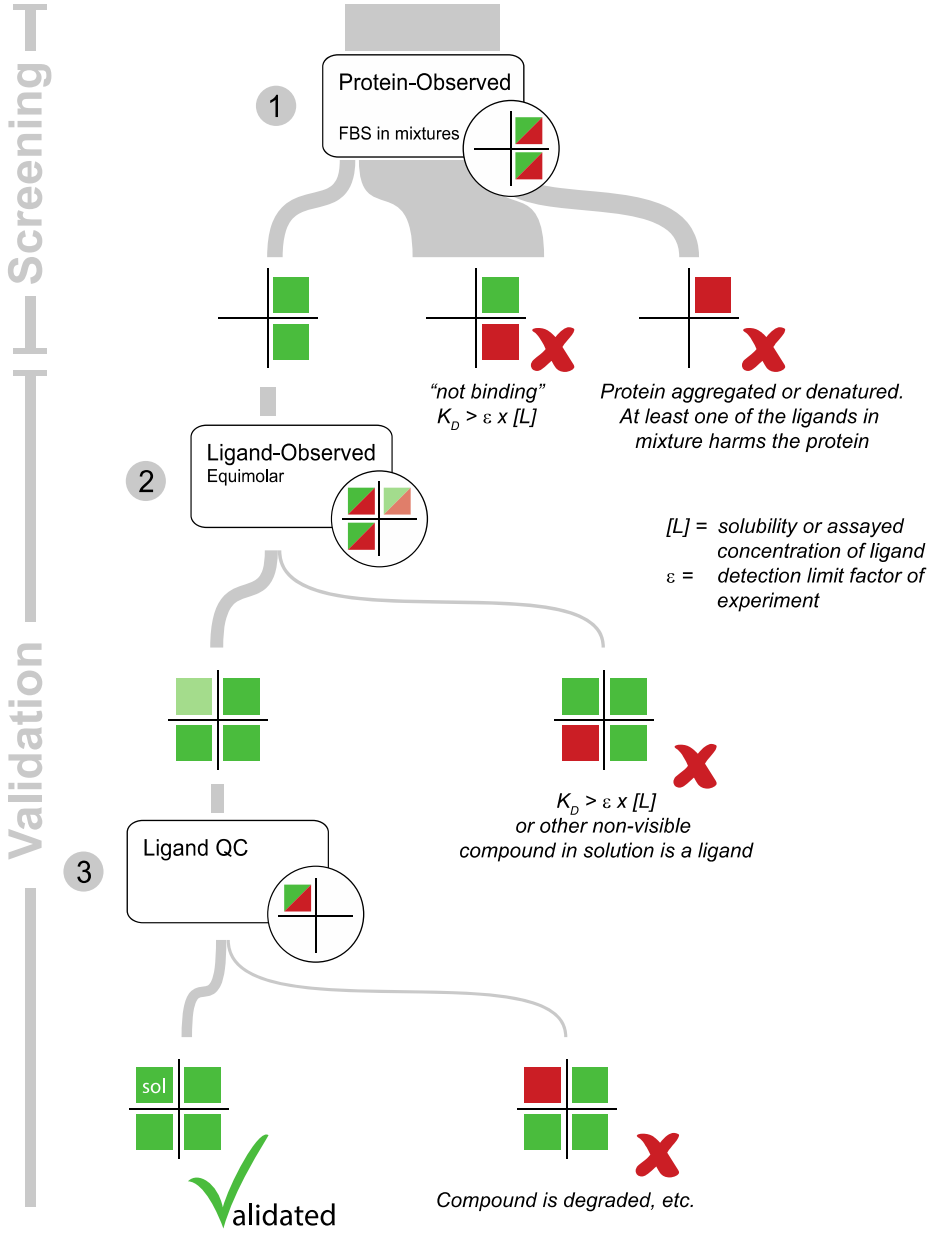

Fig. 16. Validation workflow for protein-observed FBS. Same schematic representation as in Fig. 15.

Step 3B in Fig. 15: If no high-quality protein spectra can be obtained, be it because of lack of labeled protein or crowding of the spectra, an alternative assay needs to be used in order to obtain information on protein binding and integrity. Unfortunately, without direct observation of effects on the protein, ligands cannot be stringently validated according to the validation cross scheme, under which circumstances partial validation through indirect effects is the best achievable goal. If a strong and well-characterized competitor ligand is available, indirect information on specific binding effects on the protein can be obtained. Ligands that are displaced in this assay most probably bind to the same protein binding site as the strong competitor ligand. Additionally, the fact that competition occurred, indirectly indicates that the protein is functional.

Often a competition experiment is integrated in the initial screening step. This immediately leads to highly validated ligands after the first round of experiments. Nevertheless, for proper validation, steps 2 and 3A will still be required.

Step 3C in Fig. 15: If no strong competitor ligand is known, it is often possible to develop a reporter ligand. To this end, several hits may be tested for their suitability. A reporter ligand needs to be very soluble in order not to co-aggregate with other ligands, and its affinity should be fairly low, especially in the context of validating fragments. Thus its K_D should be in the order of several hundred μM for it to be displaced by fragments that are expected to have K_Ds in the same order. However, in the context of fragment screening, a word of caution is needed: a weak reporter and weak hit may not show much competition, even if they bind to the same site, as both may only bind to the protein at low occupancy. If chemistry allows, the reporter ligand could be fluorinated or a ^{13}C-labeled methyl group could be introduced, in order to make measurements more efficient and to simplify analysis. Sometimes, the aim of a fragment screen is just to find a suitable reporter molecule in order to efficiently screen potential ligands found by other methods (see Section 3.5.3).

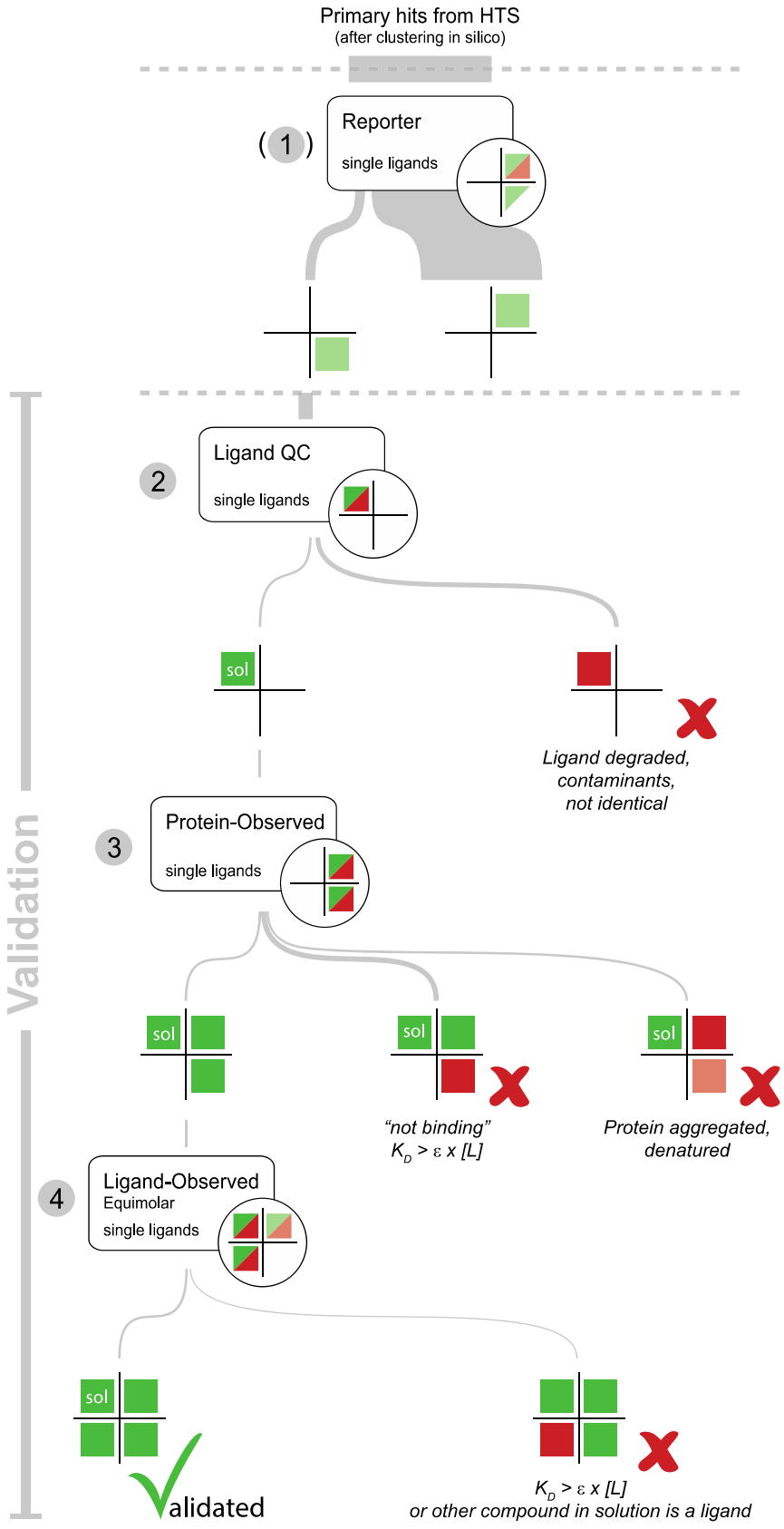

Fig. 17. Validation workflow for biochemical HTS. Same schematic representation as in Fig. 15. Step 1 is optional and only serves for pre-selection in order to reduce the number of hits that need to be validated. Steps 3 and 4 could be swapped and equimolar experiments could be run in mixtures of four compounds. If no labeled proteins are available, the same decision-tree can be used for step 3 as for steps A, B, C in Fig. 15.

zgesgp

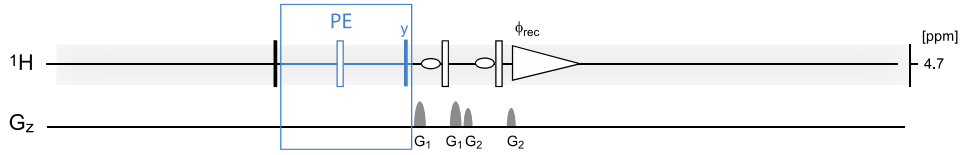

T1rho

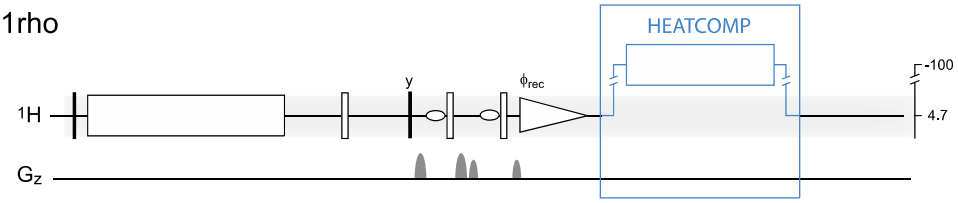

STD

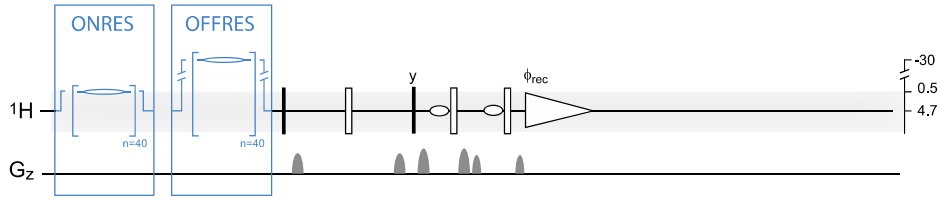

wLOGSY

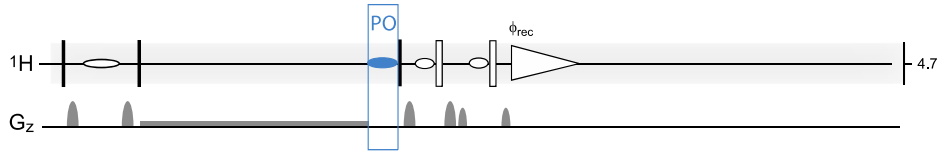

19F-T2

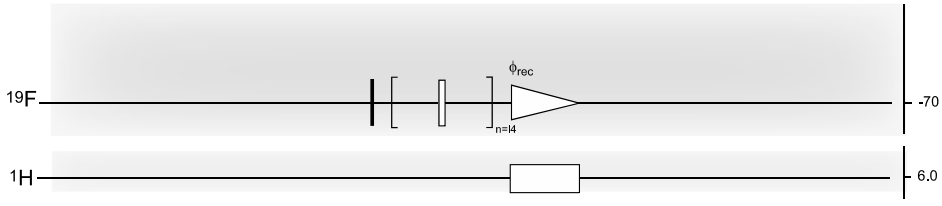

15N-ALSOFAST-HMQC

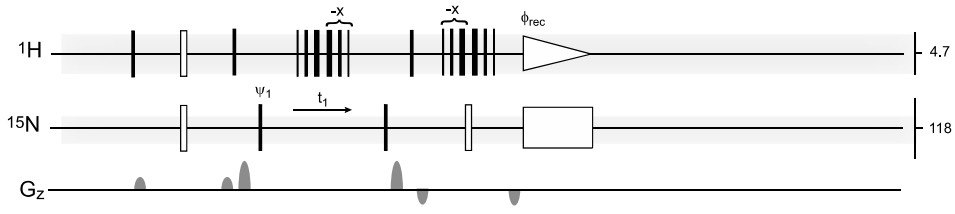

In summary, in this workflow ligands that have properties typical for fragments will be found (low affinity and fast binding kinetics), while for example compounds that bind in slow exchange will (consciously) be missed. However, it is highly unlikely that a fragment would bind in slow exchange and it would be a colossal effort to rescue all potential binders in such a campaign. Therefore, this is the most prevalent fragment screening and validation strategy used in NMR.

3.5.2. Workflow for a protein-observed FBS

A workflow starting with a protein-observed FBS is generally more costly than a ligand-observed FBS, since rather large amounts of labeled protein are required. Additionally, there is a limitation on the protein size; proteins above 30 kDa will require long measurement times or large amounts of protein (Fig. 13). On the other hand, there are no limitations on binding kinetics allowing detection of slowly exchanging compounds and typically there are fewer artifacts encountered in this method.

Ligand screening in mixtures. Step 1 in Fig. 16*:* A protein-observed FBS is typically run using mixtures of 8–12 compounds. We consider three outcomes of the screen (from right to left):

(i) Protein aggregation or denaturation: in this case at least one of the ligands harmed the protein. In most cases it is impractical to identify the culprit ligand, as this essentially means measuring each ligand individually.
(ii) No effects are seen from a mixture and the protein is intact: in this case it is safe to de-validate all ligands in the mixture, provided their presence was confirmed in a control experiment. Of course the usual limitations of protein-observed experiments apply: No observation of effects means that the K_D of the ligands is larger than ε times the employed ligand concentration. Since ε is about 3 and [*L*] is typically 500 μM, such ligands all would have K_D > 1.5 mM.
(iii) Binding effects are observed: at least one of the ligands in the mixture binds to the protein with K_D < 1.5 mM (following the considerations above). These ligands will be taken to the next step.

Identification of individual ligands by equimolar ligand-observation. Step 2 in Fig. 16*:* In this step the particular ligand from the mixture of compounds that was responsible for a positive result needs to be identified. This could be achieved by running protein-observed experiments of single compounds. However, it is more efficient in terms of measurement time and protein consumption, to run a ligand-observed experiment using the mixtures. Often, the ligand observed experiment can be run on exactly the same samples as for the protein-observed screen. However, in this format – with ligand in large excess – ligands exhibiting slow binding kinetics will not be observed (Fig. 12). Therefore, mixtures for which no binding effect can be detected on any ligand must be taken into an equimolar ligand-observed experiment; this is the safest experiment to identify and/or de-validate ligand binding.

Quality control of ligands. Step 3 in Fig. 16*:* This step is only needed because in equimolar experiments ligand QC is often not trivial, as lines are broadened and concentrations are low. Therefore, a quick ^{1}H 1D of the compound is needed in order to properly assess its integrity.

In summary, this simple workflow results in fully validated and de-validated ligands, as it combines the experiments with highest information content.

3.5.3. Workflow for validation of HTS hits

There are three important differences between hits from a fragment based screen and hits from a biochemical high-throughput screen. (i) HTS hits are more potent, (ii) there are typically more artifacts and (iii) there is a much higher number of hits.

(i) The sensitivity of biochemical screens is usually in the K_D-range of double-digit μM. Therefore, hits that are weaker than 10–100 μM are usually not detected (depending on the assay). HTS libraries contain compounds that are larger than fragments (typically ~500 Da vs. <250 Da) and therefore hits can be more potent. This needs to be considered in designing the validation workflow, because these more potent compounds will often show slow binding kinetics and will not be detectable by classical ligand observed experiments with ligand in high excess (Fig. 12).
(ii) A high throughput screen is rather prone to artifacts due to the several components in the reaction mixture that are required for a simple read-out. All of these components can be inhibited by compounds that are not specific for the target and lead to a false positive result. As the huge libraries (of more than a million of compounds) used for HTS are not quality controlled as rigorously as libraries for FBS, there are many promiscuous compounds that may just precipitate one or more of the assay components. The aim of an HTS validation workflow is not only to positively select true ligands, but also to de-select artifactual ligands, which usually represent the majority of HTS hits.
(iii) The third difference to the above workflows is that number of hits from the screen is usually orders of magnitude higher. The number of initial hits from an HTS may be as high as 30,000, for FBS it is rather around 5–30, depending of course on the target. The numbers of HTS hits need to be brought

Fig. 18. Selected pulse programs deposited in Bruker's user library [11]. Simplified pulse schemes for several pulse programs used for drug discovery are shown. The carrier frequency is depicted as a black horizontal line. Its position on the vertical ppm axis on the right hand side indicates the frequency at which pulses are applied. Filled and empty shapes represent 90° and 180° pulses, respectively. Rectangular and rounded shapes represent hard and selective pulses, respectively. The height of selective pulses approximately depicts their intended excitation bandwidth. The 1D experiments can easily be applied with double solvent suppression using pulses with the shape function 600_H2O_DMSO instead of simple rectangular pulses; the pulse-length may be adapted to the actual field. Details on phase cycles, etc. can be seen in the individual pulse programs, here the focus lies on highlighting the different options (blue), which can be set using the ZGOPTNS field (e.g., for a excitation sculpting experiment (zgesgp) with a perfect echo, –DPE is set in ZGOPTNS.) The individual options are as follows: zgesgp: PE (for "perfect echo"). This will add an echo element (blue) to suppress phasing artifacts from scalar couplings that evolve in conventional zgesgp experiments. For more details on the experimental setup see Section 2.1. T1rho: HEATCOMP (for heating compensation). With HEATCOMP a spin lock of duration d3 is applied far off-resonance during the recovery delay to compensate for differential heating during the reference experiment (relaxation delay d2 = 10 ms, heating compensation d3 = 400 ms) and the $T_1\rho$-filter experiment (d2 = 400 ms, d3 = 10 ms) (Section 2.2.2). STD: The default experiment will record a difference spectrum. ONRES and OFFRES (for on-resonance and off-resonance saturation) can be set as options. With ONRES the saturation pulses will be applied at a ppm value of cnst8 (0.5 ppm); with OFFRES at the one of cnst9 (−30 ppm) (Section 2.2.3). wLOGSY: PO (for polarization optimized). With PO a water flip-back pulse is applied so that water magnetization is preserved along the +z-axis after each scan. Additionally, the relaxation delay d1 is omitted in every second scan (Section 2.2.3). 19F-T2: d2 represents the entire relaxation period, which is set to 20 ms for the reference experiment and between 100 and 300 ms for the CPMG-filter. The offset must be adapted according to the resonance frequencies of the ^{19}F-nuclei in the sample (Section 2.2.2). 15 N-ALSOFAST-HMQC: The same pulse sequence is used for the ^{13}C-edited version of the experiment (Section 2.4.1).

down to below 1000 in order to be manageable by most biophysical techniques. This can be achieved by using chemoinformatics to cluster hits and select only a few representatives from each cluster for full validation. Even a thousand compounds may be too many for them all to be subjected to an expensive rigorous validation procedure. We suggest bringing numbers down to below 100 in an optional first step, which can be done with other biophysical assays than NMR. However, in a pure NMR workflow, the best-suited assay for this is a reporter assay.

Optional pre-selection of compounds to be validated. Step 1 in Fig. 17 (optional): This is an initial selection step to reduce the number of hits that need to be rigorously validated using expensive protein-observed NMR. The requirement for this step is of course to have a reporter molecule at hand, which may have been found using an FBS. (For ideal properties of a reporter see Section 2.2.8.) The results of the reporter assay are a set of compounds that displace the reporter, and a set that do not. Those which displace the reporter are taken into the next validation step. Those that do not are not actually de-validated hits; they may just not be binding at the same binding site, or not to a site which influences binding at the reporter binding site. However, in order to manage the numbers the validation workflow is continued only with compounds that compete with the reporter.

Quality control of individual ligands. Step 2 in Fig. 17: The next step is quality control of the ligand. As opposed to FBS, the ligands in high-throughput libraries are not well quality controlled beforehand and therefore many compounds will likely be de-validated at this stage. However, low solubility is not a de-validation criterion, and such compounds should be carried over into the next step.

Identification of binders in protein observed experiment. Step 3 in Fig. 17: The protein-observed assay is the step that adds most information in this workflow. Ligands should be de-validated if they cause the protein to aggregate or if they do not show any binding effects. The only inconclusive situation arises for low-solubility compounds that do not show any binding effects. For example, if a compound is only soluble to 2 μM and is assayed in an experiment using 20 μM protein, even if the compound was extremely potent it would probably not be detectable in this assay. Therefore it cannot be properly de-validated. If no protein-observed assay is available, the same decision tree as in Fig. 15 can be used to define the next best assay for this step.

Confirmation of ligands by ligand-observation. Step 4 in Fig. 17: When looking at the validation cross of a putative ligand, it is obvious that the last required step is a ligand-observed assay in order to rule out, for example, binding of a contaminant in the solution. As mentioned in the introduction to this workflow, ligand-observed experiments with ligands in excess are not suited for HTS hits, which often exhibit slow binding kinetics (Fig. 12). Therefore, the equimolar format is chosen, which does not suffer from these limitations. Importantly, however, there is a limit on the solubility of the ligand. Solubility should be at least a few μM in order to be able to obtain a meaningful spectrum. Ligands that also show effects in this assay are fully validated.

3.6. Some comments on "Validation and De-validation" and on "Selection, Annotation and Filtering"

In the above workflows the aim was focused on validating compounds as "true" ligands. In the continuation of a drug discovery project, these validated ligands will be further characterized by measuring their affinity or by determining their structure in complex with the target protein (Fig. 1). Such well-characterized ligands will then be optimized by synthetic chemistry in order to develop them into a potent and safe drug.

Along the way of a drug discovery project there are numerous hurdles for a ligand to overcome before becoming a drug candidate. Most ligands will actually not make it, even if they are true ligands, because they may not be permeable, they may be toxic or be degraded too fast, just to name a few causes. If all fully validated ligands are eliminated during the drug development process, ligands that were initially not fully validated may need to be "rescued". The validation cross may help to identify ligands that are worth revisiting, and to eliminate those that can safely be disregarded.

So far we have mainly focused on validating compounds, and applied a suite of experiments which aim at obtaining direct positive information on all four aspects of the validation cross. In this process many compounds have also been de-validated (as indicated by red crosses in Figs. 15–17). Following our definitions, there are only four patterns of the validation cross that can rigorously de-validate a compound (Fig. 3), corresponding to direct observation of negative effects in any of the fields; a lack of binding effects, as well as the presence and integrity of both ligand and protein must all be demonstrated at the same time in order to lead to full de-validation. In conducting a "rescuing attempt", such de-validated compounds can therefore be safely left aside.

It is useful to define a nomenclature for annotating compounds in a hit list, so that one can "filter out" de-validated compounds. Assays that can lead to safe de-validation are therefore often called "filtering" assays. In Fig. 17 the ligand quality control (step 2) and the protein observation experiment (step 3) are true filtering experiments. Compounds that do not pass the test are de-validated. In contrast, the reporter assay (step 1) is only a "selection" step, where the compounds showing the desired effect are taken forward, because they have a much higher probability of being true ligands than those that do not. However, the compounds that are not selected could still be true ligands that fail to compete with the reporter because they have different binding sites. Such compounds should therefore not be de-validated. We can only "annotate" that they do not displace the reporter – and that they leave the protein functional. In a rescuing attempt, these compounds would be worth testing in another type of assay.

When analyzing the validation workflow based on ligand-observed screening (Fig. 15), it is evident that there are many compounds that are not validated or de-validated properly. This can have many causes, such as experimental shortcomings and lack of labeled protein. All these compounds merely carry an "annotation". Such annotations can be represented in the compact form of the validation cross, and compounds can be ranked according to the number of green fields they have obtained throughout the workflow. For the sake of rescuing, compounds can therefore be prioritized according to their validation cross pattern.

When classifying compounds and analyzing outcomes of individual experiments, the nomenclature derived from the validation cross can help clarifying complex situations that are often encountered.

Conclusions

NMR is regarded as a "gold-standard" method for the validation of molecular interactions in the early phase of drug discovery; but actually this is not because of the merits of any particular single experiment. It is rather because of the ability to access many differ-

ent aspects of molecular interactions by using complementary experiments and without the need of altering any components in the sample, e.g. by chemical modification. It is therefore probably the method that is most robust with respect to experimental artifacts. At the same time, for most applications it is the most expensive and most time consuming method. The high investments in NMR for the purpose of drug discovery can only be justified if NMR continues to fulfill the highest quality standards. We hope that this review may help those who are not so familiar with the subject to apply NMR in an effective way to drug discovery, by helping them to choose the most appropriate experiments, carry them out with suitable controls, and interpret their outcomes.

Acknowledgements

This work would not have been possible without numerous discussions held during a year with Sascha Gutmann, Jean-Michel Rondeau, César Fernández and Marcel J.J. Blommers. Several parts of this text on experimental aspects and information content of experiments were based on fruitful discussions with Lukasz Skora, Simon Rüdisser, Paulus Erbel, Andreas Lingel, Andi Frank, Jaison Jacob, Jasna Fejzo and Xiaolu Zhang. We would like to thank them all for providing such a stimulating working atmosphere. We would like to thank Chrystèle Henry for her input on many practical aspects. We also thank Helena Kovacs for her valuable comments, her generous sharing of NMR knowledge and her essential help with pulse sequences together with Stefan Jehle. Last but not least, we thank Geoffrey Bodenhausen and David Neuhaus for their well-considered edits, which improve the clarity, accuracy and the general readability of this text.

Appendix A. NMR experiments in Bruker's user library

As a complement to this review, we have deposited full parameter sets for selected experiments (Fig. 18) in the Bruker user library for downloading [11]. This should enable readers seamlessly to install and run these experiments. The pulse sequences are all compatible with the 'prosol' command. Water suppression is generally achieved using excitation sculpting. An acceptable initial value for the selective pulses to handle water signals can be obtained using the command "getprosol 1H 8.0 10W", which will calculate the theoretical values for the soft pulses based on the values of the hard 90° ^{1}H pulse (here 8.0 μs corresponds to 10 W). Double solvent suppression can be achieved using 600_H2O_DMSO pulses instead of simple rectangular pulses; the pulse-length may be adapted to the actual field.

We recommend preparing dedicated samples for testing these experiments. A mixture of 1 mM L-tryptophan (Sigma-Aldrich Cat. No. 93,659) and 20 μM serum albumin (06,470) is a well-established test sample. It is advisable also to add a non-binding compound like L-tyrosine (93829) for internal reference. For ^{19}F-based experiments we recommend 4-(triflouromethyl) benzamidine (CVT00069) with trypsin (T8003), while trifluoroacetic acid (T6508) can serve as an internal control.

References

[1] A.L. Hopkins, C.R. Groom, A. Alex, Ligand efficiency: a useful metric for lead selection, Drug Discov. Today. 9 (2004) 430–431.
[2] I.D. Kuntz, K. Chen, K.A. Sharp, P.A. Kollman, The maximal affinity of ligands, Proc. Natl. Acad. Sci. 96 (1999) 9997–10002.
[3] G. Holdgate, S. Geschwindner, A. Breeze, G. Davies, N. Colclough, D. Temesi, L. Ward, Biophysical methods in drug discovery from small molecule to pharmaceutical, in: M.A. Williams, T. Daviter (Eds.), Protein-Ligand Interactions, Humana Press, Totowa NJ, 2013, pp. 327–355.
[4] A. Ciulli, Biophysical screening for the discovery of small-molecule ligands, in: M.A. Williams, T. Daviter (Eds.), Protein-Ligand Interactions, Humana Press, Totowa, NJ, 2013, pp. 357–388.
[5] H.L. Silvestre, T.L. Blundell, C. Abell, A. Ciulli, Integrated biophysical approach to fragment screening and validation for fragment-based lead discovery, Proc. Natl. Acad. Sci. 110 (2013) 12984–12989.
[6] D.A. Erlanson, W. Jahnke, Fragment-Based Drug Discovery, Wiley-VCH, 2016.
[7] J.W. Peng, J. Moore, N. Abdul-Manan, NMR experiments for lead generation in drug discovery, Prog. Nucl. Magn. Reson. Spectrosc. 44 (2004) 225–256.
[8] B. Davis, Screening protein-small molecule interactions by NMR, in: M.A. Williams, T. Daviter (Eds.), Protein-Ligand Interactions, Humana Press, Totowa, NJ, 2013, pp. 389–413.
[9] B. Meyer, T. Peters, NMR spectroscopy techniques for screening and identifying ligand binding to protein receptors, Angew. Chem. Int. Ed. 42 (2003) 864–890.
[10] W. Jahnke, Perspectives of biomolecular NMR in drug discovery: the blessing and curse of versatility, J. Biomol. NMR 39 (2007) 87–90.
[11] E. Kupce, Bruker User Library, n.d.
[12] M.H. Levitt, Spin Dynamics: Basics of Nuclear Magnetic Resonance, John Wiley & Sons, Chichester, 2001.
[13] K.A. Connors, Binding Constants - the Measurement of Molecular Complex Stability, John Wiley & Sons, New York, 1987.
[14] N.M. Green, Avidin: 1. The use of [^{14}C]biotin for kinetic studies and for assay, Biochem. J. 89 (1963) 585–591.
[15] G. Dahl, T. Akerud, Pharmacokinetics and the drug–target residence time concept, Drug Discov. Today. 18 (2013) 697–707.
[16] R.A. Copeland, D.L. Pompliano, T.D. Meek, Drug–target residence time and its implications for lead optimization, Nat. Rev. Drug Discov. 5 (2006) 730–739.
[17] C.R. Cantor, P.R. Schimmel, Biophysical Chemistry Part II: Techniques for the Study of Biological Structure and Function, W. H. Freeman and Company, New York, 1980.
[18] H.C. Berg, Random Walks in Biology, Princeton University Press, Princeton, 1993.
[19] A. Abragam, Principles of Nuclear Magnetism, Oxford University Press, Oxford, 1961.
[20] A. Furukawa, T. Konuma, S. Yanaka, K. Sugase, Quantitative analysis of protein–ligand interactions by NMR, Prog. Nucl. Magn. Reson. Spectrosc. 96 (2016) 47–57.
[21] L. Fielding, NMR methods for the determination of protein–ligand dissociation constants, Prog. Nucl. Magn. Reson. Spectrosc. 51 (2007) 219–242.
[22] T.J. Swift, R.E. Connick, NMR-relaxation mechanisms of O17 in aqueous solutions of paramagnetic cations and the lifetime of water molecules in the first coordination sphere, J. Chem. Phys. 37 (1962) 307–320.
[23] C.W. Haigh, R.B. Mallion, Ring current theories in nuclear magnetic resonance, Prog. Nucl. Magn. Reson. Spectrosc. 13 (1980) 303–344.
[24] N. Bloembergen, E.M. Purcell, R.V. Pound, Relaxation effects in nuclear magnetic resonance absorption, Phys. Rev. 73 (1948) 679–712.
[25] J. Cavanagh, W.J. Fairbrother, A.G. Palmer III, N.J. Skelton, Protein NMR Spectroscopy, Principles and Practice, Academic Press, Burlington, MA, 1996.
[26] P. Luginbühl, K. Wüthrich, Semi-classical nuclear spin relaxation theory revisited for use with biological macromolecules, Prog. Nucl. Magn. Reson. Spectrosc. 40 (2002) 199–247.
[27] J.W. Peng, G. Wagner, Investigation of protein motions via relaxation measurements, Meth. Enzymol. 239 (1994) 563–596.
[28] I. Solomon, Relaxation processes in a system of two spins, Phys. Rev. 99 (1955) 559–565.
[29] A. Kalk, H. Berendsen, Proton magnetic relaxation and spin diffusion in proteins, J. Magn. Reson. 24 (1976) 343–366.
[30] G.M. Clore, A.M. Gronenborn, Theory of the time dependent transferred nuclear overhauser effect: applications to structural analysis of ligand-protein complexes in solution, J. Magn. Reson. 53 (1983) 423–442.
[31] F. Ni, Y. Zhu, Accounting for ligand-protein interactions in the relaxation-matrix analysis of transferred nuclear overhauser effects, J. Magn. Reson. B 102 (1994) 180–184.
[32] H.N.B. Moseley, E.V. Curto, N.R. Krishna, Complete relaxation and conformational exchange matrix (CORCEMA) analysis of NOESY spectra of interacting system; two-dimensional transferred NOESY, J. Magn. Reson. B 108 (1995) 243–261.
[33] P. Crews, J. Rodriguez, M. Jaspars, Organic Structure Analysis, Oxford University Press, Oxford, 1998.
[34] U. Holzgrabe, Quantitative NMR spectroscopy in pharmaceutical applications, Prog. Nucl. Magn. Reson. Spectrosc. 57 (2010) 229–240.
[35] G. Wider, L. Dreier, Measuring protein concentrations by NMR spectroscopy, J. Am. Chem. Soc. 128 (2006) 2571–2576.
[36] G.F. Pauli, B.U. Jaki, D.C. Lankin, Quantitative ^{1}H NMR: development and potential of a method for natural products analysis, J. Nat. Prod. 68 (2005) 133–149.
[37] G.F. Pauli, T. Gödecke, B.U. Jaki, D.C. Lankin, Quantitative ^{1}H NMR. Development and potential of an analytical method: an update, J. Nat. Prod. 75 (2012) 834–851.
[38] T.-L. Hwang, A.J. Shaka, Water Suppression that works. Excitation sculpting using arbitrary waveforms and pulsed field gradients, J. Magn. Reson. A. 112 (1995) 275–279.
[39] J.A. Aguilar, M. Nilsson, G. Bodenhausen, G.A. Morris, Spin echo NMR spectra without J modulation, Chem. Commun. 48 (2012) 811.
[40] M. Piotto, V. Saudek, V. Sklenář, Gradient-tailored excitation for single-quantum NMR spectroscopy of aqueous solutions, J. Biomol. NMR 2 (1992) 661–665.

[41] R.W. Adams, C.M. Holroyd, J.A. Aguilar, M. Nilsson, G.A. Morris, "Perfecting" WATERGATE: clean proton NMR spectra from aqueous solution, Chem. Commun. 49 (2013) 358–360.
[42] F. Ni, Recent developments in transferred NOE methods, Prog. Nucl. Magn. Reson. Spectrosc. 26 (1994) 517–606.
[43] B.W. Koenig, D.C. Mitchell, S. König, S. Grzesiek, B.J. Litman, A. Bax, Measurement of dipolar couplings in a transducin peptide fragment weakly bound to oriented photo-activated rhodopsin, J. Biomol. NMR 16 (2000) 121–125.
[44] B.W. Koenig, G. Kontaxis, D.C. Mitchell, J.M. Louis, B.J. Litman, A. Bax, Structure and orientation of a G protein fragment in the receptor bound state from residual dipolar couplings, J. Mol. Biol. 322 (2002) 441–461.
[45] T. Carlomagno, I.C. Felli, M. Czech, R. Fischer, M. Sprinzl, C. Griesinger, Transferred cross-correlated relaxation: application to the determination of sugar pucker in an aminoacylated tRNA-mimetic weakly bound to EF-Tu, J. Am. Chem. Soc. 121 (1999) 1945–1948.
[46] M.J.J. Blommers, W. Stark, C.E. Jones, D. Head, C.E. Owen, W. Jahnke, Transferred cross-correlated relaxation complements transferred NOE: structure of an IL-4R-derived peptide bound to STAT-6, J. Am. Chem. Soc. 121 (1999) 1949–1953.
[47] P.J. Hajduk, E.T. Olejniczak, S.W. Fesik, One-dimensional relaxation-and diffusion-edited NMR methods for screening compounds that bind to macromolecules, J. Am. Chem. Soc. 119 (1997) 12257–12261.
[48] J.T. Gerig, Fluorine nuclear magnetic resonance of fluorinated ligands, Meth. Enzymol. 177 (1989) 3–23.
[49] C. Dalvit, P.E. Fagerness, D.T.A. Hadden, R.W. Sarver, B.J. Stockman, Fluorine-NMR experiments for high-throughput screening: theoretical aspects, practical considerations, and range of applicability, J. Am. Chem. Soc. 125 (2003) 7696–7703.
[50] J.T. Gerig, Fluorine NMR, Online Textb., 2001.
[51] Y. Lee, H. Zeng, S. Ruedisser, A.D. Gossert, C. Hilty, Nuclear magnetic resonance of hyperpolarized fluorine for characterization of protein-ligand interactions, J. Am. Chem. Soc. 134 (2012) 17448–17451.
[52] J.H. Ardenkjaer-Larsen, B. Fridlund, A. Gram, G. Hansson, L. Hansson, M.H. Lerche, R. Servin, M. Thaning, K. Golman, Increase in signal-to-noise ratio of >10,000 times in liquid-state NMR, Proc. Natl. Acad. Sci. 100 (2003) 10158–10163.
[53] C. Dalvit, A.D. Gossert, J. Coutant, M. Piotto, Rapid acquisition of ^{1}H and ^{19}F NMR experiments for direct and competition ligand-based screening, Magn. Reson. Chem. 49 (2011) 199–202.
[54] K. Kobzar, S. Ehni, T.E. Skinner, S.J. Glaser, B. Luy, Exploring the limits of broadband 90 and 180 universal rotation pulses, J. Magn. Reson. 225 (2012) 142–160.
[55] K. Kobzar, T.E. Skinner, N. Khaneja, S.J. Glaser, B. Luy, Exploring the limits of broadband excitation and inversion pulses, J. Magn. Reson. 170 (2004) 236–243.
[56] S. Hiller, H. Arthanari, G. Wagner, The T-lock: automated compensation of radio-frequency induced sample heating, J. Biomol. NMR 44 (2009) 69–76.
[57] H. Kovacs, A.D. Gossert, Improved NMR experiments with ^{13}C-isotropic mixing for assignment of aromatic and aliphatic side chains in labeled proteins, J. Biomol. NMR 58 (2014) 101–112.
[58] W. Jahnke, Spin labels as a tool to identify and characterize protein–ligand interactions by NMR spectroscopy, ChemBioChem 3 (2002) 167–173.
[59] B. Meyer, T. Weimar, T. Peters, Screening mixtures for biological activity by NMR, Eur. J. Biochem. 246 (1997) 705–709.
[60] A.L. Breeze, Isotope-filtered NMR methods for the study of biomolecular structure and interactions, Prog. Nucl. Magn. Reson. Spectrosc. 36 (2000) 323–372.
[61] M. Mayer, B. Meyer, Characterization of ligand binding by saturation transfer difference NMR spectroscopy, Angew. Chem. Int. Ed. 38 (1999) 1784–1788.
[62] M. Kobayashi, K. Retra, F. Figaroa, J.G. Hollander, E. Ab, R.J. Heetebrij, H. Irth, G. Siegal, Target immobilization as a strategy for NMR-based fragment screening: comparison of TINS, STD, and SPR for fragment hit identification, J. Biomol. Screen. 15 (2010) 978–989.
[63] S. Vanwetswinkel, R.J. Heetebrij, J. van Duynhoven, J.G. Hollander, D.V. Filippov, P.J. Hajduk, G. Siegal, TINS, target immobilized NMR screening: an efficient and sensitive method for ligand discovery, Chem. Biol. 12 (2005) 207–216.
[64] M.L. Rowe, J.L. Wagstaff, M.J. Howard, NMR in ligand binding studies, in: J. Fisher (Ed.), Modern NMR Techniques for Synthetic Chemistry, CRC Press, Boca Raton, FL, 2014, pp. 63–123.
[65] B. Claasen, M. Axmann, R. Meinecke, B. Meyer, Direct observation of ligand binding to membrane proteins in living cells by a saturation transfer double difference (STDD) NMR spectroscopy method shows a significantly higher affinity of integrin $\alpha_{iib}\beta_3$ in native platelets than in liposomes, J. Am. Chem. Soc. 127 (2005) 916–919.
[66] C. Dalvit, G. Fogliatto, A. Stewart, M. Veronesi, B. Stockman, WaterLOGSY as a method for primary NMR screening: practical aspects and range of applicability, J. Biomol. NMR 21 (2001) 349–359.
[67] C. Dalvit, P. Pevarello, M. Tatò, M. Veronesi, A. Vulpetti, M. Sundström, Identification of compounds with binding affinity to proteins via magnetization transfer from bulk water, J. Biomol. NMR 18 (2000) 65–68.
[68] Q. Chappuis, J. Milani, B. Vuichoud, A. Bornet, A.D. Gossert, G. Bodenhausen, S. Jannin, Hyperpolarized water to study protein-ligand interactions, J. Phys. Chem. Lett. 1674–1678 (2015).
[69] A.D. Gossert, C. Henry, M.J.J. Blommers, W. Jahnke, C. Fernández, Time efficient detection of protein–ligand interactions with the polarization optimized PO-WaterLOGSY NMR experiment, J. Biomol. NMR 43 (2009) 211–217.
[70] P. Sun, X. Jiang, B. Jiang, X. Zhang, M. Liu, Biomolecular ligands screening using radiation damping difference WaterLOGSY spectroscopy, J. Biomol. NMR 56 (2013) 285–290.
[71] R.E. London, Theoretical analysis of the inter-ligand overhauser effect: a new approach for mapping structural relationships of macromolecular ligands, J. Magn. Reson. 141 (1999) 301–311.
[72] V.M. Sánchez-Pedregal, M. Reese, J. Meiler, M.J.J. Blommers, C. Griesinger, T. Carlomagno, The INPHARMA method: protein-mediated interligand NOEs for pharmacophore mapping, Angew. Chem. Int. Ed. 44 (2005) 4172–4175.
[73] J. Orts, C. Griesinger, T. Carlomagno, The INPHARMA technique for pharmacophore mapping: a theoretical guide to the method, J. Magn. Reson. 200 (2009) 64–73.
[74] J. Orts, J. Tuma, M. Reese, S.K. Grimm, P. Monecke, S. Bartoschek, A. Schiffer, K. U. Wendt, C. Griesinger, T. Carlomagno, Crystallography-independent determination of ligand binding modes, Angew. Chem. Int. Ed. 47 (2008) 7736–7740.
[75] J. Chen, Z. Zhang, J.L. Stebbins, X. Zhang, R. Hoffman, A. Moore, M. Pellecchia, A fragment-based approach for the discovery of isoform-specific p38α inhibitors, ACS Chem. Biol. 2 (2007) 329–336.
[76] Y. Lee, H. Zeng, A. Mazur, M. Wegstroth, T. Carlomagno, M. Reese, D. Lee, S. Becker, C. Griesinger, C. Hilty, Hyperpolarized binding pocket nuclear overhauser effect for determination of competitive ligand binding, Angew. Chem. Int. Ed. 51 (2012) 5179–5182.
[77] M. Carravetta, M.H. Levitt, Long-lived nuclear spin states in high-field solution NMR, J. Am. Chem. Soc. 126 (2004) 6228–6229.
[78] R. Sarkar, P. Ahuja, P.R. Vasos, A. Bornet, O. Wagnières, G. Bodenhausen, Long-lived coherences for line-narrowing in high-field NMR, Prog. Nucl. Magn. Reson. Spectrosc. 59 (2011) 83–90.
[79] R. Buratto, D. Mammoli, E. Chiarparin, G. Williams, G. Bodenhausen, Exploring weak ligand-protein interactions by long-lived NMR states: improved contrast in fragment-based drug screening, Angew. Chem. Int. Ed. 53 (2014) 11376–11380.
[80] N. Salvi, R. Buratto, A. Bornet, S. Ulzega, I. Rentero Rebollo, A. Angelini, C. Heinis, G. Bodenhausen, Boosting the sensitivity of ligand-protein screening by NMR of long-lived states, J. Am. Chem. Soc. 134 (2012) 11076–11079.
[81] R. Buratto, A. Bornet, J. Milani, D. Mammoli, B. Vuichoud, N. Salvi, M. Singh, A. Laguerre, S. Passemard, S. Gerber-Lemaire, S. Jannin, G. Bodenhausen, Drug screening boosted by hyperpolarized long-lived states in NMR, ChemMedChem 9 (2014) 2509–2515.
[82] J.A. Peters, J. Huskens, D.J. Raber, Lanthanide induced shifts and relaxation rate enhancements, Prog. Nucl. Magn. Reson. Spectrosc. 28 (1996) 283–350.
[83] I. Bertini, C. Luchinat, New applications of paramagnetic NMR in chemical biology, Curr. Opin. Chem. Biol. 3 (1999) 145–151.
[84] G. Pintacuda, A. Moshref, A. Leonchiks, A. Sharipo, G. Otting, Site-specific labelling with a metal chelator for protein-structure refinement, J. Biomol. NMR 29 (2004) 351–361.
[85] O.K. Baryshnikova, T.C. Williams, B.D. Sykes, Internal pH indicators for biomolecular NMR, J. Biomol. NMR 41 (2008) 5–7.
[86] D. Wu, A. Chen, C.S. Johnson Jr., Flow imaging by means of 1D pulsed-field-gradient NMR with application to electroosmotic flow, J. Magn. Reson. A. 115 (1995) 123–126.
[87] C.S. Johnson Jr., Diffusion ordered nuclear magnetic resonance spectroscopy: principles and applications, Prog. Nucl. Magn. Reson. Spectrosc. 34 (1999) 203–256.
[88] X. Zhang, A. Sänger, R. Hemmig, W. Jahnke, Ranking of high-affinity ligands by NMR spectroscopy, Angew. Chem. Int. Ed. 48 (2009) 6691–6694.
[89] C. Dalvit, M. Flocco, S. Knapp, M. Mostardini, R. Perego, B.J. Stockman, M. Veronesi, M. Varasi, High-throughput NMR-based screening with competition binding experiments, J. Am. Chem. Soc. 124 (2002) 7702–7709.
[90] W. Jahnke, P. Floersheim, C. Ostermeier, X. Zhang, R. Hemmig, K. Hurth, D.P. Uzunov, NMR reporter screening for the detection of high-affinity ligands, Angew. Chem. Int. Ed. 41 (2002) 3420–3423.
[91] Y. Kim, C. Hilty, Affinity screening using competitive binding with fluorine-19 hyperpolarized ligands, Angew. Chem. Int. Ed. 54 (2015) 4941–4944.
[92] M.A. McCoy, D.F. Wyss, Spatial localization of ligand binding sites from electron current density surfaces calculated from NMR chemical shift perturbations, J. Am. Chem. Soc. 124 (2002) 11758–11763.
[93] C. Aguirre, O. Cala, I. Krimm, Overview of probing protein-ligand interactions using NMR, in: J.E. Coligan, B.M. Dunn, D.W. Speicher, P.T. Wingfield (Eds.), Current Protocols in Protein Science, John Wiley & Sons, Inc., Hoboken, NJ, USA, 2015, pp. 17.18.1–17.18.24.
[94] I. Shimada, T. Ueda, M. Matsumoto, M. Sakakura, M. Osawa, K. Takeuchi, N. Nishida, H. Takahashi, Cross-saturation and transferred cross-saturation experiments, Prog. Nucl. Magn. Reson. Spectrosc. 54 (2009) 123–140.
[95] M. Reibarkh, T.J. Malia, G. Wagner, NMR distinction of single- and multiple-mode binding of small-molecule protein ligands, J. Am. Chem. Soc. 128 (2006) 2160–2161.
[96] Z. Kelman (Ed.), Isotope Labeling of Biomolecules - Labeling Methods, Elsevier, Waltham, MA, 2015.
[97] H.S. Atreya (Ed.), Isotope Labeling in Biomolecular NMR, Springer, Dordrecht, 2012.

[98] J. Fiaux, E.B. Bertelsen, A.L. Horwich, K. Wüthrich, NMR analysis of a 900K GroEL–GroES complex, Nature 418 (2002) 207–211.
[99] R. Sprangers, L.E. Kay, Quantitative dynamics and binding studies of the 20S proteasome by NMR, Nature 445 (2007) 618–622.
[100] L. Skora, B. Shrestha, A.D. Gossert, Isotope labeling of proteins in insect cells, in: Z. Kelman (Ed.), Methods in Enzymology, Academic Press, Burlington, 2015, pp. 245–288.
[101] A. Meola, C. Deville, S.A. Jeffers, P. Guardado-Calvo, I. Vasiliauskaite, C. Sizun, C. Girard-Blanc, C. Malosse, C. van Heijenoort, J. Chamot-Rooke, T. Krey, E. Guittet, S. Pêtres, F.A. Rey, F. Bontems, Robust and low cost uniform ^{15}N-labeling of proteins expressed in Drosophila S2 cells and Spodoptera frugiperda Sf9 cells for NMR applications, J. Struct. Biol. 188 (2014) 71–78.
[102] A. Sitarska, L. Skora, J. Klopp, S. Roest, C. Fernández, B. Shrestha, A.D. Gossert, Affordable uniform isotope labeling with ^{2}H, ^{13}C and ^{15}N in insect cells, J. Biomol. NMR 62 (2015) 169–177.
[103] C. Opitz, S. Isogai, S. Grzesiek, An economic approach to efficient isotope labeling in insect cells using homemade ^{15}N-, ^{13}C- and ^{2}H-labeled yeast extracts, J. Biomol. NMR 62 (2015) 373–385.
[104] P. Lundström, A. Ahlner, A.T. Blissing, Isotope labeling methods for large systems, in: H.S. Atreya (Ed.), Isotope Labeling in Biomolecular NMR, Springer, Netherlands, Dordrecht, 2012, pp. 3–15.
[105] N. Guthertz, J. Klopp, A. Winterhalter, C. Fernández, A.D. Gossert, Auto-inducing media for uniform isotope labeling of proteins with ^{15}N, ^{13}C and ^{2}H, J. Biomol. NMR 62 (2015) 191–197.
[106] F.W. Studier, Protein production by auto-induction in high-density shaking cultures, Protein Expr. Purif. 41 (2005) 207–234.
[107] R.C. Tyler, H.K. Sreenath, S. Singh, D.J. Aceti, C.A. Bingman, J.L. Markley, B.G. Fox, Auto-induction medium for the production of [U-^{15}N]- and [U-^{13}C, U-^{15}N]-labeled proteins for NMR screening and structure determination, Protein Expr. Purif. 40 (2005) 268–278.
[108] P.J. Hajduk, D.J. Augeri, J. Mack, R. Mendoza, J. Yang, S.F. Betz, S.W. Fesik, NMR-based screening of proteins containing ^{13}C-labeled methyl groups, J. Am. Chem. Soc. 122 (2000) 7898–7904.
[109] D.M. LeMaster, Deuteration in protein proton magnetic resonance, Meth. Enzymol. 177 (1989) 23–43.
[110] J. Weigelt, M. van Dongen, J. Uppenberg, J. Schultz, M. Wikström, Site-selective screening by NMR spectroscopy with labeled amino acid pairs, J. Am. Chem. Soc. 124 (2002) 2446–2447.
[111] L. Mueller, Alternate HMQC experiments for recording HN and HC-correlation spectra in proteins at high throughput, J. Biomol. NMR 42 (2008) 129–137.
[112] P. Schanda, Ē. Kupče, B. Brutscher, SOFAST-HMQC experiments for recording two-dimensional heteronuclear correlation spectra of proteins within a few seconds, J. Biomol. NMR 33 (2005) 199–211.
[113] K. Pervushin, Impact of transverse relaxation optimized spectroscopy (TROSY) on NMR as a technique in structural biology, Quart. Rev. Biophys. 33 (2000) 161–197.
[114] R. Riek, J. Fiaux, E.B. Bertelsen, A.L. Horwich, K. Wüthrich, Solution NMR techniques for large molecular and supramolecular structures, J. Am. Chem. Soc. 124 (2002) 12144–12153.
[115] K. Pervushin, R. Riek, G. Wider, K. Wüthrich, Attenuated T_2 relaxation by mutual cancellation of dipole–dipole coupling and chemical shift anisotropy indicates an avenue to NMR structures of very large biological macromolecules in solution, Proc. Natl. Acad. Sci. 94 (1997) 12366–12371.
[116] T. Cierpicki, J. Otlewski, Amide proton temperature coefficients as hydrogen bond indicators in proteins, J. Biomol. NMR 21 (2001) 249–261.
[117] A. Ross, G. Schlotterbeck, W. Klaus, H. Senn, Automation of NMR measurements and data evaluation for systematically screening interactions of small molecules with target proteins, J. Biomol. NMR 16 (2000) 139–146.
[118] A. Ross, H. Senn, Automation of biomolecular NMR screening, Curr. Top. Med. Chem. 3 (2003) 55–67.
[119] R.F. Ludlow, M.L. Verdonk, H.K. Saini, I.J. Tickle, H. Jhoti, Detection of secondary binding sites in proteins using fragment screening, Proc. Natl. Acad. Sci. 112 (2015) 15910–15915.
[120] C.A. Lepre, Practical aspects of NMR-based fragment screening, in: Methods in Enzymology, Academic Press, Burlington, 2011, pp. 219–239.